Characterizing FDA-approved drugs targeting Staufen1 as therapeutics against Skeletal Muscle Atrophy

Dhrashti Patel

A thesis submitted in partial fulfillment of the requirements for the
Master of Science in Cellular and Molecular Medicine

Supervisors: Dr. Bernard J. Jasmin and Dr. Aymeric Ravel-Chapuis

Department of Cellular and Molecular Medicine
Faculty of Medicine
University of Ottawa

Abstract

Skeletal muscle atrophy is a debilitating condition characterized by progressive muscle mass loss and functional decline, commonly associated with aging, physical inactivity, denervation, cachexia, and various chronic diseases. Previous work from our laboratory demonstrated that transgenic overexpression of STAU1 in mouse skeletal muscle induces muscle atrophy, suggesting that STAU1 functions as a novel atrogene. More recently, we observed an early and transient increase in STAU1 expression across multiple models of muscle atrophy, including starvation-induced atrophy in C2C12 myotubes, muscle samples in a denervation model, and human participants undergoing bed rest or dry immersion. Importantly, genetic knockdown of STAU1 during atrophic condition preserved myofiber diameter, supporting a causal role for STAU1 in the initiation of muscle wasting. However, whether STAU1 can be effectively targeted using pharmacological approaches remains unknown. To explore potential therapeutic strategies, we aimed to identify FDA-approved compounds capable of reducing STAU1 expression during atrophy. A high-throughput ELISA-based screen of 770 FDA-approved drugs was conducted in myoblasts to assess their ability to downregulate STAU1 protein levels. Using our established in *vitro* atrophy model, three candidate drugs (11, 12, and 15) were identified that significantly reduced STAU1 mRNA and protein expression and preserved myotube diameter, thereby attenuating atrophy. Subsequently, Drugs 12 and 15 were evaluated both in *vitro* and in *vivo* using C2C12 myotubes and male and female mice subjected to sciatic nerve denervation followed by daily drug administration. STAU1 inhibition preserves myotube integrity during acute atrophic stress in *vitro*. However, in *vivo* treatment following denervation did not significantly prevent muscle loss, indicating that while STAU1 contributes to early atrophic responses, its inhibition alone is insufficient to mitigate denervation-induced skeletal muscle atrophy. Collectively, these findings indicate that although STAU1 inhibition is protective in *vitro*, it does not confer significant protection against denervation-induced muscle atrophy in *vivo*. Further studies are warranted to identify more effective modulators of STAU1 or complementary pathways to mitigate skeletal muscle atrophy.

Table of Contents

List of Abbreviations

Atrogin-1 (MAFbx)

Forkhead Box O (FoxO)

Insulin-like Growth Factor-1 (IGF-1)

Liquid-liquid phase separation (LLPS)

mammalian target of rapamycin (mTOR)

Muscle RING Finger 1 (MuRF1)

Phosphate and tension homolog (PTEN)

Phosphoinositide 3-kinase (PI3K)

Ribonucleoprotein (RNP)

RNA-binding proteins (RBPs)

Staufen1 (STAU1)

Staufen1-binding sites (SBSs)

Ubiquitin-Proteasome System (UPS)

List of Figures

List of Tables

Acknowledgment

I would like to express my deepest gratitude to my supervisors, Dr. Bernard J. Jasmin and Dr. Aymeric Ravel-Chapuis, for their invaluable guidance, support, and encouragement throughout the course of my graduate studies. Their mentorship has been instrumental in shaping my scientific thinking and research skills, and I am sincerely thankful for the opportunity to learn under their supervision. I would also like to acknowledge the Canadian Space Agency (CSA) and the River Phillip Foundation for providing financial support for this project. Their funding made it possible to carry out this research and contribute to our understanding of skeletal muscle atrophy in space-related and terrestrial models. My heartfelt thanks go to all the members of both laboratories for their collaboration, advice, and camaraderie. In particular, I am deeply grateful to Jonathan Gobin, whose guidance and hands-on training were essential for the successful completion of my experiments. His patience, expertise, and willingness to share knowledge greatly enriched my research experience. I also extend my thanks to Marc Charron for his continuous support and insightful discussions, as well as to the CBIAcore team for their valuable assistance with microscopy analysis and technical expertise.

1. Introduction and Background

The term "healthy muscle" refers to the preservation of sufficient muscle mass, composition, and integrity throughout a person's life rather than the presence of muscle tissue (Frontera and Ochala, 2015). Healthy muscles are essential for mobility, strength, and overall well-being. Skeletal muscle is an important part of overall physiological health and comprises approximately 30-40% of total body mass (Wong et al., 2025). In the recent years; it has become a key component in determining quality of life with a significant correlation between muscle functioning, and risk of diseases. Increased risks of frailty, disability, hospitalization, and death are associated with loss of muscle mass and decrease in muscle quality, which are frequently seen in aging (sarcopenia), muscle atrophy and chronic diseases (Prado et al., 2024; McCullough, Jessu, and Callahan, 2025). As a result, maintaining skeletal muscle is widely recognized as a central purpose in therapeutic and preventative approaches meant to improve long-term health outcomes. This rising awareness highlights the significance of skeletal muscle in clinical and research settings as a crucial indication of overall health condition in addition to its role in preserving physical independence.

1.1 Overview of Skeletal Muscle Structure and Function

Skeletal muscle has a precisely sequenced, hierarchical structure that facilitates effective force production and mechanical coordination. Macroscopically, skeletal muscle is made up of bundles of muscle fibers, each of which is a multinucleated cell, wrapped in the sarcolemma, a specialized plasma membrane (Tortora and Derrickson, 2018). Numerous cylindrical structures called myofibrils, which give muscles their contractile characteristics, are found inside each muscle fiber. These myofibrils run longitudinally throughout the fiber's length and are closely packed with contractile proteins. Sarcomeres, which are the fundamental contractile units of skeletal muscle, continue to arise functional units that make up myofibrils at the subcellular level (Tortora and Derrickson, 2014; Mukund and Subramaniam, 2019). Z discs define each sarcomere, which is made up of intricately arranged thin (actin) and thick (myosin) filaments. Different banding patterns, such as the A band (thick filaments), I band (thin filaments), and H

zone (center region with solely thick filaments), are produced by the spatial arrangement of these filaments (Figure 1) (Tortora and Derrickson, 2018; Mukund and Subramaniam, 2019). The Z discs establish the limits of the sarcomere and attach the thin filaments, while the M line, which is situated in the heart of the sarcomere, maintains the thick filaments. Skeletal muscle fibers have specific features that support their function in addition to the contractile machinery. Myofibrils are surrounded by the sarcoplasmic reticulum, which stores calcium ions that are necessary to control contraction. To provide the ATP needed for prolonged muscular action, mitochondria are scattered throughout the fiber (Mukund and Subramaniam, 2019).

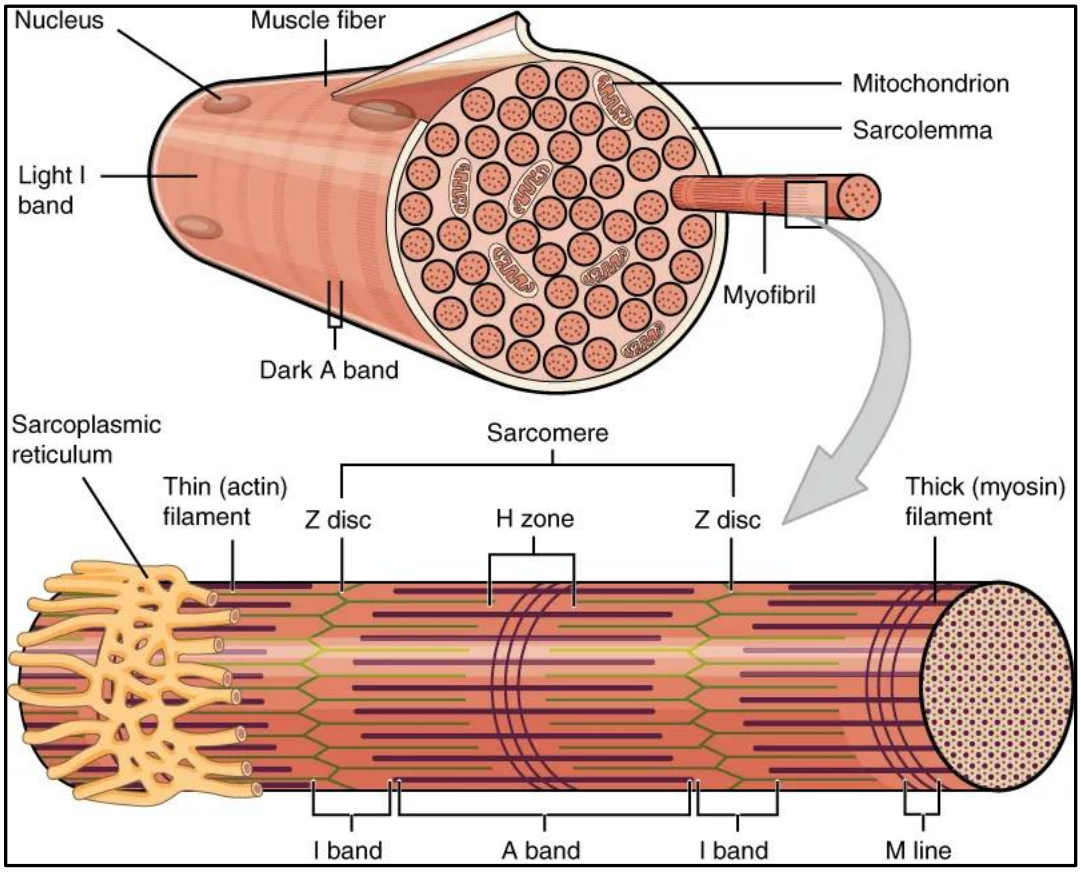

Figure 1. Hierarchical organization of skeletal muscle structure.

Skeletal muscles are made up of multinucleated muscle fibers that are densely packed with myofibrils. Actin (thin) and myosin (thick) filaments are arranged to create repeated sarcomeres, the basic contractile units that make up myofibrils. Muscle contraction is caused by the coordinated sliding of these filaments. Image from Tortora and Derrickson, 2018.

Skeletal muscle performs a range of essential physiological functions that extend beyond voluntary movement. Its major function is to generate force by coordinated contractions, which allows the somatic nervous system to control stability of joints, posture maintenance, and movement (Tortora and Derrickson, 2018). Furthermore, skeletal muscle is a major regulator of

whole-body metabolism, including contributing to the preservation of core body temperature by generating heat (McCullough, Jessu, and Callahan, 2025), a key location for the absorption of glucose, the storage of glycogen, and the oxidation of fatty acids, all of which are critical for preserving energy homeostasis and insulin sensitivity (DeFronzo and Tripathy, 2009; Richter and Hargreaves, 2025). Additionally, myokines secreted by skeletal muscle act as an endocrine organ, modulating immune responses, inflammation, and inter-organ communication, among other systemic processes (Pedersen and Febbraio, 2012; Severinsen and Pedersen, 2020). At the molecular level, the sliding filament mechanism of contraction is driven by the highly organized interaction of actin and myosin filaments within sarcomeres, which is controlled by calcium ions and other proteins like troponin and tropomyosin (Mukund and Subramaniam, 2019; Dave, Shook, and Varacallo, 2023). When taken as a whole, these many functions highlight how vital skeletal muscle is to human wellness and disease as a mechanical and metabolic organ.

1.2 Skeletal Muscle Atrophy: Definition and Clinical Relevance

Skeletal muscle atrophy is a debilitating condition characterized by a loss, shrinking, or decrease in muscle mass, force-generating ability, and cross-sectional areas of the muscle fibers (Figure 2) (Bonaldo and Sandri, 2013; Frontera and Ochala, 2015). This decline is caused by an imbalance between protein synthesis and protein degradation pathways, eventually leading to the loss of myofibril proteins, particularly actin and myosin (Bonaldo and Sandri, 2013; Duan, Gao, and Zhu, 2021). Although sarcopenia, or the loss of muscle mass, is a common aspect of aging, atrophy can also be brought on by several pathological and physiological conditions, such as malnutrition, denervation (nerve injury), chronic illnesses (such as cancer, kidney disease, or heart failure), and particular drugs (such as corticosteroids) (Bonaldo and Sandri, 2013; McCuller, Jessu, and Callahan, 2025)

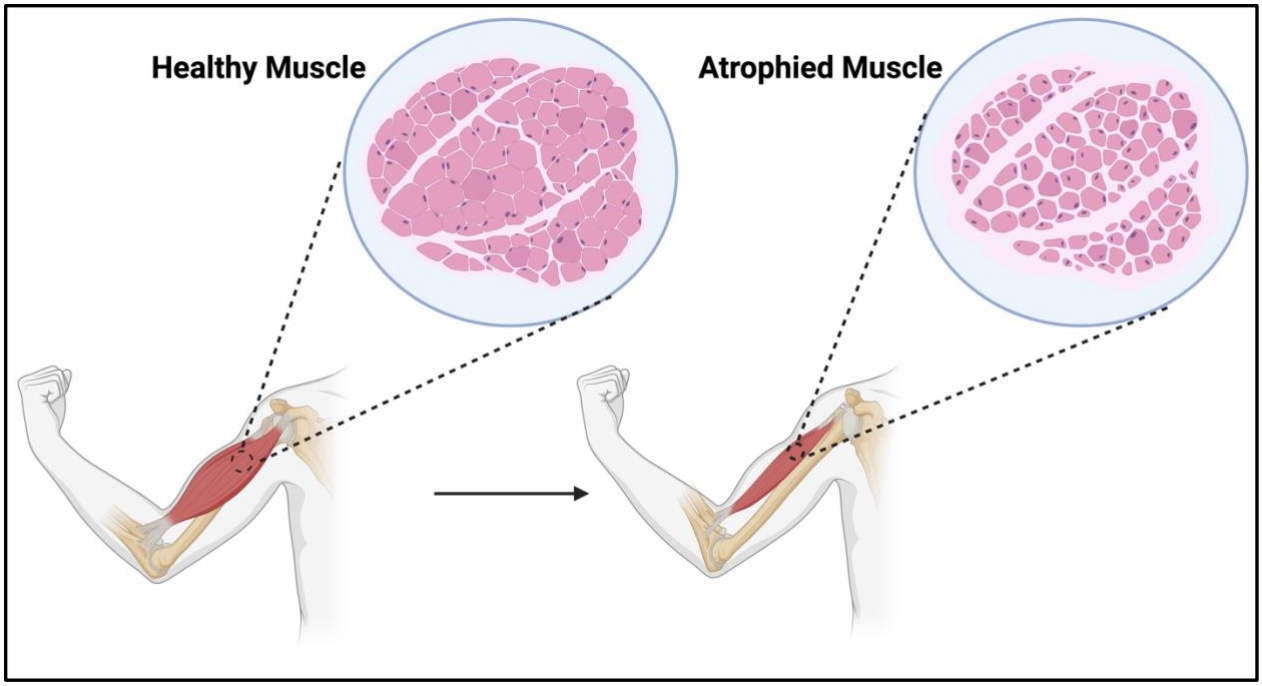

Figure 2. Structural changes associated with skeletal muscle atrophy.

Schematic representation of healthy and atrophied skeletal muscle. In healthy muscle, myofibers are large and densely packed, contributing to normal muscle mass and strength. In contrast, atrophied muscle is characterized by a reduction in myofiber cross-sectional area and increased spacing between fibers, leading to decreased muscle size and functional capacity. Figure created on BioRender.

Skeletal muscle atrophy has substantial and diverse clinical implications, including decreased lifespan, loss of independence, and poor functional ability in a variety of patient populations. (McCuller, Jessu, and Callahan, 2025). Maintaining muscle mass is important for survival and prognosis, as evidenced by studies showing that disorders like cancer cachexia, which involves major muscle wasting, are frequently the direct cause of mortality in afflicted individuals (Schmidt et al., 2018; Nishikawa et al., 2021).

1.3 Molecular Mechanisms Underlying Muscle Atrophy

Skeletal muscle atrophy occurs due to a disruption in muscle protein homeostasis, in which protein degradation surpasses protein synthesis (Bonaldo and Sandri, 2013). This imbalance is caused by inhibition of anabolic signaling pathways like IGF-1/Akt/mTOR and enhanced proteolysis via the ubiquitin-proteasome and autophagy-lysosome systems (Pang et al., 2023; Chen et al., 2025). In addition to being closely controlled by transcription factors like FoxO, these processes are also impacted by oxidative stress, inflammation, and mitochondrial dysfunction (Joshi et al., 2025).

1.3.1 Catabolic Pathways

1.3.1.1 The Ubiquitin-Proteasome System (UPS)

The Ubiquitin-Proteasome System (UPS) is an important process for the selective destruction of most intracellular proteins, including essential contractile and structural proteins in skeletal muscle (Bonaldo and Sandri, 2013; Pang et al., 2023). In muscles, the UPS is necessary for the removal of sarcomeric proteins as muscular activity varies. A reduction in muscle mass is linked to: (1) heightened attachment of ubiquitin to muscle proteins; (2) elevated activity of the ATP-dependent proteasome; (3) increased protein degradation that proteasome blockers can effectively inhibit; and (4) an upsurge in transcripts that code for ubiquitin, certain ubiquitin-conjugating enzymes (E2), some ubiquitin-protein ligases (E3), and several subunits of the proteasome (Figure 3A) (Bonaldo and Sandri, 2013; Sartori et al., 2021; Souza et al., 2025).

In many models of skeletal muscle atrophy, the muscle-specific E3 ubiquitin ligases MuRF1 and Atrogin-1 are transiently upregulated and contribute to increased protein degradation (Bodine and Baehr., 2014; Sartori et al., 2021). These atrogenes are recognized as dependable molecular indicators of muscle loss in scenarios such as disuse, fasting, and various chronic illnesses (Lecker, Goldberg, and Mitch, 2006; Kitajima, Yoshioka, and Suzuki, 2020; Pang et al., 2023). Research has demonstrated that MuRF1 targets crucial myofibrillar proteins, including myosin heavy chains and troponin I, for degradation, whereas Atrogin-1 focuses on regulatory proteins, such as the eukaryotic initiation factor 3 subunit f (eIF3-f) and the muscle regulatory factor MyoD. The elevated expression of these specific E3 ligases directs vital muscle proteins into the UPS pathway, resulting in the loss of muscle mass that characterizes atrophy (Kitajima, Yoshioka, and Suzuki, 2020; Pang et al., 2023).

1.3.1.2 Forkhead Box O (FoxO) Transcription Factors

The FoxO family of transcription factors plays a crucial role as negative regulators of muscle mass, acting as key mediators in the catabolic response during conditions that induce atrophy. The main FoxO isoforms found in skeletal muscle include FoxO1, FoxO3a, and FoxO4, all of which are significant contributors to the process of muscle protein breakdown (Sandri, 2010; Santos et al., 2023; Song et al., 2025). The regulatory activity of FoxO factors is closely

associated with the IGF-1/PI3K/Akt anabolic signaling pathway. Typically, the protein kinase Akt is active and phosphorylates FoxO proteins (Figure 4). This phosphorylation leads to the export of FoxO factors from the nucleus to the cytoplasm, deactivating them and preventing them from facilitating gene transcription (Bonaldo and Sandri, 2013; Permpoon et al., 2025).

The nuclear FoxO factors have two main roles; first is the upregulation of atrogenes - FoxO factors directly promote the expression of muscle-specific E3 ubiquitin ligases, atrogin-1 (MAFbx) and MuRF1 (Bonaldo and Sandri, 2013; Souza et al., 2025; Li et al., 2025). These ligases play an important role in marking myofibrillar proteins for degradation through the UPS. Secondly, is the stimulation of autophagy genes. FoxO3a serves as a strong initiator of genes related to the autophagy-lysosome pathway, such as LC3, GabarapL1, ATG4b, and Bnip3 (Sandri, 2010; Liu et al., 2025). This function promotes the extensive turnover of muscle components.

The synchronized activation of both the UPS and the autophagy mechanisms by FoxO transcription factors highlights their critical function as a molecular switch in regulating muscle protein turnover. The capacity of FoxO factors to transition muscle fibers from an anabolic phase to a catabolic phase makes them an important focus for therapeutic approaches aimed at addressing muscle-wasting conditions.

1.3.1.3 The Autophagy-Lysosome System

Autophagy, which translates to "self-eating," is an essential catabolic mechanism that involves the dynamic breakdown of long-lasting proteins, aggregated proteins, and entire cellular organelles like damaged mitochondria and the sarcoplasmic reticulum (Sandri, 2010; Leduc-Gaudet et al., 2023; Gopal Krishnan et al., 2025). While the UPS is tasked with the quick turnover of individual proteins, the autophagy-lysosome system serves as a key pathway for bulk degradation, critical for maintaining cellular balance, recycling nutrients during periods of starvation, and facilitating the overall remodeling of muscle fibers (Sandri, 2010; Chu et al., 2024).

The autophagy process in skeletal muscle consists of several essential stages: sequestration (autophagosome formation), in which a double-membrane vesicle known as the autophagosome encircles the cellular material intended for degradation; fusion, where the autophagosome subsequently merges with a lysosome, an organelle filled with a powerful array of hydrolytic enzymes; and degradation, during which the contents of the resulting autolysosome are broken down into amino acids, fatty acids, and other fundamental components that the cell recycles to sustain energy balance or build new structures (Figure 3B) (Levine and Kroemer, 2019).

In situations that trigger muscle atrophy such as, denervation, or chronic illness, the rate of autophagic flux (the process of forming and clearing autophagosomes) is generally increased (Bonaldo and Sandri, 2013; Pang et al., 2023; Chen et al., 2025). This elevation is frequently driven by the same signaling pathways that stimulate the UPS, particularly the dephosphorylation of FoxO3 transcription factors, leading to the upregulation of various autophagy-related genes (ATG genes, Bnip3, LC3) (Sandri, 2010; Vainshtein and Sandri, 2020; Permpoon et al., 2025; Liu et al., 2025).

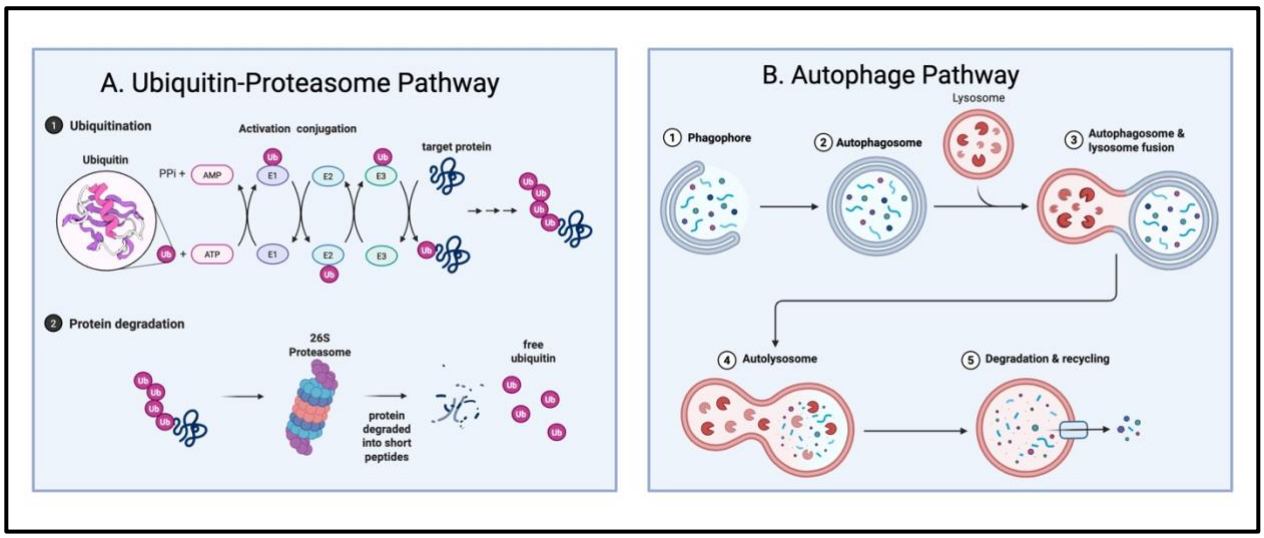

Figure 3. Major catabolic pathways regulating skeletal muscle protein breakdown during atrophy.

(A) The ubiquitin-proteasome system (UPS) facilitates the selective breakdown of myofibrillar proteins via the processes of ubiquitin activation (E1), conjugation (E2), and ligation (E3), which leads to the poly-ubiquitination of target proteins and their subsequent degradation by the 26S proteasome into shorter peptides. (B) The autophagy-lysosome pathway plays a role in the extensive breakdown of cellular constituents through the formation of phagophores, maturation of autophagosomes, fusion with lysosomes, and subsequent recycling of degraded macromolecules. Collectively, these interconnected pathways promote muscle protein degradation and contribute to skeletal muscle atrophy. Created on BioRender.

1.3.2 Anabolic Pathway

1.3.2.1 IGF-1/PI3K/Akt/mTOR Pathway

The main anabolic pathway in skeletal muscle is the IGF-1/PI3K/Akt/mTOR signaling pathway, which is a key regulator of muscle mass (Sandri, 2010; Vainshtein and Sandri, 2020). Under normal physiological circumstances, skeletal muscle mass is maintained by simultaneously promoting protein synthesis and supressing protein degradation. (Vainshtein and Sandri, 2020). This coordinated regulation is accomplished by activating Akt, which inhibits the transcriptional activity of FoxO proteins that cause muscle atrophy while stimulating anabolic signaling via mTOR.

This pathway is activated when IGF-1 binds to its receptor (IGF-1R) located on the surface of muscle cells, leading to a sequence of phosphorylation events (Figure 4) (Rommel et al., 2001; Yoshida and Delafontaine, 2020). This binding event leads to the phosphorylation and activation of downstream proteins, including the lipid kinase phosphatidylinositol-3-kinase (PI3K). Activated PI3K phosphorylates a membrane lipid, PIP_2, to PIP_3, creating a binding site for the kinase Akt (also known as Protein Kinase B). Akt is then recruited to the membrane and activated by other kinases, like PDK1 (Rommel et al., 2001; Yoshida and Delafontaine, 2020). Once activated, Akt phosphorylates several downstream targets including mammalian target of rapamycin (mTOR), and FoxO transcription factors (Figure 4). The activation of mTOR enhances protein synthesis and encourages cell proliferation, while simultaneously hindering processes such as autophagy and protein degradation, which contribute to cell growth and survival (Rommel et al., 2001; Yoshida and Delafontaine, 2020).

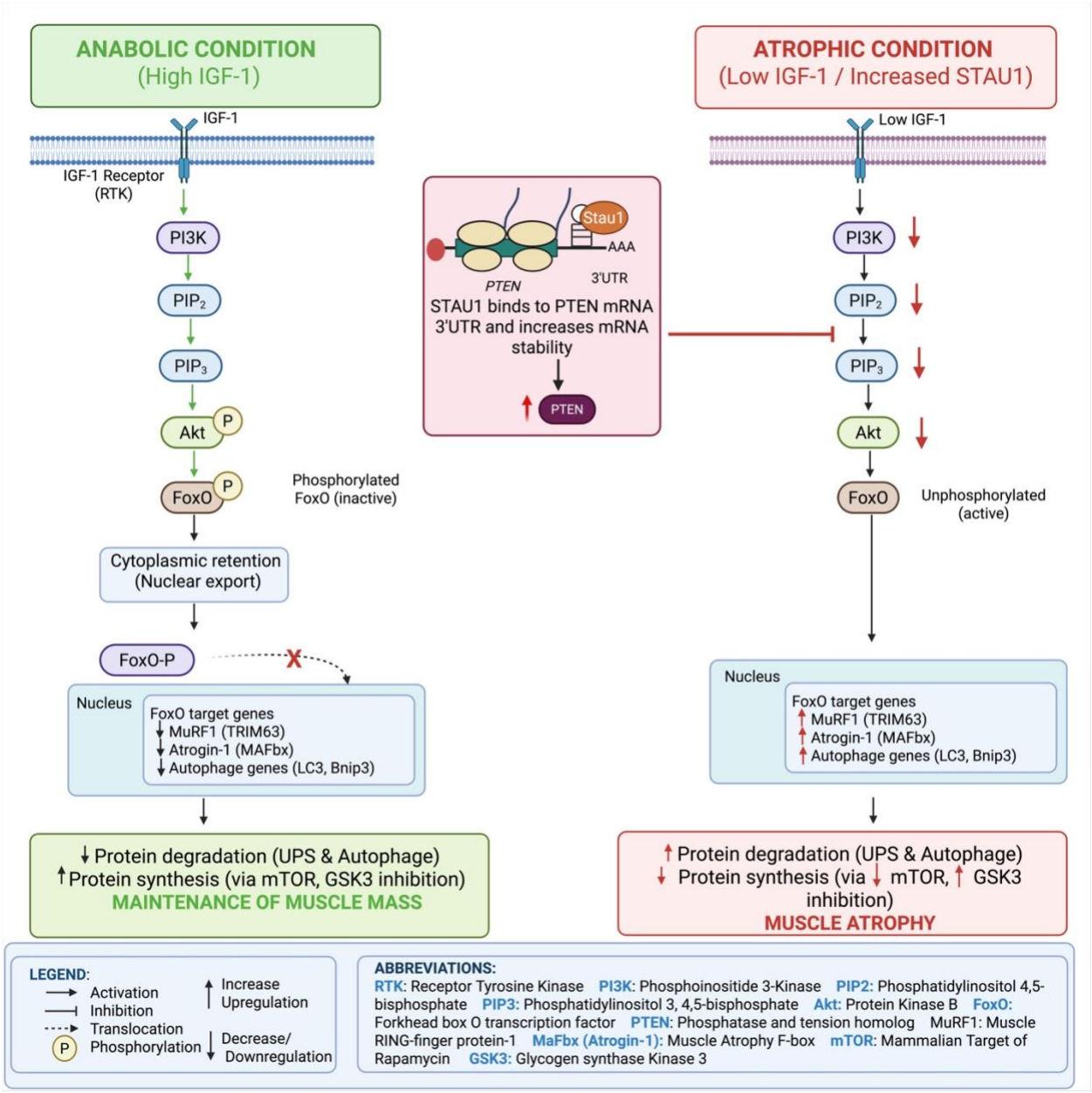

Figure 4. IGF-1/PI3K/AKT/mTOR signaling pathway regulating skeletal muscle mass.

STAU1's potential function in the IGF-1/PI3K/Akt/FoxO signaling cascade during skeletal muscle atrophy. IGF-1 promotes muscle maintenance under anabolic conditions by activating PI3K/Akt signaling, which results in FoxO phosphorylation, cytoplasmic retention, and inhibition of atrophy-related genes. Reduced PI3K/Akt signaling and STAU1-mediated upregulation of PTEN reduce Akt activity during atrophic conditions, which permits unphosphorylated FoxO to translocate to the nucleus and induce the expression of atrogenes, such as MuRF1, Atrogin-1 (MAFbx), and autophagy-related genes, leading to increased muscle atrophy and protein degradation. STAU1's putative PTEN regulation is based on previous research by Parks et al. (2017).

A key feature of this signaling pathway is its ability to coordinate both anabolic and catabolic processes. Members of the Forkhead box O (FoxO) transcription factor family (FoxO1, FoxO3, and FoxO4) are phosphorylated by Akt in anabolic conditions, which causes them to be exported

from the nucleus and retained in the cytoplasm. This phosphorylation-dependent nuclear exclusion suppresses ubiquitin-proteasome and autophagy-lysosome mediated protein degradation by preventing FoxO from activating atrogenes like Fbxo32 (Atrogin-1/MAFbx) and Trim63 (MuRF1), as well as other autophagy-related genes (Figure 4) (Bonaldo and Sandri, 2013; Vainshtein and Sandri, 2020).

Anabolic signaling is reduced in atrophic conditions due to decreased IGF-1 stimulation, which results in decreased FoxO phosphorylation and PI3K/Akt activation. As a result, unphosphorylated FoxO builds up in the nucleus, where it triggers the transcription of genes related to protein degradation mediated by autophagy-lysosome and ubiquitin-proteasome, ultimately causing skeletal muscle atrophy. (Bonaldo and Sandri, 2013; Chen et al 2025; Joshi et al., 2025).

Recent data suggests that STAU1 further influences this signaling network via post-transcriptional regulation of PTEN. STAU1 interacts with the 3′ untranslated region (3′UTR) of PTEN mRNA, therefore increasing its stability and PTEN expression (Parks et al., 2017). Elevated PTEN suppresses Akt activation, allowing FoxO nuclear localization and activation of atrophy-associated genes because PTEN inhibits PI3K signaling by turning PIP3 back to PIP2. During skeletal muscle atrophy, STAU1 serves as an upstream post-transcriptional regulator that connects RNA metabolism with PI3K/Akt/FoxO signaling (Figure 4).

1.4 Therapeutic Strategies and Countermeasures Targeting Skeletal Muscle Atrophy

Considering the significant clinical and societal impact of skeletal muscle atrophy, extensive research endeavors have been directed towards creating therapeutic approaches designed to maintain muscle mass and functionality in various pathological scenarios, such as sarcopenia, immobilization, cachexia, and neuromuscular disorders (Bonaldo and Sandri, 2013; McCullough, Jessu, and Callahan, 2025). Nonetheless, despite these initiatives, no single therapy has shown to be uniformly successful, underscoring the intricate and multifaceted characteristics of muscle loss. Skeletal muscle atrophy, whether resulting from disuse, or disease, continues to

be a significant health concern linked to a higher cost of healthcare and a reduced lifestyle (Sayed et al., 2023; Mao et al., 2025). Its prevalence increases with age and medical conditions, exacerbating chronic illnesses including diabetes, cardiovascular diseases and increased mortality, and frailty (Guenhneau et al., 2018; Nunes et al., 2022). Collectively, these impacts strain health-care systems, reducing the quality of many people, and increase societal expenses due to the loss of productive years and substantial need for medical and social support services.

Various pharmacological strategies have focused on key signaling pathways that play a role in muscle protein turnover (Table 1). The inhibition of the ubiquitin-proteasome system, especially by altering the activity of E3 ubiquitin ligases like muscle RING finger-1 (MuRF1) and muscle atrophy F-box (MAFbx/Atrogin-1), has shown protective effects in preclinical studies (Bodine et al., 2001; Pang et al., 2023). Nonetheless, the extensive involvement of the proteasome in maintaining cellular homeostasis has restricted the practical application of these methods due to the concerns about specificity and potential systemic toxicity. Bimagrumab, a monoclonal antibody that inhibits activin-type II receptors, decreases UPS-mediated protein breakdown and promotes anabolic signaling (Table 1) (Nunn et al., 2024). A study involving older adults indicated that it leads to better preservation of lean mass compared to standard optimized care, emphasizing the potential therapeutic importance of UPS inhibition (Rooks et al., 2020). Likewise, the stimulation of anabolic pathways such as the insulin-like growth factor-1 (IGF-1)/Akt/mTOR signaling axis has been demonstrated to enhance muscle growth and mitigate atrophy in experimental conditions (Schiaffino et al., 2013; Chen et al., 2025; Joshi et al., 2025), but prolonged activation of these pathways could lead to metabolic imbalances and a heightened risk of cancer.

Other pharmacological approaches have targeted the reduction of inflammation and oxidative stress, both of which play a role in muscle wasting associated with chronic diseases. The effectiveness of anti-inflammatory drugs like ibuprofen and the COX-2 inhibitor celecoxib has been evaluated in trials for sarcopenia and cachexia, demonstrating slight preservation of muscle mass but variable functional improvements, likely due to inflammation being just one of several contributing factors (Table 1) (Kubat et al., 2023; Liu et al., 2021; Rolland et al., 2023). Antioxidants including N-acetylcysteine (NAC) and the polyphenol resveratrol are often

mentioned for their ability to scavenge reactive oxygen species and enhance mitochondrial redox status (Cacciatore et al., 2024; Domaniku et al., 2023). Mitochondrial-targeted therapies promote mitophagy, biogenesis, or dynamics (such as urolithin A, and GlyNAC) aim to restore mitochondrial quality control, which is a fundamental defect in sarcopenia and cachexia (Zhang et al., 2025; Broome et al., 2024). Overall, all these regimens have been inconsistent, influenced by the specific causes of muscle atrophy (Bonetto et al., 2009; Powers et al., 2016).

Nutritional and nutraceutical strategies have been widely explored as accessible countermeasures to muscle loss (Table 1). Supplementing with essential amino acids, especially leucine, has demonstrated the ability to promote muscle protein synthesis, particularly in older adults and during periods of disuse (Phillips and Van Loon, 2011). Coenzyme Q10 supplementation has shown potential in mitigating exercise-related oxidative damage and may assist in muscle recovery among older adults (Qu H. and Qu Y. 2025). Additional substances, such as creatine, omega-3 fatty acids, and vitamin D, have shown slight advantages in promoting muscle mass and performance (Smith et al., 2011; Wall et al., 2013; Zhang et al., 2025). Nonetheless, these interventions by themselves are typically inadequate to stop muscle loss in severe atrophy models and frequently necessitate combination with other therapeutic or mechanical stimuli.

Non-pharmacological countermeasures, including resistance training (Table 1) consistently increases muscle mass, strength, and functional capabilities in patients with sarcopenia and those hospitalized, and even low-volume “minimal-dose” regimens can be beneficial for frail individuals (Sanchez et al., 2025; Sharma et al., 2023; Fyfe et al., 2022). Aerobic or physical activity including regular walking, cycling, or programs that are involved in enhancing muscle quality and overall physical function, particularly when integrated with resistance exercises, which can help preserve muscle mass and strength (Gonzalez et al., 2022; Govindasamy et al., 2025). Synergistic outcomes occur when resistance training is combined with protein or amino-acid supplementation, leading to greater increases in lean mass and strength (Hu et al., 2024; Lim et al., 2022). Gut-microbiome approaches including probiotics and prebiotics may modulate inflammation and muscle metabolism, representing emerging supplements to classic exercise-nutrition regimens (Hu et al., 2024). However, their use is restricted in clinical situations that involve immobilization, denervation, or critical illness, where voluntary muscle

activation is impaired. This constraint highlights the necessity for molecularly targeted treatments that can maintain muscle integrity regardless of mechanical stimulus.

Table 1: Therapeutic Strategies Targeting Skeletal Muscle Atrophy

Category	Intervention	Mechanism of Action	Outcome	Reference
Pharmacological	Bimagrumab (anti-ActRII)	Inhibits myostatin/activin signaling → ↑ muscle growth, ↓ protein degradation	↑ lean mass; variable functional improvement	Rooks et al., 2017
	mTOR modulators (e.g., sirolimus)	Regulates protein synthesis and autophagy via mTORC1 inhibition	Improved muscle function	Harrison et al., 2009
	Anti-inflammatory drugs (NSAIDs, COX-2 inhibitors)	↓ chronic inflammation contributing to muscle wasting	Modest preservation of muscle mass	Rolland et al., 2023
	Mitochondrial-targeted therapies (e.g., urolithin A)	↑ mitophagy, mitochondrial biogenesis	Improved muscle endurance and mitochondrial health	Singh et al., 2022
Nutritional / Nutraceutical (non-pharmacological)	Amino acids (leucine)	↑ muscle protein synthesis via mTOR activation	Effective in older adults and disuse conditions	Phillips and Van Loon, 2013
	Creatine	↑ ATP availability; supports muscle performance	Modest gains in strength and lean mass	Zhang et al., 2025
	Omega-3 fatty acids	Anti-inflammatory; enhances anabolic sensitivity	May improve muscle mass and function	Smith et al., 2011
	Coenzyme Q10	Supports mitochondrial function and redox balance	May aid recovery in older adults	Qu H. and Qu Y, 2025

Lifestyle / non-pharmacological	Resistance training	↑ muscle protein synthesis; activates mTOR	effective intervention for muscle mass and strength naturally	Lan, Caini, and Wei, 2026
	Aerobic exercise	Improves mitochondrial function and endurance	Enhances muscle quality and metabolic health	González-Rocha et al., 2022
	Combined exercise + nutrition	Synergistic effect on hypertrophy and strength	Greater gains than either intervention alone	Hu et al., 2024; Lim et al., 2022

1.5 RNA-Binding Proteins and Post-Transcriptional Regulation of Atrophy

Skeletal muscle atrophy is characterized by significant post-transcriptional regulations, and increasing evidence highlights the role of RNA-binding proteins (RBPs) as key regulators of these adaptive mechanisms. Multiple RBPs have been associated with the control of skeletal muscle atrophy by influencing mRNA stability, splicing, localization, and translation (Gebauer et al., 2021; Sun et al., 2025). The RBP Human antigen R (HuR) (ELAVL1) attaches to AU-rich sequences in the 3′ untranslated regions of target mRNAs and enhances the stability of mRNAs (Figure 5) related to atrophy signaling, including those regulated by FoxO, like Atrogin-1 and MuRF1 (Acharyya et al., 2004; Dormoy-Raclet et al., 2007; Mynatt et al., 2019). TDP-43 (TARDBP) is linked to the dynamics of stress granules and has been found in cytoplasmic aggregates within denervated or affected muscle, where its misregulation impairs RNA processing and leads to muscle pathology (Colombrita et al., 2009; Weihl et al., 2008). The splicing regulator CUG-binding protein 1 (CUGBP1/CELF1) is increased in atrophic environments and myotonic dystrophy, where it modifies alternative splicing and mRNA degradation of muscle-specific transcripts, thus facilitating atrophic gene expression programs (Timchenko et al., 2001; Cox et al., 2020).

Poly(A)-binding protein nuclear 1 (PABPN1) decreases with aging, and its slight knockdown in the tibialis anterior muscle of mice initiates myofiber atrophy, extracellular matrix remodeling,

and a transition to fast-type fibers, primarily due to diminished distal-PAS usage that increases the expression of the atrogenic factor Atrogin-1 (Riaz et al., 2016). The N6-methyladenosine (m^6A) reader YTHDF2 regulates post-transcriptional proteostasis; deleting YTHDF2 specifically in skeletal muscle shortens muscle fibers and reduces strength by disrupting the ubiquitin ligase ASB2 and subsequent SMAD3 signaling, highlighting its crucial role in preserving muscle mass (Figure 5) (Gilbert et al., 2024). Broad examinations of RBPs highlight their ability to influence translation and the dynamics of stress granules amid catabolic stress, with proteins like Fragile X mental retardation protein (FMRP) and cytoplasmic poly(A)-binding protein (PABP) modifying ribosome recruitment and shielding mRNAs from breakdown (Shi and Grifone, 2021). IGF2BP2 interacts with growth-associated transcripts to stimulate anabolic signaling (Liu et al., 2025), whereas the cold-shock protein RBM3 improves overall translation and provides defense against atrophy caused by disuse (Van Pelt et al., 2018) both have been noted to reduce muscle loss in experimental studies. Collectively, these RBPs illustrate that the disruption of RNA processing and post-transcriptional regulation is a key aspect of muscle atrophy, working in conjunction with proteolytic mechanisms like the ubiquitin-proteasome and autophagy pathways offering multiple therapeutic entry points for combating muscle wasting.

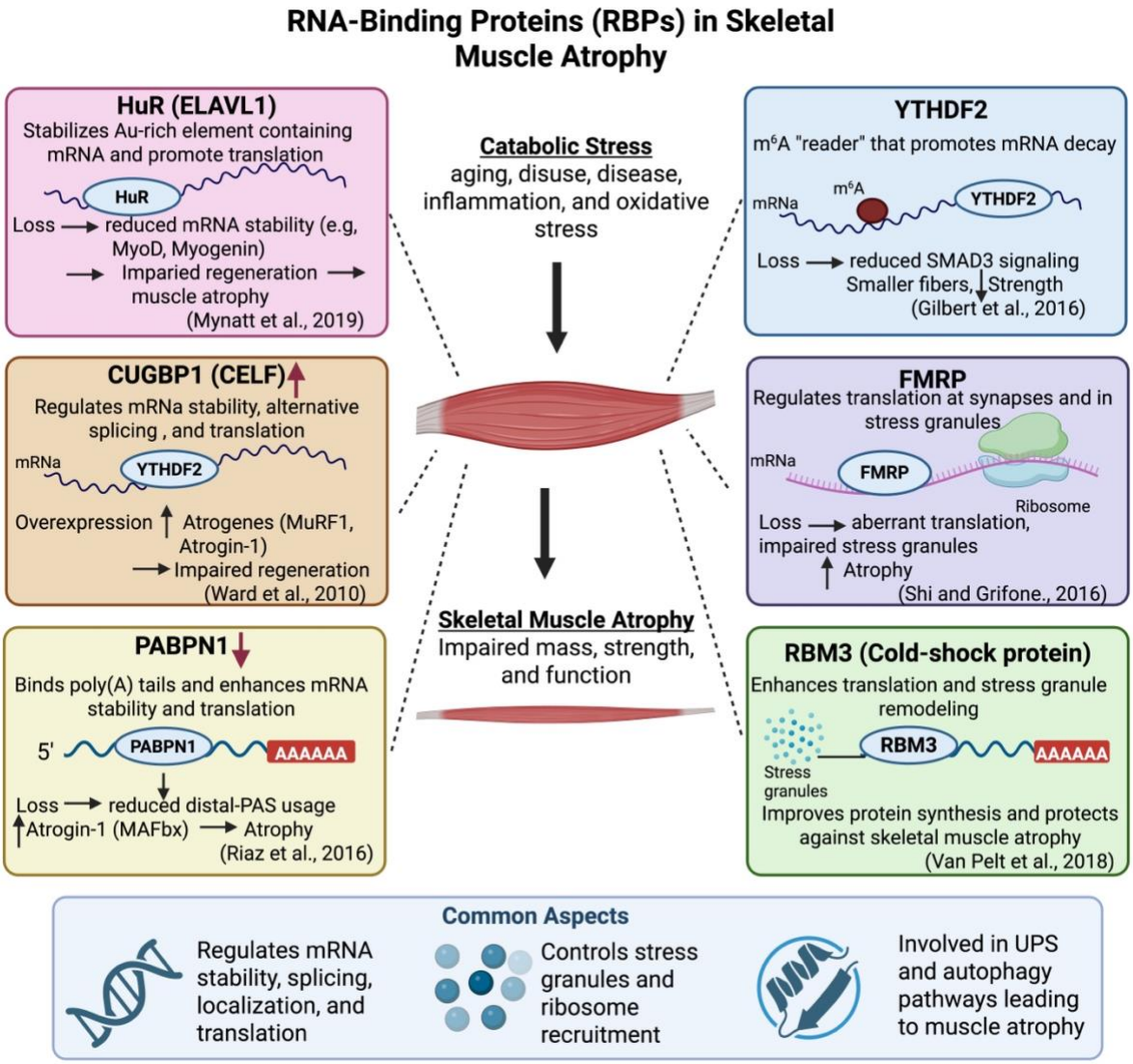

Figure 5. Schematic illustration of RNA-binding proteins (RBPs) implicated in skeletal muscle atrophy.

Through their interactions with the ubiquitin-proteasome and autophagy pathways, RBPs control mRNA stability, translation, and stress granule dynamics, which in turn affects proteostasis and muscle mass. Created on BioRender.

1.6 The RNA Binding Protein Staufen1 (STAU1)

Staufen1 (STAU1) is a double-stranded RNA-binding protein (dsRBP) that functions as a versatile post-transcriptional regulator of gene expression, participating in multiple RNA metabolisms. Initially identified in Drosophila for its role in mRNA localization during early embryonic development. The mammalian homologs STAU1 and STAU2 have also been shown to be involved in mRNA transport, localization, translation, and decay in various cell types, including muscle cells, which support myogenic differentiation and stress responses; neurons,

which regulate dendritic mRNA transport; and epithelial cells, which play an essential part in mRNA decay pathways. (Wickham et al., 1999; Kiebler et al., 1999; Duchaine et al., 2002; and Ravel-Chapuis et al., 2012). Building on these foundational bases, STAU1 has now been recognized as an important modulator of cellular homeostasis across a variety of tissues, including its novel roles in controlling stress responses, alternative splicing and disease-associated pathways (Marcellus et al., 2021; Zhang et al., 2025).

1.6.1 Staufen Proteins: Structure, Isoforms, and Tissue Expression

The human STAU1 gene generates various splice variants, with STAU1^{55} and STAU1^{63} being the primary isoforms named based on their estimated molecular weights (~55 kDa and ~63 kDa) (Figure 6) (Almasi and Jasmin, 2021). STAU1^{55} and STAU1^{63} arise from one STAU1 gene via alternative splicing of the identical pre-mRNA, instead of being produced from distinct genes or through post-translational cleavage (Bondy-Chorney et al., 2016; Almasi and Jasmin, 2021). Following transcription, the STAU1 pre-mRNA undergoes processing by the spliceosome in the nucleus, with the presence or absence of an extra N-terminal exon dictating which isoform is generated. Omitting this exon results in a shorter mRNA transcript, which is translated into the approximately 55 kDa STAU1^{55} protein, while the inclusion of this exon allows for a longer transcript that encodes an extended N-terminal region, leading to the approximately 63 kDa STAU1^{63} isoform (Wickham et al., 1999; Quesada and DesGroseillers, 2022). Both isoforms keep the conserved double-stranded RNA-binding domains (dsRBDs) and tubulin-binding domain, indicating that their essential RNA-binding and transport roles are maintained, while the N-terminal extension in STAU1^{63} might affect subcellular localization or interaction dynamics (Wickham et al., 1999; Quesada and DesGroseillers, 2022). Among the identified STAU1 isoforms, STAU1^{55} is the most prominent and thoroughly examined variant in existing research. In comparison, STAU1^{63} is less abundant and is still relatively underexplored, with limited research investigating its functional roles. Consequently, the present knowledge of STAU1's role in muscle and disease scenarios is mainly based on studies of the STAU1^{55} variant (Kim et al., 2005; Park et al., 2013).

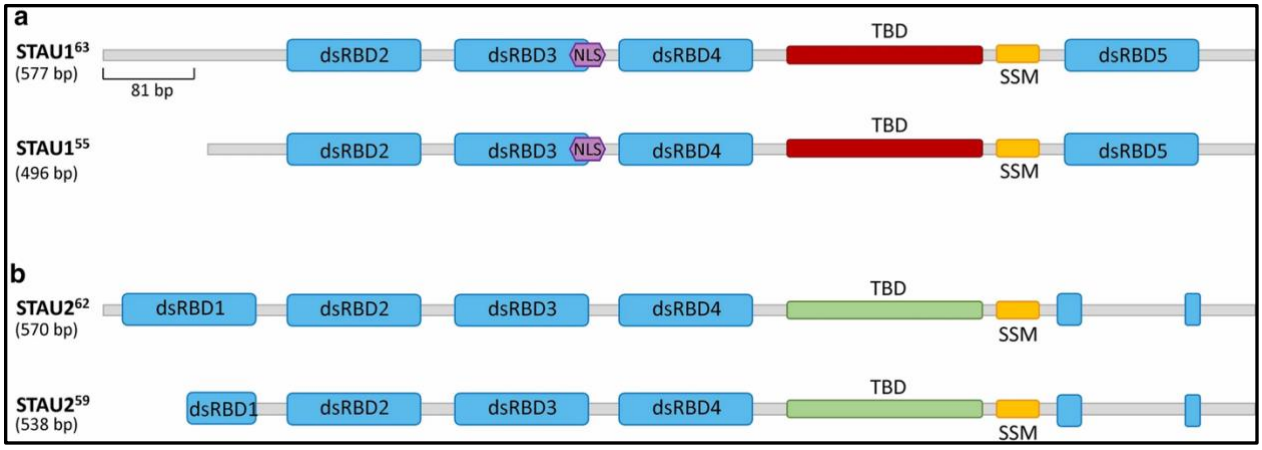

Figure 6. Schematic representation of STAU1 and STAU2 Isoforms.

a and b - each variant include the double-stranded RNA-binding domains (dsRBDs) (light blue boxes), the nuclear localization signal (NLS) (purple), the tubulin binding domain (TBD) (red and green), and the identified Staufen-swapping motif (SSM) (yellow). Even with significant sequence similarity in the dsRBDs of STAU1 and STAU2, the TBD motifs of the two proteins show considerable sequence differences (indicated in various colors, red and green). The C-terminal region shows variation across various splicing variants of each STAU protein. Image adapted from Almasi and Jasmin, 2021.

In skeletal muscle, STAU1 is present in myoblasts and myofibers and governs transcripts related to differentiation, stress responses, and muscle homeostasis, with its dysregulation associated with atrophy and myogenic abnormalities (Ravel-Chapuis et al., 2014; Dugré-Brisson et al., 2016; Parks et al., 2017). Additionally, STAU1 has been demonstrated to affect myogenic development in C2C12 myoblasts, where its depletion promotes differentiation and modifies the expression of genes specific to muscles, underscoring its regulatory function in myogenesis (Yamaguchi et al., 2008; Almasi and Jasmin, 2021). Beyond skeletal muscle, STAU1 is extensively expressed in the central nervous system, where it is essential for localized translation and neuronal mRNA transport, especially in dendrites, supporting synaptic function and neuronal development (Vessey et al., 2012; Kiebler et al., 1999). Detectable levels of STAU1 are also found in the heart, where it plays a role in RNA regulatory networks that affect cardiomyocyte function (Vessey et al., 2012). Moderate expression is noted in metabolically active tissues like the liver and kidney, indicating a wider function in post-transcriptional gene regulation (Duchaine et al., 2002). Furthermore, STAU1 expression in germ cells, such as the testis and ovary, indicates a role in the regulation of developmental mRNA (Wickham et al., 1999). These patterns are maintained in mice, with STAU1 mRNA and protein identified throughout the brain, skeletal muscle, heart, liver, kidney, and reproductive tissues, emphasising both extensive and tissue-specific roles (Duchaine et al., 2002; Ravel-Chapuis et al., 2012)

STAU1 possesses a conserved molecular structure defined by several dsRBDs that tend to engage with structured RNA features instead of sequences (Kim et al., 2005). In STAU1, these domains include functionally distinct dsRBDs and have protein-interaction domains that promote the formation of messenger ribonucleoprotein (mRNP) complexes and engage with cytoskeletal elements, allowing for intracellular RNA transport (Doyle and Kiebler, 2011; Lazzaretti et al., 2018). Apart from these conventional domains, STAU1 has regions that promote its multifunctional role in post-transcriptional regulation by facilitating interactions with decay factors and translation machinery (Quesada and DesGroseillers, 2022). Given their structural arrangement, STAU1 proteins can function as molecular scaffolds that connect RNA activity to a variety of regulatory pathways, such as Staufen-mediated mRNA decay (SMD), which interacts with the nonsense-mediated decay machinery to selectively degrade target transcripts (Park and Maquat, 2013). Recent studies have demonstrated that STAU1 undergoes liquid-liquid phase separation (LLPS), creating dynamic cytoplasmic condensates that attract mRNAs and translation factors, thereby regulating protein synthesis (Zhao et al., 2024). The dysregulation of this process can result in aberrant activation of pathways like mTOR signaling and compromised autophagy (Park and Maquat, 2013; Zhao et al., 2024).

STAU2 exhibits considerable structural similarity to STAU1, featuring several dsRBDs and preserved interaction motifs, although its expression and role are more prevalent in the nervous system. Multiple STAU2 splice variants (e.g., STAU2^{59}, STAU2^{62}) are generated through alternative splicing, influencing regulatory components while maintaining essential RNA-binding function (Figure 6b) (Kiebler et al., 1999; Wickham et al., 1999). STAU2 shows high expression in the brain, where it governs dendritic mRNA transport and synaptic plasticity processes critical for learning and memory (Kiebler et al., 1999; Heraud-Farlow et al., 2013). Its function in neurons emphasizes the significance of RNA positioning and localized translation in specialized cells with intricate structure. STAU2 is widely expressed in other tissues outside of the brain system, such as the heart, lung, kidney, and reproductive organs, suggesting a more widespread function in RNA metabolism (GeneCards; Human Protein Atlas). STAU2 is also found in skeletal muscle, where transcriptome and proteomic data show its existence in myocytes, suggesting possible participation in muscle RNA regulation, despite its expression

being lower compared to neural tissues (Human Protein Atlas). Research has showed the presence of STAU1 and STAU2 in skeletal muscle, indicating a conserved function in post-transcriptional regulation and RNA transport in muscle cells (Bélanger et al., 2003).

1.6.2 Functional Roles of Staufen1 in RNA Metabolism

STAU1 protein regulates multiple stages of mRNA metabolism, including splicing, transport, translation, and decay. These functions are mediated through STAU1 recognition of Staufen1-binding sites (SBSs) double-stranded RNA secondary structures typically located within the 3′ untranslated region (3′ UTR) of target mRNAs (Almasi and Jasmin, 2021; Chakrabarti et al., 2023). Because STAU1 may bind double-stranded RNA structures created by inverted repeat elements, especially Alu sequences inside intronic regions, it has become a significant regulator of alternative splicing. By serving as platforms for STAU1 binding, these structured RNA fragments might impact exon inclusion and splice site selection. By interfering with adjacent splicing silencers and improving the detection of neighboring splice sites, STAU1 binding to intronic Alu elements encourages exon inclusion (Figure 7a) (Lee et al., 2024). STAU1 recruits or excludes splicing factors and stabilizes RNA secondary structures to affect the ratio of splicing enhancers to silencers. Exon inclusion events in several transcripts have been demonstrated to be impacted by this regulatory activity, indicating a more extensive involvement for STAU1 in coordinating RNA processing beyond its well-established roles in mRNA transport and decay (Ravel-Chapuis et al., 2012; Bondy-Chorney et al., 2016; Almasi and Jasmin, 2021; Jiang et al., 2023)

Upon binding, STAU1 stabilizes these RNA structures and forms ribonucleoprotein (RNP) complexes that associate with the cytoskeleton. STAU1 acts as a molecular adaptor between mRNA cargo and motor proteins. Components such as dynein intermediate chain and kinesin heavy chain have been identified in STAU1-containing RNP complexes, supporting its role in recruiting motor proteins to facilitate directional mRNA transport along microtubules (Figure 7b) (Donaldson and Jackson, 2000; Doyle and Kiebler, 2011; and Almasi and Jasmin, 2021). Through this mechanism, STAU1 enables the delivery of transcripts to specific subcellular locations where localized protein synthesis is required.

Beyond its role in transport, STAU1 actively promotes mRNA translation. STAU1 has been shown to associate with actively translating ribosomes and influence translation through interactions with both the 3′ UTR and, in some cases, the 5′ UTR of target mRNAs (Kim et al., 2005; Almasi and Jasmin, 2021). A requirement for a 5′ UTR SBS in STAU1-mediated translation activation has been observed in mammalian cells, suggesting that STAU1 can facilitate efficient translation initiation (Ricci et al., 2014). Additionally, more recent research demonstrates that STAU1 can boost translation by forming RNA-protein condensates through LLPS, which attract target mRNAs and translation machinery to improve protein synthesis (Zhao et al., 2024). Additionally, STAU1 localization to the rough endoplasmic reticulum (RER) indicates that it contributes to directing mRNAs to sites of active translation, enhancing ribosomal engagement and protein synthesis (Wickham et al., 1999; Luo, Duchaine, and DesGroseillers, 2002; Brendal et al., 2004). Through this function, STAU1 contributes to processes requiring rapid and localized protein reduction, such as neuronal plasticity, muscle maintenance, and cellular stress responses (Figure 5c) (Wickham et al., 1999; Bonnet-Magnaval et al., 2016).

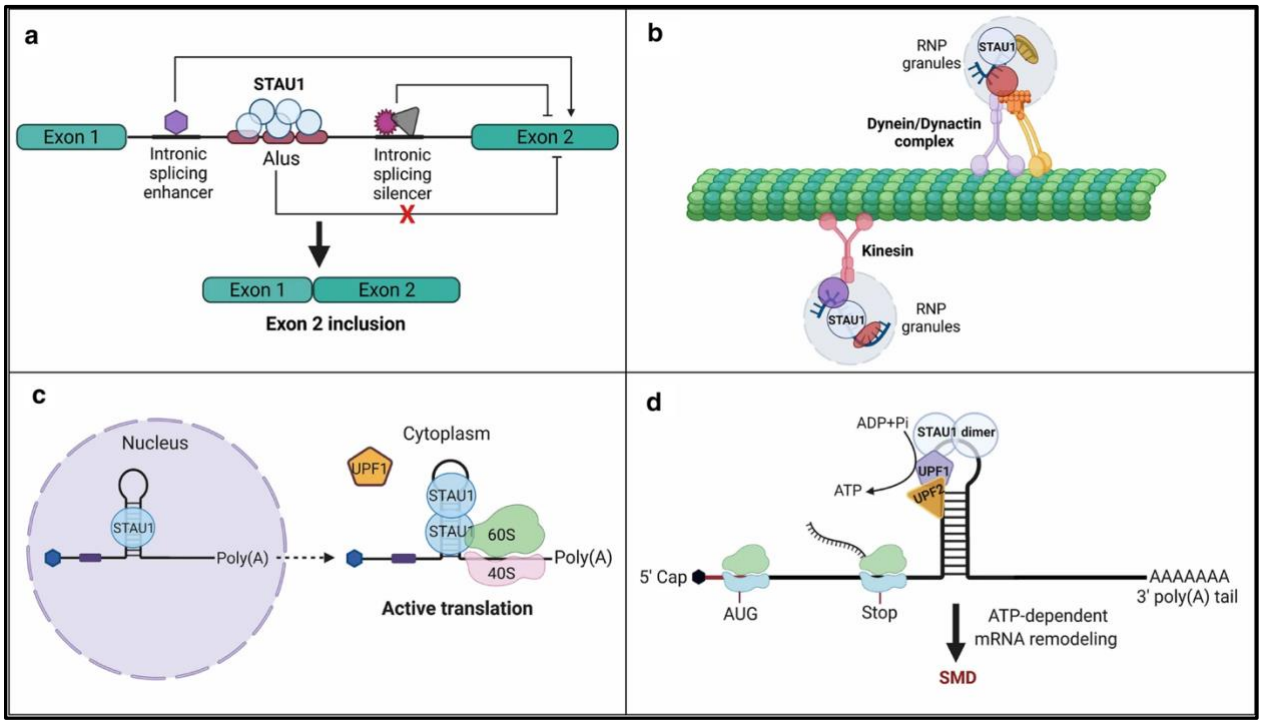

Figure 7. Role of Staufen1 in RNA Metabolism.

STAU1 regulates multiple aspects of RNA metabolism by binding to target mRNAs. **(a)** Alternative splicing events are regulated by STAU1 binding to SBS (such as Alu repeats) present in target mRNAs. **(b)** STAU1 interacts

directly with cis-acting motifs or localization signals in the 3'UTR of target mRNAs, facilitating the recruitment of motor proteins like dynein and kinesin. These proteins enable the active transport of mRNAs along the cytoskeletal network to specific subcellular locations. **(c)** STAU1 binding to both mRNAs and ribosomes enhance mRNA translation. **(d)** In STAU1-mediated mRNA decay (SMD), STAU1 binds to the STAU1-binding site (SBS) located in the 3'UTR, downstream of the stop codon, and recruits the UPF1 and UPF2 helicases, ultimately triggering mRNA degradation. Image from Almasi and Jasmin, 2021.

STAU1 also regulates mRNA turnover through SMD. In this pathway, STAU1 binds to an SBS located in the 3′ UTR downstream of the stop codon and recruits the RNA helicases UPF1 and UPF2, components also involved in nonsense-mediated decay (NMD) (Kim et al., 2005: Park and Maquat, 2014). The recruitment of UPF proteins initiates selective degradation of the bound transcript (Figure 7d). This process allows the cell to meticulously regulate gene expression by removing unnecessary or aberrant mRNAs and adjusting transcript levels in response to cellular conditions.

1.6.3 Role of STAU1 in Skeletal Muscle

As shown in Figure 7, STAU1 regulates RNA metabolism through its binding to cis-acting elements in 3′-UTRs, consequently regulating mRNA transport, increasing translation, and initiating SMD, which establishes the molecular framework for its roles in skeletal muscle development (Park and Maquat, 2013). In mouse skeletal muscle, STAU1 is present in high quantities during embryonic development but decreases significantly in mature fibers, a trend that is also observed after injury induced by cardiotoxin, suggesting its role in muscle regeneration (Ravel-Chapuis et al., 2014). Immunofluorescence studies indicate that STAU1 accumulates at the postsynaptic sarcoplasm of the neuromuscular junction, exhibiting increased levels in slow-twitch muscles and being up-regulated during myogenic differentiation, which implies its participation in the maturation of the junction (Belanger et al., 2003). Furthermore, STAU1 expression is also elevated during synaptic remodeling and following muscle denervation, suggesting a function in neuromuscular plasticity and repair mechanisms (Belanger et al., 2003; Kim et al., 2005; and Parks et al., 2017). From a mechanistic perspective, STAU1 attaches to the 3′-UTR of MyoD mRNA in resting muscle stem cells, inhibiting its translation and thus preserving satellite-cell quiescence; the removal of this inhibition allows for MyoD protein production, leading to cell-cycle entry and activation (Gan et al., 2017). On the other hand, the enforced overexpression of STAU1 in C2C12 myoblasts hinders differentiation, lowering levels of MyoD, myogenin, and MEF2A/C, while raising c-Myc translation, which

interferes with the myogenic program (Ravel-Chapuis et al., 2014). Collectively, STAU1 acts as a post-transcriptional regulator that maintains the equilibrium between stem-cell quiescence and differentiation, directing the processes of skeletal muscle formation and repair. Importantly, aberrant STAU1 expression also plays a role in muscle disorders like myotonic dystrophy type 1 and rhabdomyosarcoma, which are discussed next.

Myotonic Dystrophy Type 1 (DM1) is a neuromuscular disorder affecting multiple systems, resulting from an expanded CTG repeat in the DMPK gene, which causes extensive RNA toxicity and disruption of RNA-binding proteins (Lo Scrudato et al., 2019). STAU1 contributes to disease-associated RNA dysregulation in the skeletal muscle of individuals with DM1 and similar animal models where it is markedly elevated (Ravel-Chapuis et al., 2012; Bondy-Chorney et al., 2016). In this situation, STAU1 directly interacts with CUG-expanded DMPK mRNAs, increasing their nuclear export and improving their translation, which exacerbates downstream RNA metabolism abnormalities and encourages the buildup of hazardous RNA species (Ravel-Chapuis et al., 2012; Bondy-Chorney et al., 2016). STAU1 functions as a disease modifier that may either partially rescue or further disrupt splicing anomalies depending on the target mRNA. It also controls alternative splicing of numerous transcripts in addition to its role in RNA export and translation (Bondy-Chorney et al., 2016). Together, these results demonstrate the complex role of STAU1 in DM1 pathophysiology, connecting muscle weakness to changes in RNA processing, translation, and splicing.

Rhabdomyosarcoma (RMS) is a pediatric soft tissue sarcoma marked by dysfunctional myogenic differentiation and uncontrolled growth of muscle progenitor cells (Keller and Guttridge, 2013). STAU1 has been associated with RMS due to its role in controlling mRNA translation and the stability of transcripts that play a part in cell growth and differentiation (Parks et al., 2017; Marcellus et al., 2021). Increased STAU1 expression has been detected in RMS cells, facilitating proliferation and hindering myogenic differentiation by influencing the translation of vital regulatory mRNAs (Parks et al., 2017; Almasi et al., 2023). On the other hand, in RMS models, lowering STAU1 levels reduces tumor cell proliferation and partially restores differentiation ability, suggesting that STAU1 plays a role in maintaining the malignant phenotype (Parks et al., 2017). Together, these results demonstrate how STAU1 dysregulation significantly impacts

decisions about the fate of muscle cells and emphasize its wider function as a regulator of muscle homeostasis and disease (Marcellus et al., 2021; Almasi et al., 2023; Chakrabarti et al., 2023).

1.7 Staufen1 as a Potential Atrogene and its Regulation in Muscle Atrophy

The conventional view of skeletal muscle atrophy primarily focuses on well-known "atrogenes," like the E3 ubiquitin ligases atrogin-1 and MuRF1, whose increased activity is a common characteristic of conditions that lead to muscle wasting (McKinnell and Rudnicki, 2004; Parks et al., 2017). However, research from our lab has uncovered an additional regulatory factor that play a role in the molecular processes governing muscle mass. Staufen1 has been suggested as a non-canonical or potential "atrogene" because it can trigger atrophy when its regulation is disrupted (Parks et al., 2017). Research utilizing mouse models from our lab has shown that muscle-specific overexpression of STAU1 results in progressive muscle wasting and a myopathy phenotype (Parks et al., 2017).

As shown in figure 8, STAU1 leads to skeletal muscle atrophy through coordinated modulation of translational control and important signaling pathways that regulate protein homeostasis. STAU1 promotes transcriptional pathways related to muscle cell development and metabolism by increasing the translation of target mRNAs including c-myc (Figure 8A) (Kaur et al., 2013; Parks et al., 2017). STAU1 links RNA-binding activity to downstream signaling pathways via controlling Phosphatase and tension homolog (PTEN) expression at the transcriptional level (Figure 8B) (Furic et al., 2008; Sugimoto et al., 2015; Parks et al., 2017). In Figure 8C, STAU1 increases the production of ubiquitin ligases such as MAFbx/Atrogin-1 and MuRF1 by promoting the activation of atrogenes through FoxO3a-dependent transcription (Sandri, 2010; Parks et al., 2017; Yoshida and Delafontaine, 2020). STAU1 binds to the 3′UTR of PTEN mRNA at the post-transcriptional level, improving its translation and raising PTEN protein levels (Figure 8D) (Parks et al., 2017; Kim et al., 2005). Elevated PTEN inhibits the PI3K/AKT signaling pathway, as seen in Figure 8E. This leads to lower mTOR activity and AKT phosphorylation, both of which reduce protein synthesis while increasing FoxO3a activation and protein degradation (Parks et al., 2017; Schiaffino et al., 2013). When taken as a whole, these

processes shift the balance in favor of more proteolysis and less anabolic signaling, which eventually causes skeletal muscle atrophy.

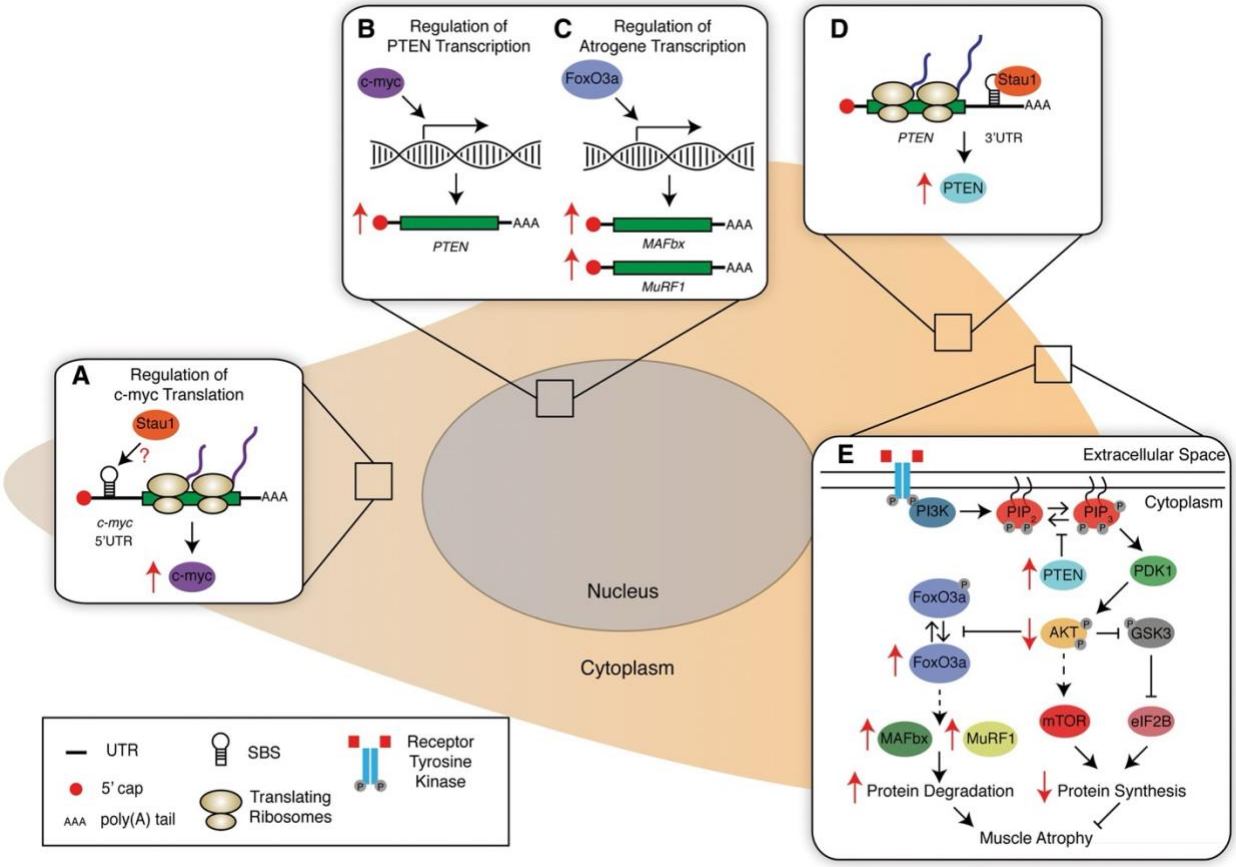

Figure 8. Proposed Mechanism of Staufen1 in Skeletal Muscle Atrophy.

Staufen1 drives skeletal muscle atrophy through a combination of interconnected cellular processes. **(A)** It facilitates c-myc translation via interactions with the 5'UTR. **(B)** The resulting increase in c-myc expression leads to the upregulation of PTEN transcription, while **(C)** FoxO3a controls the transcription of MAFbx and MuRF1, key regulators of muscle degradation. **(D)** Additionally, Staufen1 post-transcriptionally modulates PTEN mRNA stability through the 3'UTR, **(E)** further elevating PTEN expression, which in turn inhibits the PI3K/AKT signaling pathway. Together, these Staufen1-driven mechanisms enhance protein degradation and suppress protein synthesis, ultimately leading to skeletal muscle atrophy. Figure from Parks et al., 2017.

Collectively, these interrelated mechanisms illustrate that STAU1 could act as an upstream RNA-binding regulator that converges on the primary anabolic-catabolic switch regulating muscle mass. STAU1 promotes skeletal muscle atrophy by integrating post-transcriptional regulation with canonical signaling pathways through the increase of PTEN expression, stimulation of FoxO transcriptional activity, and control of mRNA metabolism.

1.8 Preliminary Findings from Our Laboratory

1.8.1 Experimental Models of Skeletal Muscle Atrophy

Skeletal muscle atrophy has been studied using a variety of experimental models, including in vitro systems, animal models, and human studies, all which capture various components of muscle loss. In vitro models (Table 2), C2C12 myoblasts and differentiated myotubes are often studied for cellular processes of atrophy under normal conditions. Atrophy can be triggered by glucocorticoid treatment, nutrient or serum deprivation, or inflammatory conditions, activating proteolytic pathways and inhibition of anabolic signaling (Sandri, 2013; Schiaffino et al., 2013; Li et al., 2023). Animal models based on disuse, including immobilization and hindlimb unloading, simulate mechanical unloading and decreased contractile activity, which leads to a reduction in protein synthesis and an increase in proteolysis (Table 2) (Morey-Holton and Globus, 2002; Dirks et al., 2016). Denervation-induced atrophy is characterized by rapid muscle shrinkage and the activation of catabolic pathways which serve as a model of neuromuscular disruption (Bonaldo and Sandri, 2013; Yokogawa et al., 2025). On the other hand, sarcopenia, a gradual kind of muscle loss linked to mitochondrial dysfunction, inflammation, and delayed regeneration, is studied using age-related models, such as natural and accelerated aging systems (Larsson et al., 2019; Sayer et al., 2024).

Table 2. Comparison of Experimental Models of Skeletal Muscle Atrophy

Model	Category	Type of Atrophy	Key Features
C2C12 (Starvation, dexamethasone, cytokines)	In Vitro	Disuse/Microgravity	Muscle unloading, rapid atrophy
Hindlimb Unloading	Animal (in vivo)	Disuse/Microgravity	Muscle unloading, rapid atrophy
Immobilization (casting)	Animal/ Human (in vivo)	Disuse	Reduced mechanical load contraction
Denervation	Animal (in vivo)	Neuromuscular	Loss of neural input, nerve injury, rapid atrophy
Natural aging	Animal/ Human (in vivo)	Sarcopenia	Gradual muscle loss, inflammation, mitochondrial dysfunction
Accelerated Aging models	Animal (in vivo)	Sarcopenia	Genetic or induced aging phenotypes

Preliminary data from our laboratory suggested an early and transient increase in STAU1 expression observed across three models of skeletal muscle atrophy. Early unpublished experiments examined different atrophic stimuli using in vitro, in vivo, and the use of human samples. In an vitro model, starvation-induced atrophy was established in differentiated C2C12 myotubes (Figure 9). In vivo, denervation-induced atrophy was generated in 12-week-old FVB/N mice by transecting a small segment of the left sciatic nerve (Figure 10). Complementary to these models, human muscle samples were obtained from two ground-based analogs of microgravity: a short-term dry immersion study in healthy young males and a long-term bed rest study. Preliminary results showed that STAU1 expression was consistently elevated in all three experimental settings, indicating that this rise is an early and universal molecular response to atrophic stimuli. Together these models suggest that STAU1 may be a common regulator of muscle remodeling under catabolic stress. Contrary to these multi-model findings, the current work mainly concentrates on utilizing in vitro C2C12 differentiated myotubes and an in vivo denervation model in 12-week-old mice, enabling controlled analysis of STAU1 activity in both cellular and physiological environments.

In this work, denervation achieved via transection of the sciatic nerve, a commonly used and thoroughly studied paradigm for causing skeletal muscle atrophy in mice (Viezuină et al., 2025). Major hindlimb muscles, such as the gastrocnemius and tibialis anterior, are innervated by the sciatic nerve, which makes it especially useful for researching strong and quick muscular atrophy after loss of neural input (Yang et al., 2022). Reduced protein synthesis, activation of the ubiquitin-proteasome system, and overexpression of atrogenes like MuRF1 and Atrogin-1 are the hallmarks of a consistent and synchronized atrophic response following sciatic nerve transection (Bodine et al., 2001; Bonaldo and Sandri, 2013). This model is notably effective for studying early regulators of muscle atrophy, such as RNA-binding proteins like STAU1, since it allows for comprehensive temporal investigation of early molecular processes after denervation. Sciatic nerve transection continues to be the standard method for examining neuromuscular disruption and muscle degeneration in vivo because of its reliability, consistency, and recognized molecular markers.

1.8.2 Increased STAU1 Expression Across Two Models of Skeletal Muscle Atrophy

1.8.2.1 Starvation-Induced Atrophy in Myotubes

Members of our lab (Aymeric Ravel-Chapuis, Shekoufeh Almasi, Catherine Calhoun, Allon Pagano, and Marc Charron) employed a well-characterized in vitro model to induce muscle atrophy in cultured myotubes, namely starvation of mouse C2C12 muscle cells (Stevenson et al., 2005). Differentiated myotubes were switched to a depleted starvation medium for varying time intervals (3 h, and 6 h; Figure 9A), selected to capture both early and later events associated with starvation-induced atrophy. Immunofluorescence staining using anti-myosin heavy chain (MyHC) antibodies was performed to visualize myotubes and quantify myotube diameter (Bodine et al., 2001; Gomes et al., 2001). As expected, a significant reduction in myotube diameter was observed following 3 and 6 hours of starvation ($p<0.001$) (Figure 9C). In this preliminary work, we also determined the levels of STAU1 during starvation. This data revealed that the total levels of STAU1 increased progressively after 15 min, 30 min and 1 hr, reaching a peak of expression at 3 hrs (Figure 9D and E). Research has also shown that increased expression of MuRF1 and MAFbx serves as a hallmark of the atrophic response, as mentioned above (Gomes et al., 2001; Belanger et al., 2003). Consistent with this, the data indicates that MuRF1 levels were increased during starvation at 15 minutes, and MAfbx levels increased at later time points (Figure 9F-I).

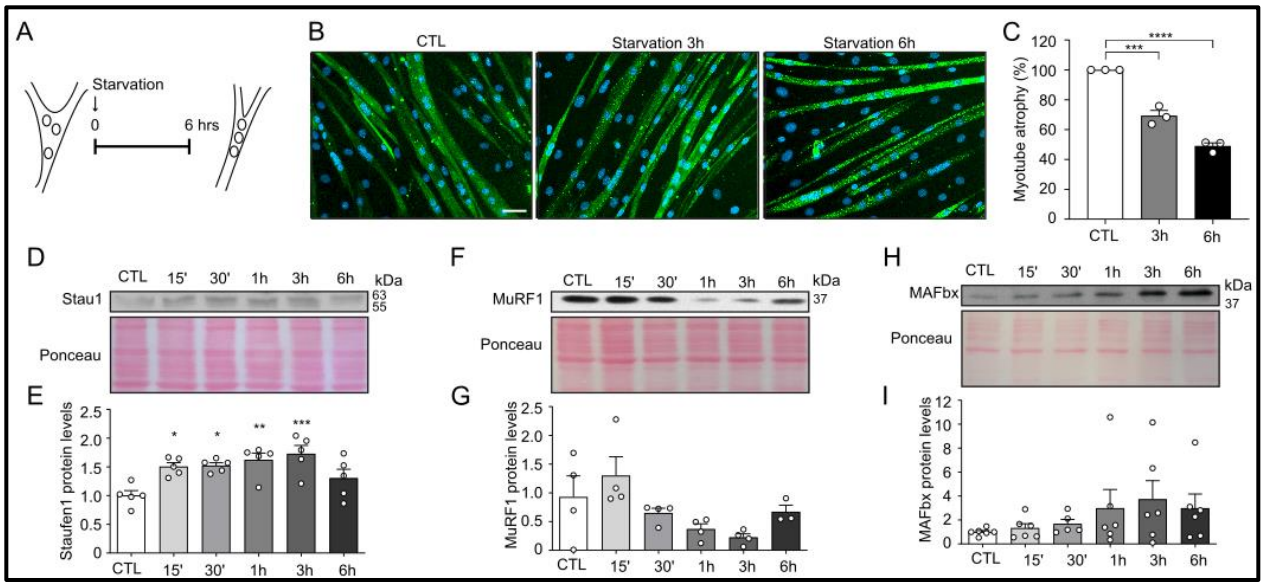

Figure 9. Staufen1 is increased early during starvation-induced myotube atrophy.

(A) 5-day differentiated myotubes were starved for the indicated time. (B, C) Representative immunofluorescence and quantifications of control (CTL) and 3hr- and 6hr-starved myotubes. MyHC (green) and DAPI (blue) were used to stain myotubes and nuclei, respectively. Scale bars, 50 µm. (D) Representative western blots and quantifications showing STAU1 and MAFbx protein levels. Ponceau were used as loading controls. n = 3. T-tests were used, and asterisks indicate significance (* $p<0.05$, *** $p<0.001$). Data from Jasmin Lab.

1.8.2.2 Denervation-induced atrophy in mouse skeletal muscle

The hindlimb muscles of 12-week-old FVB/N mice were subjected to denervation by cutting and excising a small portion of the left sciatic nerve. The muscles of the contralateral leg acted as controls, remaining innervated. At 1, 2, 3, 5, and 7 days following surgery, muscles from both the innervated and denervated legs were isolated (Figure 10A). As anticipated, denervation resulted in a reduction of muscle mass in the tibialis anterior (TA), soleus (SOL), and gastrocnemius (GAS) muscles at day 7 (Figure 10B). To further explore the molecular alterations related to hindlimb denervation, we assessed the levels of Staufen1, MuRF1, and MAFbx in TA muscles via western blot analysis. We noted a significant and transient rise in STAU1 levels at days 3, 5 and 7 of denervation ($p<0.001$). In addition, a significant increase was also observed in MuRF1 protein levels at days 2 and 3 ($p<0.05$, $p<0.01$) as well as in MAFbx at days 1, 2, and 3 ($p<0.05$, $p<0.01$, and $p<0.001$) (Figure 10C).

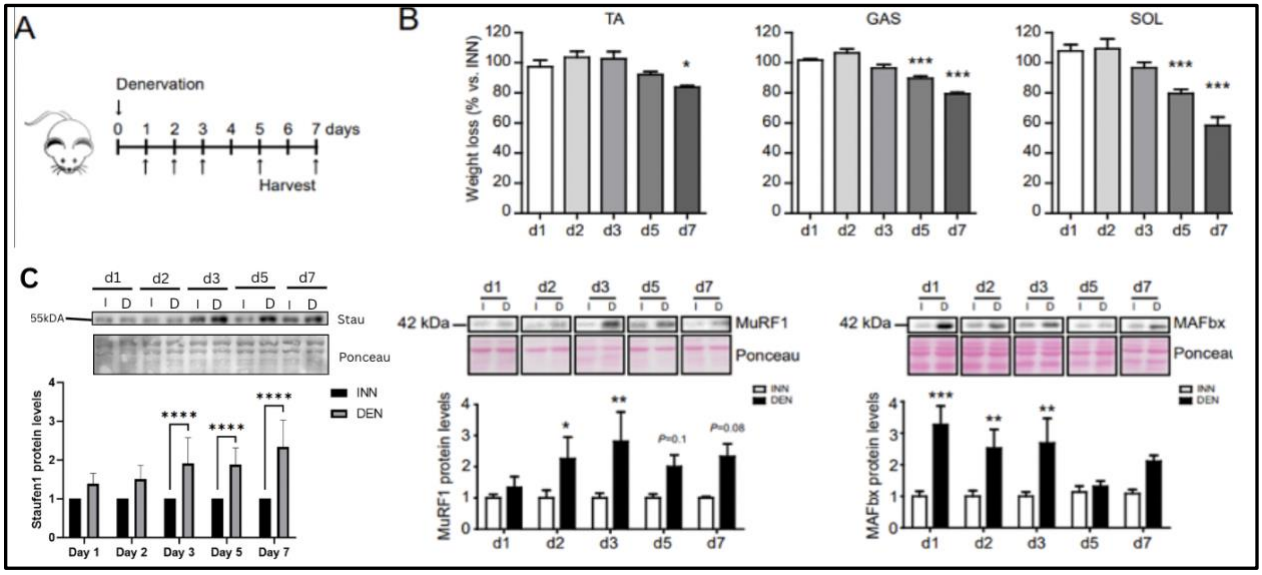

Figure 10. Staufen1 is increased during skeletal muscle denervation.

(A) Denervation for the indicated time. (B) Percentage of muscle weight loss. (C) Representative western blots and quantifications showing STAU1, MuRF1 and MAFbx protein levels in innervated (I) and denervated (D) TA

muscles. Ponceau were used as loading controls. n = 3. T-tests were used, and asterisks indicate significance (* $p \leq 0.05$, ** $p \leq 0.01$ and *** $p \leq 0.001$). Data from Jasmin Lab.

1.8.3 The decrease of Staufen1 levels shows protection against muscle atrophy.

To assess the role of STAU1 in the atrophy process, Aymeric Ravel-Chapuis conducted experiments to downregulate STAU1 by transfecting STAU1 shRNAs. Figure 11A illustrates the experimental setup for STAU1 knockdown in C2C12 cells using shRNA targeting STAU1 (shSTAU1). Prior to differentiation, cells were initially transfected with shSTAU1 constructs. This was followed by a 5-day differentiation period that allowed mature myotubes to develop. Differentiated myotubes were then starved for a maximum of 6 hours before samples were collected for further analysis. Firstly, a significant reduction ($p < 0.05$ of STAU1 levels (by 40%) through western blot analysis was confirmed (Figure 11B). Then, immunofluorescence staining was used to examine how the modulation of STAU1 levels affected the diameter of the myotubes (Figure 11C). As anticipated, myotubes that were transfected with the control empty plKO vector exhibited a response to starvation with a ($p< 0.001$) reduction in diameters. However, starvation of myotubes did not lead to atrophy when STAU1 levels were decreased, emphasizing the protective role of reduced STAU1 expression during atrophy (Figure 11D). Collectively, these findings suggest that targeting and lowering STAU1 expression during atrophy aids in maintaining muscle fiber diameter and preventing atrophy, making STAU1 an appealing target for therapeutic interventions.

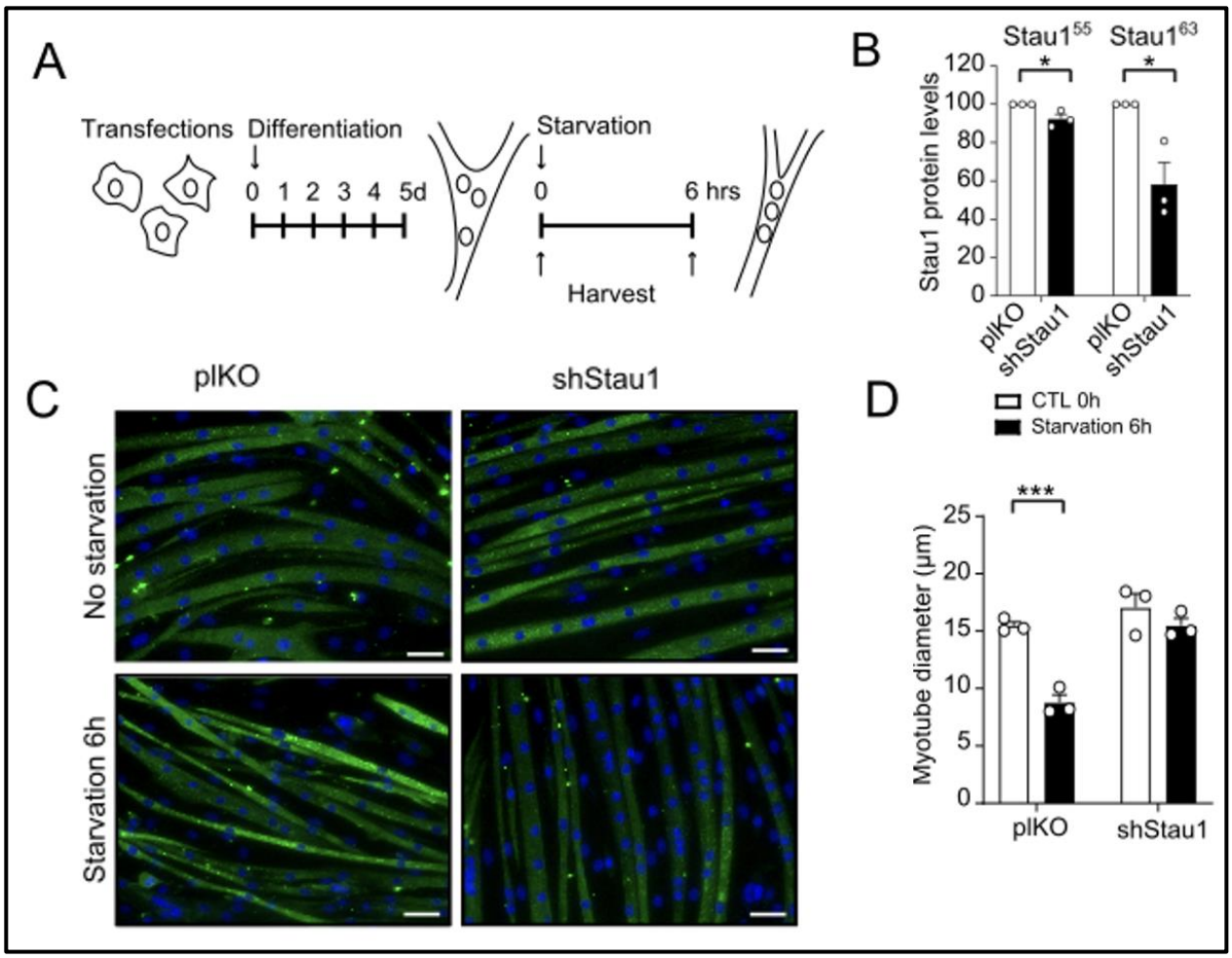

Figure 11. Lentiviral knockdown of Staufen1 prior to starvation successfully averts myotube shrinking.

(A) A graphical depiction of lentiviral transfection employing the shStau1 knockdown vector along with the respective controls. (B) Representative western blot analysis that confirms STAU1 protein levels after knockdown. (C) Representative immunofluorescent images of myotubes taken before and after starvation when transfected with the shStau1 knockdown vector, with myotubes stained for MyHC in FITC (green) and nuclear staining in DAPI (blue). Microscope analysis completed on the Zeiss AxioObserver M2 10x objective. (D) Analysis of myotube diameter of MHC stained myotubes transfected with shStau1 knockdown vector after starvation. (* $p \leq 0.05$, and *** $p \leq 0.001$). Data from Jasmin Lab.

1.9 Drug Repurposing as a Therapeutic Strategy

Developing novel therapeutics for intricate conditions like skeletal muscle atrophy is frequently impeded by the prolonged, expensive, and high-risk nature of conventional drug discovery. Typically, the development of a new medication spans over ten years and demands investments totaling billions before receiving clinical approval (Pushpakom et al., 2019). Conversely, drug repurposing is the practice of finding new medical uses for existing approved drugs that offers a faster and cost-effective route for translation research. (Ashburn, and Thor, 2004). Since the

pharmacokinetics, safety, and toxicity profiles of these drugs are already known, repurposed medications can rapidly advance to clinical trials for new uses (Ashburn, and Thor, 2004; Chong, and Sullivan, 2007). This approach has been effectively utilized in various areas, such as oncology, neurology, and infectious diseases, resulting in the discovery of new treatments like sildenafil for pulmonary hypertension and thalidomide for multiple myeloma (Nosengo, 2016).

Drug repurposing offers a promising approach for muscle atrophy by leveraging compounds with established safety and regulatory approval, enabling faster translation to clinical use. Numerous FDA-approved medications initially intended for different purposes have shown potential to combat atrophy. For example, β2-adrenergic agonists like clenbuterol have been studied for its ability to reduce skeletal muscle atrophy and promote muscle protein production through the activation of the PI3K/Akt/mTOR pathway (Table 3) (Ryall et al., 2002). Clinical data shows that clenbuterol can enhance lean muscle mass and decrease denervation-induced muscle atrophy in humans (Hostrup et al., 2025). Nevertheless, its clinical use is still restricted because of safety issues and lack of regulatory approval. Next, selective androgen-receptor modulators (SARMs) such as Enobosarm have been examined for its potential to cure skeletal muscular atrophy because of its anabolic properties. Although clinical research has shown gains in lean body mass in populations with age-related muscle loss and cancer cachexia, its practical applicability has been restricted due to inconsistent benefits in functional performance and lack of regulatory approval (Dalton et al., 2011; Crawford et al., 2016). Furthermore, the widely used antidiabetic medication metformin has been studied for possible effects on skeletal muscle metabolism through AMPK activation (Table 3). Nevertheless, clinical studies in older adults have shown that it may attenuate muscle hypertrophy and strength improvements during resistance training, limiting its efficacy as a therapeutic approach for skeletal muscle atrophy (Walton et al., 2019; Konopka et al., 2019). Mifepristone, a glucocorticoid receptor antagonist, can prevent glucocorticoids from activating proteolytic pathways because it has been suggested as a possible treatment for skeletal muscle atrophy. Although preclinical research shows that glucocorticoid receptor inhibition can reduce muscle atrophy by inhibiting FoxO-mediated atrogene production (Schakman et al., 2013), there is currently little clinical proof, and its application is mostly limited to the treatment of hypercortisolism rather than muscle atrophy.

Table 3. Representative advanced agents repurposed for the potential treatment of skeletal muscle atrophy

Drug Class	Representative agent	Primary mechanism in muscle	Clinical evidence
β2-adrenergic agonists	Clenbuterol	PI3K/Akt/mTOR activation → ↑ protein synthesis	Denervation-induced atrophy (Ryall et al., 2002; Hostrup et al., 2025)
SARM	Enobosarm (GTx-024)	Direct activation of androgen receptor → anabolic signaling	Cancer-cachexia trials (Dalton et al., 2011; Crawford et al., 2016)
Biguanide	Metformin	AMPK activation → ↓ mTOR signaling, ↑ autophagy and metabolic adaptation	Attenuate muscle hypertrophy and improves strength (Walton et al., 2019; Konopka et al., 2019)
Glucocorticoid antagonists	Mifepristone (RU-486)	Glucocorticoid receptor antagonism → ↓ proteolysis (↓ MuRF1, Atrogin-1)	Proposed to treat skeletal muscle atrophy (Schakman et al., 2013; Permpoon et al., 2025)

There are presently no FDA-approved pharmaceutical therapies explicitly used for skeletal muscle atrophy or sarcopenia, despite extensive investigation. Although substances like growth hormone and testosterone can boost muscle mass in some therapeutic settings (Sinclair et al., 2016; Connor et al., 2023), their application is constrained by safety issues and varied functional advantages. Myostatin/activin inhibitors and selective androgen receptor modulators are examples of emerging medications that have demonstrated a promise in clinical trials but have not yet received regulatory approval, underscoring the continuous difficulty in creating safe and effective treatments for muscle wasting.

The identification of Staufen1 (STAU1) as a potential atrogene has unveiled a new pathway for therapeutic innovation. Considering STAU1's function in facilitating catabolic signaling and hindering differentiation (Parks et al., 2017; Ravel-Chapuis et al., 2014), medications that can

reduce its expression or function may act as new anti-atrophy agents. High-throughput screening technologies utilizing established compound offer an effective way to identify candidate molecules with potential for clinical application quickly. Therefore, repurposing not only speed up the identification of compounds relevant to clinical practice but also provide a mechanistic understanding of the regulatory networks that govern muscle mass (Corsello et al., 2017). Ultimately, drug repurposing with the molecular characterization of targets like STAU1 represents a promising new strategy for creating treatments for skeletal muscle atrophy and related wasting disorders.

1.9.1 High-Throughput Screening for STAU1 Modulators

The Jasmin Lab conducted additional experiments to determine if lowering STAU1 levels can offer protection against muscle atrophy. Reduced STAU1 expression maintained myofiber integrity and reduced atrophic alterations, as shown by STAU1 knockdown using shRNA (Figure 11). An In-Cell ELISA Colorimetric Detection System was used in an ELISA-based high-throughput screen of FDA-approved drugs to identify pharmacological compounds that might downregulate STAU1. STAU1-expressing myoblasts were placed in 384-well microplates with 770 FDA-approved compounds that were accessible in our lab. STAU1 protein levels were measured after cells were exposed to either vehicle controls or drugs for 24 hours. The top candidate compounds exhibiting the greatest reduction in STAU1 expression were selected for further analysis.

A secondary screening of the 20 most promising candidates was performed to identify drugs that could effectively reduce STAU1 expression while maintaining C2C12 myoblast viability (Figure 12A). From this screen, five drugs designated as compounds 1, 2, 11, 12, and 15 demonstrated significant downregulation of STAU1 protein levels. These five compounds were subsequently tested in differentiated C2C12 myotubes under both basal and starvation-induced atrophic conditions. Myotubes were exposed to each compound (or DMSO control) for either 1 hour or 24 hours, followed by incubation in either control differentiation medium or starvation medium for 6 hours to induce atrophy. Exposure to compound 11 for 1 hour effectively prevented starvation-induced atrophy compared to the control. Similarly, treatments with compounds 12 and 15 also reduced the extent of myotube atrophy, although their protective effects were less

pronounced than compound 11. In contrast, compounds 1 and 2 did not significantly influence myotube diameters under either condition (Figure 12B).

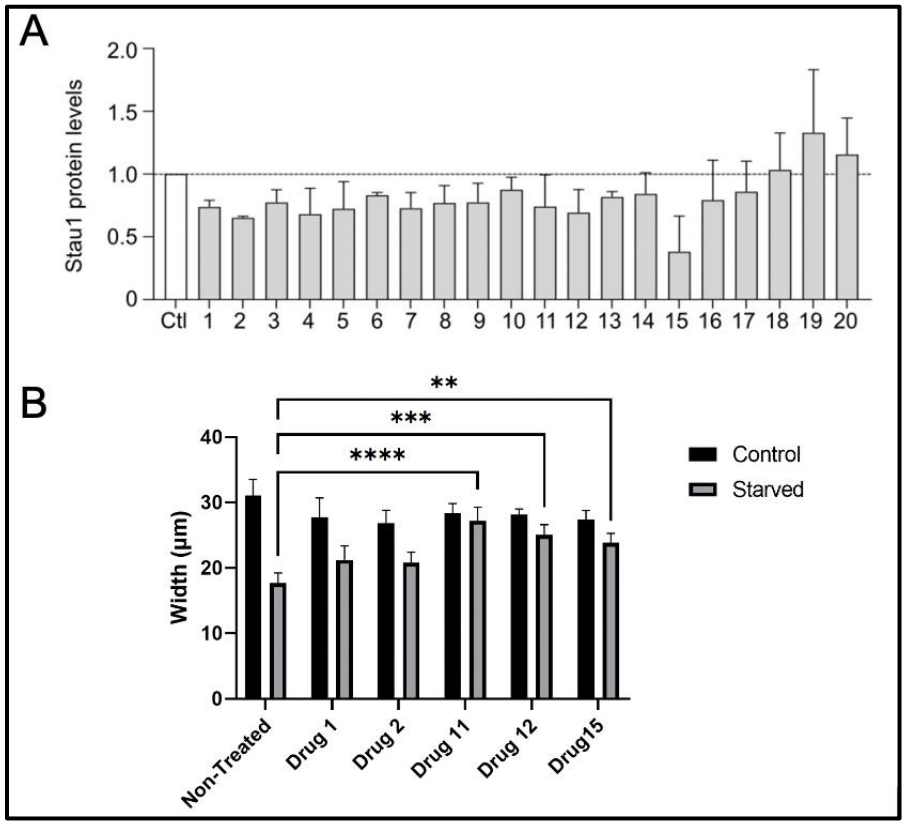

Figure 12. Pharmacological screening identifies compounds that modulate STAU1 expression and effects of myotube atrophy under starvation conditions.

(A) Quantification of STAU1 protein levels in differentiated C2C12 myotubes following treatment with a panel of candidate compounds (1-20). Protein levels are normalized to control (Ctl; dashed line = 1.0). **(B)** Myotube diameters using immunofluorescence analyses were measured under control (black bars) and starvation (grey bars) conditions following treatment with selected compounds (Drug 1, Drug 2, Drug 11, Drug 12, and Drug 15) compared to non-treated cells. Statistical significance is indicated as **p < 0.01, ***p<0.001, and ****p < 0.0001. Data are presented as mean ± SEM. Data from the Jasmin Lab.

Collectively, these preliminary findings indicate that both genetic suppression of STAU1 via shRNA (Figure 11) and pharmacological downregulation using select FDA-approved drugs specifically compounds 11, 12, and 15 can attenuate skeletal muscle atrophy in cultured muscle cells (Figure 12). These results highlight STAU1 as a promising therapeutic target and support further investigation into its modulation as a potential strategy to prevent muscle wasting.

2. Rationale, Hypothesis, and Research Objectives

Recent research from our lab has identified the RNA-binding protein Staufen1 (STAU1) as a novel regulator of skeletal muscle atrophy. Unpublished findings show that STAU1 expression is consistently and transiently elevated at the onset of muscle atrophy across multiple models, including starved myotubes, denervated and hindlimb-suspended mice, and humans undergoing bed rest and dry immersion. Moreover, shRNA-mediated knockdown of STAU1 attenuates myofiber atrophy, supporting a functional role for STAU1 in early atrophic responses. Despite this growing evidence, no pharmacological strategies currently exist to specifically target STAU1. Therefore, drug repurposing of FDA-approved compounds offers a practical approach to identify potential modulators. Hence, this study aimed to determine whether pharmacological reduction of STAU1 could mitigate skeletal muscle atrophy by functional validation in vitro using a starvation-induced model and in vivo using a denervation-induced atrophy model.

The overarching objective of my MSc thesis is to characterize FDA-approved drugs that modulate STAU1 expression and evaluate their potential as therapeutic agents against skeletal muscle atrophy based on the recent finding from the Jasmin Lab. My thesis project aims to understand the regulatory role of Staufen1 (STAU1) in skeletal muscle atrophy and to evaluate whether targeting STAU1 with FDA-approved drugs can mitigate early molecular changes and prevent muscle wasting in vitro and in vivo. We hypothesize that pharmacological downregulation of Staufen1 (STAU1) can mitigate skeletal muscle atrophy. Specifically, it is proposed that certain FDA-approved drugs can reduce STAU1 expression in muscle cells, thereby preventing the molecular and morphological features of atrophy. I have two specific project objectives:

Aim 1: Investigating the Effect of FDA-Approved Drugs on STAU1 Expression in Starved C2C12 Myotubes

This objective confirms whether FDA-approved drugs are successful in decreasing STAU1 levels and mitigating muscle atrophy in an in vitro model of skeletal muscle atrophy.

Aim 2: Assessing the Therapeutic Potential of FDA-Approved Drugs Targeting STAU1 in a Mouse Model of Denervation-Induced Muscle Atrophy

2.1 To evaluate whether Drugs 12 reduces STAU1 expression and prevent skeletal muscle atrophy following sciatic nerve denervation in mice.

2.2 To evaluate the ability of Drug 15 to decrease STAU1 expression and limit skeletal muscle loss in denervated mice.

By addressing these aims, this project builds the framework needed to investigate the mechanistic role of STAU1 in muscle atrophy and to determine whether pharmacological inhibition can mitigate its effects.

3. Materials and Methods

3.1 Thawing and Initial Culture of C2C12 Myoblasts

Growth medium (GM) consisted of Dulbecco's Modified Eagle 1X Medium (DMEM) (Multicell with 4.5g/L Glucose, L-glutamine and Sodium Pyruvate) supplemented with 10% fetal bovine serum (FBS) (Thermofisher) and penicillin-streptomycin (Pen/strep) (Multicell), while differentiation medium (DM) consisted of DMEM supplemented with 2% horse serum (HS) (Corning) and penicillin-streptomycin. Media were prepared under sterile conditions and used for maintenance and differentiation of C2C12 myoblasts.

Frozen C2C12 myoblast stock vials were retrieved from liquid nitrogen storage and rapidly thawed in a 37 °C water bath for approximately 2 minutes, until only a small ice crystal remained. Once the cells were thawed, 1mL of C2C12 stock were transferred into a 15ml Falcon tube containing 5mL GM. A 10 cm tissue culture dish was labeled with the experimenter's initials, cell type, experiment number, passage number, and date. An additional 5 mL of growth medium was added to the Falcon tube to bring the total volume to 10 mL, which was then transferred to the 10 cm dish using a gentle zig-zag motion to ensure even cell distribution. Growth medium was replaced 24 hours after plating to remove residual cryoprotectant and non-adherent cells. C2C12 myoblasts were subsequently cultured for 2-3 days until they reached approximately 80% confluency, at which point they were used for downstream differentiation experiments.

3.2 Cell Seeding and Differentiation of C2C12 Myoblasts into Myotubes

Growth medium (GM), differentiation medium (DM), and 0.25% trypsin (Multicell - 2.21mM EDTA 4Na) were thawed in a 37 °C water bath for approximately 30 minutes. Prior to cell seeding, 35 mm plates were coated with Matrigel to promote cell attachment, differentiation, and growth. Growth medium was aspirated from the 10 cm culture dish, and cells were washed once with 5 mL of 1× PBS. Subsequently, 5 mL of trypsin was added, and the plate was gently mixed to ensure even coverage. Cells were incubated at 37 °C for 5 minutes to allow detachment from the plate. Cell detachment was confirmed microscopically, after which 1 mL of FBS was added to neutralize trypsin activity. The cell suspension was transferred into a 15 mL Falcon tube, and the plate was rinsed with an additional 5-10 mL of GM to collect any remaining cells. The combined suspension was gently mixed to ensure homogeneity and centrifuged at 300 × g for 5 minutes. Following centrifugation, the supernatant was aspirated, and the cell pellet was resuspended in 1 mL of differentiation medium. Cell concentration was determined using an auto countess. Briefly, 10 µL of the cell suspension was mixed with 10 µL of Trypan Blue dye and loaded onto a cell count slide. Viable cells were counted, and cell density was calculated. Cells were seeded at a density of 200,000 cells per well in 35 mm dishes containing differentiation medium. Seeded cells were placed in a 37 °C humidified incubator with 5% CO_2 to allow differentiation of myoblasts into myotubes. Differentiation medium was replaced every 24-48 hours.

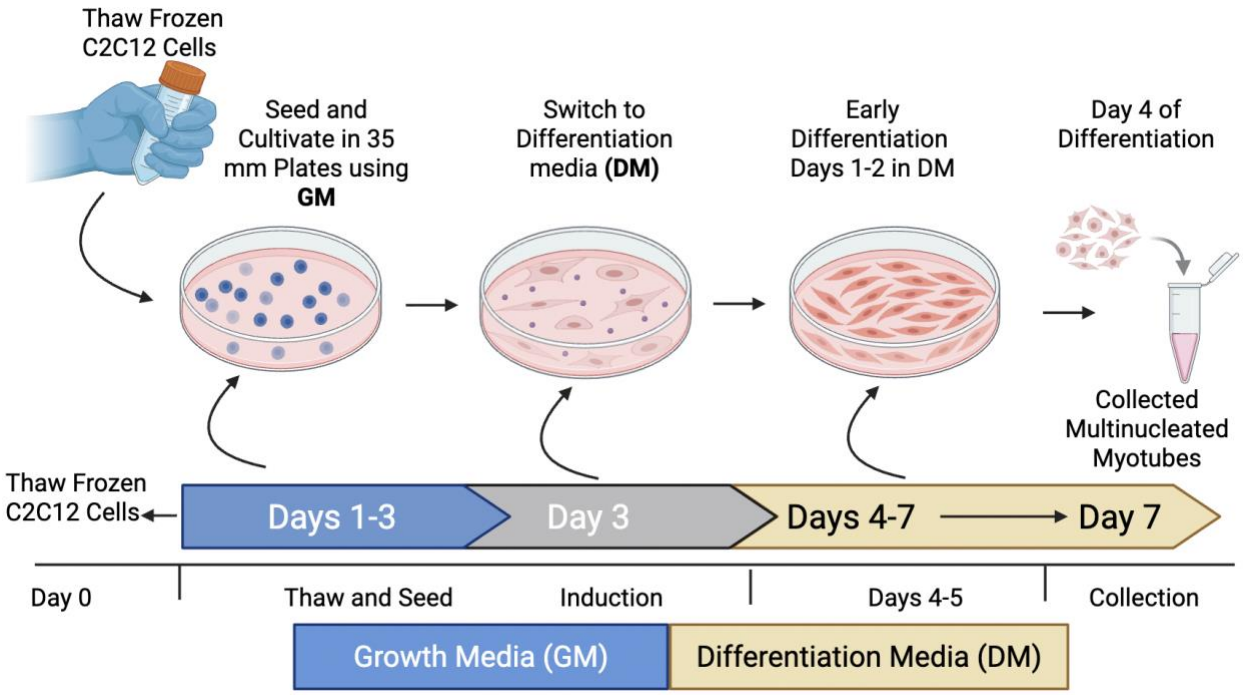

Figure 13. Timeline of C2C12 myoblast culture, differentiation, and treatment protocol used for in vitro atrophy experiments.

C2C12 myoblasts were thawed and cultured in growth media (GM) for 2-3 days until they reached 80-90% confluency. The cells were then plated onto coated 35 mm plates and transitioned to differentiation media (DM) to promote myotube development. Differentiation occurred over 4-5 days, with multinucleated myotubes becoming evident by Day 3 of the differentiation process. On Day 4 of differentiation, the myotubes underwent drug treatment and/or were collected for subsequent immunofluorescence and protein analysis. Image created on BioRender.

3.3 Drug Treatment and Induction of In Vitro Muscle Atrophy

C2C12 myoblasts were differentiated into multinucleated myotubes as described above (Figure 13). Differentiated myotubes were treated with media making a final concentration in the plate of 1 µM of Drug 12 or Drug 15, or untreated control (in DM), for 1 hour. Following drug treatment, one set of myotubes was subjected to 6 hours of starvation using starvation medium (SM) (1X PBS + 2% HS + pen/strep) to induce an in vitro model of skeletal muscle atrophy. These samples were subsequently used for immunofluorescence staining and myotube diameter analysis. In parallel, a separate set of differentiated myotubes was treated with Drug 12, Drug 15, or vehicle control for 1 hour without starvation. These samples were collected for protein extraction and Western blot analysis to assess STAU1 protein expression.

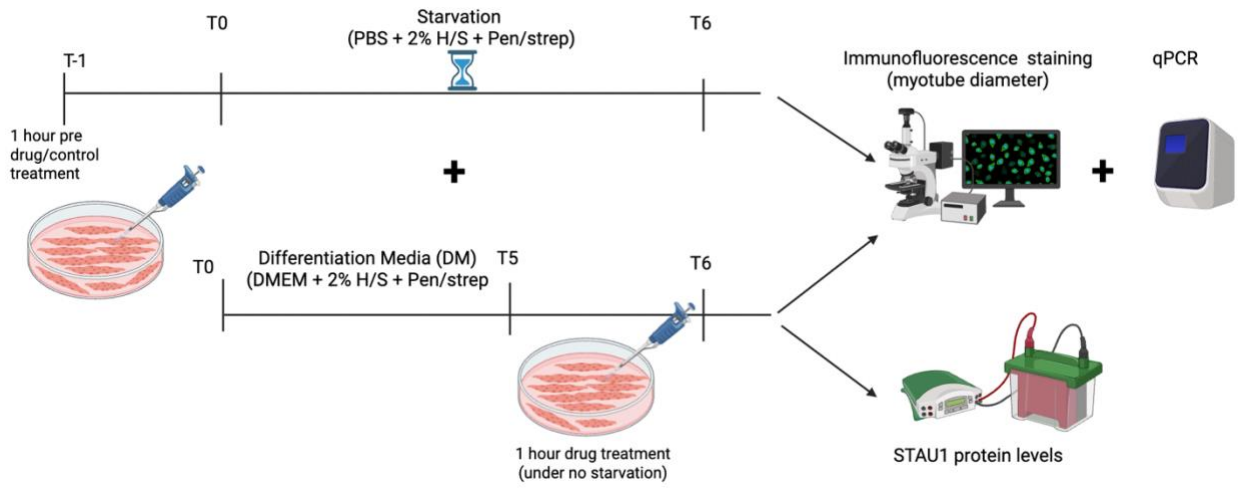

Figure 14. Experimental design for in vitro drug treatment and starvation-induced atrophy in C2C12 myotubes.

Differentiated C2C12 myotubes were subjected to two parallel treatment conditions. In the starvation condition (top), cells received a 1-hour pre-treatment with drug or vehicle (T-1), followed by 6 hours of serum starvation in starvation medium (PBS + 2% horse serum + penicillin/streptomycin) from T0 to T6. In the non-starved condition (bottom), myotubes were maintained in differentiation medium (DMEM + 2% horse serum + penicillin/streptomycin) and treated with drug or vehicle for 1 hour at the 5-hour timepoint (T5-T6). At T6, cells from both conditions were collected for immunofluorescence staining to assess myotube diameter, qPCR analysis, and Western blot analysis to evaluate STAU1 protein levels. Image created on BioRender.

3.4 Immunofluorescence Staining and Myotube Diameter Analysis

Differentiation medium (DM) or starvation medium was aspirated from the 35mm plates, and C2C12 myotubes were washed twice with 1 mL of 1× PBS. Cells were fixed by adding 1 mL of 3.7% formaldehyde diluted in PBS to each well and incubating for 10 minutes at room temperature (RT). Following fixation, wells were washed twice with 1× PBS, and 1 mL of PBS was added to each well to maintain hydration and prevent drying. Plates were sealed with parafilm and stored at 4°C until immunofluorescence staining. For immunofluorescence staining, PBS was aspirated from each well, and cells were permeabilized using 0.5% Triton X-100 in 10% donkey serum diluted in 1× PBS for 20 minutes at RT on a rocking platform. The permeabilization solution was removed, and cells were blocked with 1% bovine serum albumin (BSA) in PBS for 10 minutes at RT. Wells were then washed twice with 1× PBS. Primary antibody incubation was performed using mouse MF20 (anti-myosin heavy chain) diluted 1:100 in 0.1% Triton X-100 with 5% serum. Approximately 500 µL of the primary antibody solution was added to each well, and plates were incubated for 1 hour at RT on a rocker. Following incubation, wells were washed three times with PBS for 10 minutes each. Secondary antibody incubation was performed using a CY3 donkey anti-

mouse secondary antibody diluted 1:500 in 0.1% Triton X-100 with 5% serum. Approximately 500 µL of secondary antibody solution was added to each well, and plates were incubated for 1 hour at RT in the dark to prevent photobleaching. Wells were then washed three times with PBS for 10 minutes each. Cells were mounted using Vectashield mounting medium containing DAPI, covered with glass coverslips, and sealed around the edges using clear nail polish. Samples were stored at 4°C in the dark until imaging and analysis.

Immunofluorescence-stained C2C12 myotubes were imaged using a Zeiss AxioObserver 7-Apollo fluorescence microscope equipped with a 20X objective lens, 0.8 Numerical Aperture and lens with 25mm field of view. All images were acquired using identical microscope settings, including exposure time, gain, and illumination intensity, to ensure consistency across experimental conditions. Fluorescence signals were captured using the appropriate fluorophore channel for myotube labeling and the DAPI channel for nuclear staining. For each condition, five to ten randomly selected fields of view were imaged per experimental replicate.

Quantification of myotube diameter was performed using Fiji/ImageJ software. Individual myotubes were manually measured using line tool, and diameter measurements were taken at three distinct positions along the length of each myotube, the top, middle, and bottom regions. These values were averaged to obtain a mean diameter per myotube, accounting for local variations in thickness. A minimum of 80-100 myotubes per condition were analyzed across independent biological replicates.

3.5 Protein Extraction and Western Blot Analysis of STAU1 Expression

Protein Extraction from Differentiated C2C12 Myotubes

C2C12 myotubes were subjected to drug treatment as described in section 3.1.3. Following treatment, culture medium was aspirated, and 150-200 µL of ice-cold 1× RIPA lysis buffer was added to each well. Plates were immediately placed on ice under a chemical fume hood and incubated for approximately 5 minutes to allow efficient cell lysis. Cells were then manually detached using a cell scraper, and the lysate from each well was collected and transferred into individually labeled 1.5 mL microcentrifuge tubes. Lysates were centrifuged at 14,000 × g for 10 minutes at 4°C to pellet insoluble debris. Without disturbing the pellet, the clarified supernatant

was carefully transferred to a new labeled microcentrifuge tube. Protein samples were stored at -20°C until further use for protein quantification and Western blot analysis.

Protein Quantification by Bicinchoninic Acid (BCA) Assay (ThermoScientific - using Bicinchoninic Acid)

Protein concentration was determined using the bicinchoninic acid (BCA) assay kit (Thermo Fisher Scientific), according to the manufacturer's instructions for microplate procedure. A serial dilution was performed to generate a standard curve with concentrations from 2000 mg/mL to 31.25 µg/mL, with MilliQ water serving as the blank. Protein samples were diluted 1:20 by mixing 9 µL of the sample with 36 µL of distilled water. For both samples and standards, 10 µL was pipetted in duplicate into a 96-well plate. Working reagent was prepared by mixing Reagent A and Reagent B at a 50:1 ratio, adjusted according to the total number of wells required. Subsequently, 200 µL of BCA working reagent was added to each well. The plate was incubated at 37°C for 30 minutes, after which absorbance was measured at 595 nm using a microplate reader. Protein concentrations were calculated from the BSA standard curve and used to normalize samples for downstream Western blot analysis.

Sample Preparation for Western Blotting

Protein samples were normalized to equal concentrations, and 20-30 µg of total protein from each sample was mixed with 4x Laemmli buffer containing 10% b-mercaptoenthanol to a final concentration of 1X. Samples were vortexed thoroughly to ensure homogenous mixing and then denatured at 95°C for 5 minutes on a heat block. Following denaturation, samples were briefly centrifuged and vortexed again before loading onto SDS-polyacrylamide gels.

SDS-Polyacrylamide Gel Preparation

Western blot gels were casted for the Biorad Mini-Protein Teta system with 5 % stacking and 10 % resolving as indicated below (1.5mm gel). Volumes of each component required to prepare the gel was prepared using a 30% acrylamide/bis-acrylamide solution, Tris buffer (pH 8.8), Tris buffer (pH 6.8), SDS, ammonium persulfate (APS), and TEMED for polymerization.

While the resolving gel was polymerizing, a 5% stacking gel (5 mL total volume) for Tris-glycine SDS-PAGE was prepared according to Table 5. A 10-well, 1.5 mm comb was inserted carefully,

ensuring proper alignment with the edge of the short plate. The stacking gel was then allowed to polymerize for 30 minutes.

SDS-Polyacrylamide Gel Electrophoresis

Solutions were prepared using 10X and 1X running and transfer buffers using glycine, SDS, and topped with ddH_2O. A 10 µL PageRuler™ Prestained Protein Ladder (Thermo Fisher Scientific) was loaded into one well, starting from the right side of the gel. Protein samples were then loaded into the remaining wells from right to left, ensuring that no air bubbles were introduced during dispensing. An additional running buffer was gently added to the tank as needed. Electrophoresis was performed at a constant voltage of 80 V for approximately 20-30 minutes, allowing proteins to migrate through the stacking gel. The voltage was then increased to 100-120 V until adequate protein separation within the resolving gel was achieved.

Protein Transfer and Immunoblotting

The transfer sandwich was placed into a pre-filled transfer tank, and protein transfer was performed at 90 V for 80 minutes. Upon completion, the membrane was removed, rinsed briefly with distilled water, and equilibrated in TBS-T buffer. Molecular weight markers were marked using a non-ethanol permanent marker to ensure visibility after subsequent processing. To assess protein transfer and loading uniformity, the membrane was stained with Ponceau S (5-10 mL) for 5-10 minutes until protein bands became visible. The membrane was then rinsed with ddH_2O and scanned using a ChemiDoc imaging system (Bio-Rad). Ponceau staining was removed by washing the membrane three times with TBS-T for 2 minutes each. The membrane was blocked in 25 mL of 5% bovine serum albumin (BSA) in TBS-T for 1 hour at room temperature. Following blocking, the membrane was incubated overnight at 4°C with a primary antibody against STAU1 (Abcam; 1:2000 dilution) on a rocking platform. After primary antibody incubation, membranes were washed three times with TBS-T for 10 minutes each. Membranes were then incubated with a horseradish peroxidase (HRP)-conjugated secondary antibody (goat anti-rabbit; 1:5000 dilution) for 1 hour at room temperature, followed by three additional washes with TBS-T. Protein bands were visualized using enhanced chemiluminescence (ECL) prepared at a 1:1 dilution, with membranes incubated for 5 minutes prior to imaging on the ChemiDoc system (Bio-Rad).

3.6 Animals and Ethical Approval

All animal experiments were conducted in accordance with the guidelines of the Canadian Council on Animal Care (CCAC) and were approved by the University of Ottawa Animal Care Committee (ACC). All experimental procedures were designed to minimize animal suffering and to reduce the number of animals used. Twelve-week-old male and female FVB/N mice were used in this study. Animals were housed in a temperature and humidity-controlled facility under a 12-hour light/dark cycle, with ad libitum access to food and water. Mice were group-housed in standard cages with appropriate environmental enrichment and were allowed to acclimate to the animal facility prior to the initiation of experimental procedures.

Mice were randomly assigned to experimental groups, including innervated control, denervated, and drug-treated denervated groups, as outlined in the experimental design. All surgical procedures were performed under isoflurane anesthesia, and perioperative analgesia was administered to minimize discomfort. Animals were monitored daily twice a day following surgery for signs of distress, infection, or impaired mobility, and humane endpoints were applied when necessary.

3.7 Sciatic Nerve Denervation Procedure

Mouse Preparation

Mice were initially anesthetized using 5% isoflurane to induce unconsciousness. After approximately 2-3 minutes, a reduction in respiratory rate was observed, indicating adequate induction of anesthesia (Figure 17). Depth of anesthesia was confirmed by assessing reflex responses to a tail pinch and/or interdigital pinch of the hind paw; absence of a withdrawal response indicated sufficient anesthesia. Once anesthetized, mice were transferred to a nose cone to maintain anesthesia at a concentration of 2-3% isoflurane for the duration of the surgical procedure. Ophthalmic ointment was applied to both eyes to prevent corneal drying during anesthesia. To maintain hydration, a subcutaneous injection of 1.0 mL sterile 0.9% saline was administered into the scruff of the neck (Figure 17). Hair was removed using an electric shaver or razor from the left lateral thigh and buttock region, extending from the sciatic notch to the knee, to expose the surgical site. The shaved area was disinfected using povidone-iodine or an appropriate antiseptic substitute (Figure 5) before incision.

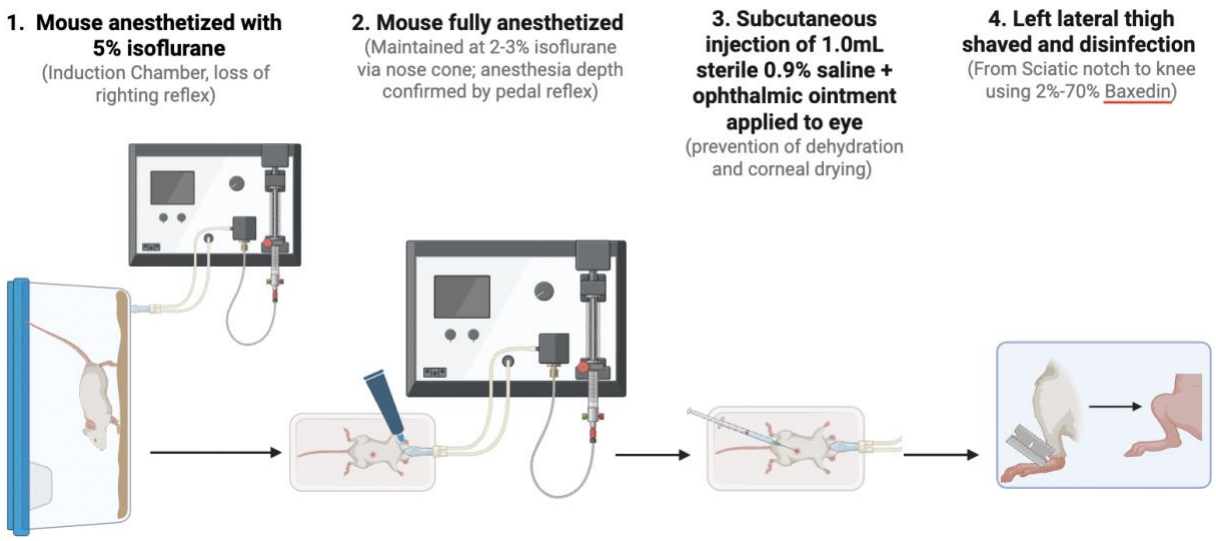

Figure 15. Pre-operative preparation of mice before sciatic nerve denervation surgery.

Mice were first anesthetized with 5% isoflurane in an induction chamber until loss of the righting reflex was observed. Anesthesia was then maintained at 2-3% isoflurane via a nose cone, and depth of anesthesia was confirmed by the absence of the pedal reflex. To prevent dehydration and corneal drying during the procedure, 1.0 mL of sterile 0.9% saline was administered subcutaneously, and ophthalmic ointment was applied to both eyes. The left lateral thigh was shaved from the sciatic notch to the knee and disinfected before surgical incision. Image created on BioRender.

Surgical Procedure for Sciatic Nerve Denervation

Following completion of pre-surgical preparations, mice were anesthetized with isoflurane, which was maintained at approximately 2% throughout the procedure. Anesthetic depth was continuously monitored by assessing respiratory rate and reflex responses, and isoflurane concentration was adjusted as necessary to maintain an adequate plane of anesthesia. A small 1-2 cm incision was made in the posterolateral cutaneous region using fine surgical scissors, beginning near the sciatic notch and extending toward the knee (Figure 18). The skin was carefully separated from the underlying musculature surrounding the incision site. The superficial fascia was then incised, and the hamstring and gluteal muscles were gently separated to expose the sciatic nerve. Sciatic nerve denervation was performed by a mid-point axotomy, in which an approximately 3 mm segment of the nerve was excised to prevent reinnervation (Figure 18). Following nerve transection, the incision was closed using one to two wound clips. For analgesia, animals received buprenorphine hydrochloride (0.1 mg/kg) pre-operatively and buprenorphine (1.2 mg/kg, subcutaneous) post-operatively to aid recovery. Animals were monitored twice daily following surgery for signs of pain, distress, or infection in accordance with approved animal care protocols.

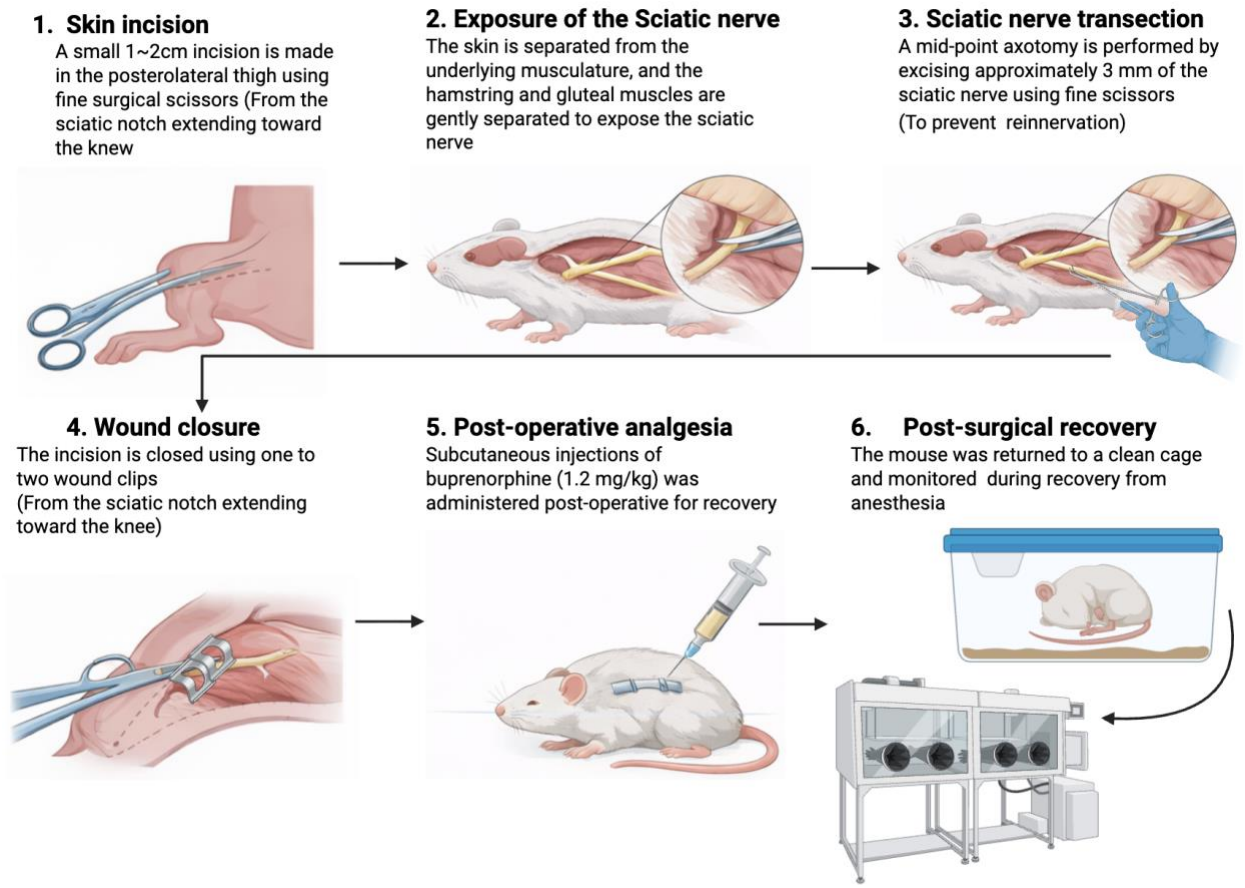

Figure 16. Schematic representation of sciatic nerve denervation surgery in mice.

Following skin incision and muscle separation, a 3 mm segment of the sciatic nerve is excised to prevent reinnervation. The incision is closed with wound clips, and animals receive post-operative analgesia prior to recovery. Created on BioRender.

3.8 Drug Preparation and Administration

Drug 12 and Drug 15 were prepared according to approved animal use protocols and administered to mice following unilateral sciatic nerve denervation. All drugs and control solutions were prepared fresh under sterile conditions on the day of injection. Drug 12 was administered at a dose of 1.0 mg/kg, while Drug 15 was administered at a dose of 30 mg/kg. Both drugs were delivered via intraperitoneal (IP) injection in a fixed volume of 50 µL per mouse. Injections were performed once daily beginning on the day of denervation surgery (Day 0) and continued for up to 14 consecutive days, depending on the experimental endpoint. For Drug 12 experiments, 0.9% sterile saline was used as the vehicle control and administered via IP injection at an equivalent volume (50 µL). For Drug 15 experiments, a vehicle solution consisting of 8% dimethylformamide (DMF), 20% ethanol (EtOH), 15% glycerol, and 15% polyethylene glycol 300 (PEG300) was used.

Vehicle control mice for Drug 15 received the same formulation without the active compound at a volume of 50 µL, corresponding to doses of 125.8 mg/kg DMF, 263 mg/kg EtOH, 315 mg/kg glycerol, and 280 mg/kg PEG300, representing approximately 20% of the reported LD_{50} as a maximum for each component.

Table 4. In Vivo Drug Dosing and Administration Parameters

Substance	Species	Route	Dose Administered	Volume	Dosing Frequency
Drug 12	Mouse	Intraperitoneal (IP)	1.0mg/kg	50uL	Once daily
Saline (0.9% NaCl)	Mouse	Intraperitoneal (IP)	N/A	50uL	Once daily
Drug 15	Mouse	Intraperitoneal (IP)	30mg/kg	50uL	Once daily
Vehicle control (Drug #15) 8% DMF 20% EtOH: 15% Glycerol 15% PEG300	Mouse	Intraperitoneal (IP)	DMF = 125.8mg/kg EtOH: = 263mg/kg Glycerol = 315mg/kg PEG300 = 280mg/kg	50uL	Once daily

3.9 Muscle Collection and Processing

At day 5 post-denervation, mice were euthanized by cervical dislocation following administration of Euthanol (120 mg/mL) in accordance with approved animal care protocols. The tibialis anterior (TA), extensor digitorum longus (EDL), soleus (SOL), and gastrocnemius (GA) muscles were carefully dissected from both the denervated limb and the contralateral control limb. Muscles were immediately weighed to determine wet muscle mass, snap-frozen in liquid nitrogen, and stored at -80 °C for subsequent RNA and protein extraction. At day 14 post-denervation, an additional portion of each muscle from both hindlimbs was collected for histological analysis (Figure 19). Muscles were embedded in Tissue-Tek optimal cutting temperature (OCT) compound within embedding molds to fully cover the tissue. A cold-resistant beaker containing 2-methylbutane was cooled using liquid nitrogen, and embedded muscle samples were frozen by immersion in the cooled 2-methylbutane for approximately 30 seconds. Frozen samples were then transferred to 1 mL labeled cryotubes, placed in liquid nitrogen, and stored at -80 °C until cryosectioning.

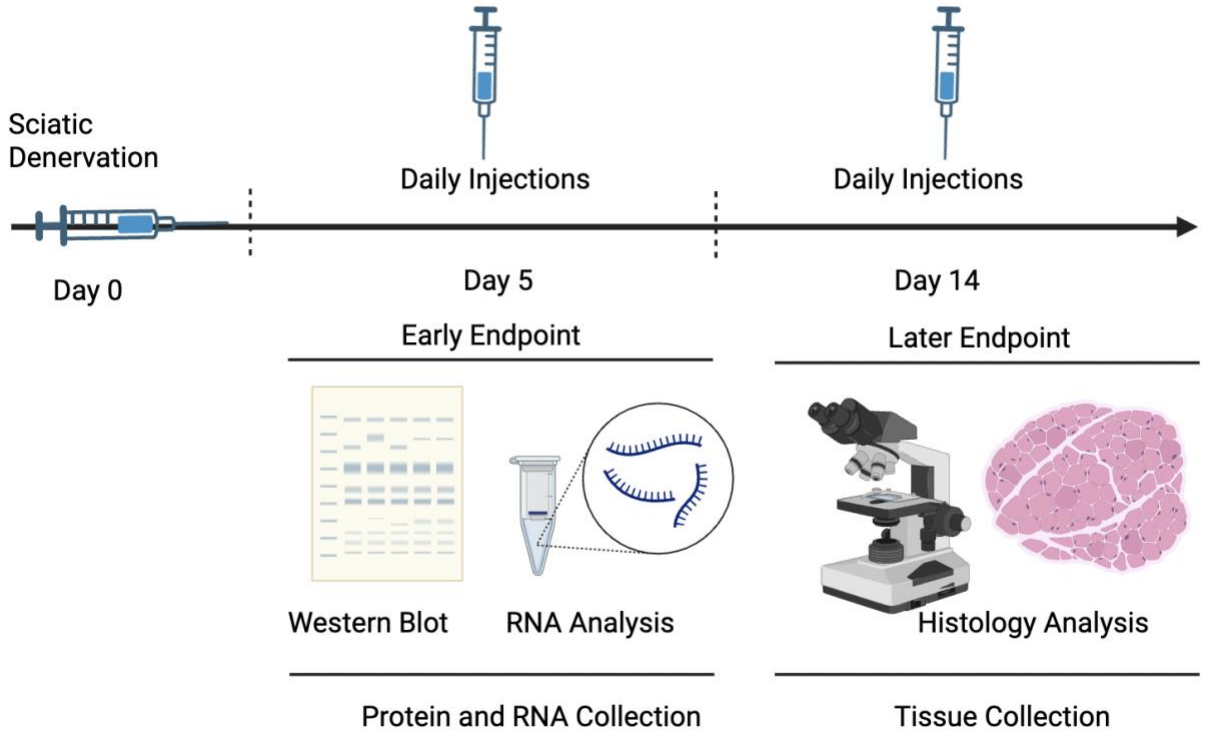

Figure 17. Experimental timeline showing daily drug administration and two collection endpoints.

Mice received daily intraperitoneal injections from Day 0 onward. One cohort was euthanized on Day 5 for early endpoint analyses, including protein extraction for Western blot and RNA isolation. A second cohort continued to receive daily injections until Day 14, at which point muscles were collected for histological assessment. This design enabled evaluation of both early molecular changes and later morphological outcomes following drug treatment. Created on BioRender.

Prior to sectioning, the cryostat (Thermo Scientific TS-HM525, MX-3531) was pre-cooled to -17 °C. Muscle samples were equilibrated inside the cryostat for at least 5 minutes. Excess OCT was trimmed from both ends of the muscle using a blade, and samples were mounted onto round metallic specimen holders using Tissue-Tek OCT. Frozen muscles were sectioned at a thickness of 10 μm at the midpoint region and mounted onto Superfrost Plus positively charged microscope slides (Fisherbrand, 25 × 75 × 1.0 mm). Each slide contained 5-6 serial muscle sections and was returned to a slide box within the cryostat immediately after sectioning. Slides were subsequently processed for hematoxylin and eosin (H&E) staining.

3.10 Histological Analysis and Myofiber Morphometry

Hematoxylin and Eosin (H&E) Staining of Frozen Tissue Sections

Frozen tissue sections were removed from -80 °C storage and allowed to air-dry at room temperature for 30 minutes. Once completely dried, slides were placed in a slide rack and immersed in filtered hematoxylin for 3-10 minutes, depending on staining intensity. Slides were then gently rinsed under running distilled deionized water (ddH_2O) for 2 minutes. Differentiation was performed by briefly dipping the slides several times in 1% acid alcohol solution (prepared as 5 drops of concentrated HCl in 250 mL of 70% ethanol). Slides were immediately rinsed again under running water for 2 minutes. To promote nuclear bluing, tissue sections were immersed in 1% lithium carbonate solution for 1 minute, followed by an additional 2-minute rinse in running water. Slides were then placed in 70% ethanol for 1 minute. Sections were counterstained with eosin for 90 seconds. To ensure uniform staining, slides were gently dipped and removed repeatedly for the full duration of the staining period. Following eosin staining, slides were dehydrated in 95% ethanol for approximately 30 seconds, taking care not to exceed this time, as prolonged exposure can result in loss of eosin staining. Complete dehydration was achieved by incubating slides in 100% ethanol twice for 2 minutes each. Slides were then cleared in toluene for 5 minutes under a chemical fume hood. Finally, tissue sections were mounted using 2-3 drops of Permount mounting medium and covered with 24 × 50 mm glass coverslips. Slides were allowed to dry prior to imaging and analysis.

Microscopic Imaging and Analysis

Slides were imaged using a Thermo Fisher Scientific EVOS FL Auto 2 microscopes equipped with a color camera and a 20X, 0.4 Numerial Aperture objective lens. For each experimental condition, 4-5 cross-sections per slide were imaged, resulting in the analysis of approximately 800-1,000 individual muscle fibers per condition. Image analysis was performed using Fiji/ImageJ and the Anaconda Navigator software (Version 4.1.0). Images were first imported into Fiji and uniformly cropped using identical dimensions across all samples to ensure consistency. The cropped images were then processed using a custom myofiber analysis workflow implemented through the Anaconda Python environment, using cellpose (version 3.0.11 - via Anaconda/pip) where individual myofiber boundaries were identified and segmented. Images representing both the

original cropped field and the corresponding segmented myofiber areas were generated and saved. The segmented images were subsequently re-imported into Fiji and analyzed using a dedicated plugin to quantify individual myofiber cross-sectional area (CSA). Mean CSA values were calculated for each condition and used to assess changes in muscle fiber size and evaluate potential drug-induced protection against denervation-induced muscle atrophy.

3.11 RNA Extraction and Quantitative PCR (qPCR) Analysis

RNA Extraction from Skeletal Muscle

Frozen skeletal muscle samples were pulverized and aliquoted into pre-labeled tubes designated for RNA isolation. 1 mL of Phenol:chloroform (Tripure) reagent was added to each sample, and samples were vortexed for 15 minutes at 2000 rpm at room temperature using a Vortex-Genie Plus (Scientific Industries) to ensure complete tissue homogenization. Samples were briefly centrifuged using an Eppendorf 5425 R centrifuge to collect condensation from the tube caps.

Subsequently, 200 µL of chloroform was added to each tube under a chemical fume hood, and samples were vortexed for 15-30 seconds. Phase separation was achieved by centrifugation at 13,000 rpm for 15 minutes at 4 °C. Following centrifugation, samples were separated into three distinct phases: an organic (pink) phase at the bottom, an interphase (white) in the middle, and an aqueous (clear) phase at the top. Approximately 400 µL of the aqueous phase was carefully transferred to a new tube containing 500 µL of 100% isopropanol and 1 µL of glycogen as a carrier. Samples were gently inverted 3-4 times to mix and incubated at room temperature for 10 minutes to allow RNA precipitation. Samples were then centrifuged at 13,000 rpm for 15 minutes at 4 °C, after which the supernatant was discarded. RNA pellets were washed with 500 µL of RNase-free 70% ethanol and centrifuged at 13,000 rpm for 10 minutes at 4 °C. This wash step was repeated once, and residual ethanol was carefully removed using a pipette. Pellets were allowed to air-dry under a fume hood for 10-15 minutes. Once fully dry, RNA pellets were resuspended in 32 µL of RNase-free water.

DNase Treatment for Genomic DNA Removal

RNA samples and reagents (Table 8) were thawed on ice, and a DNase master mix was prepared containing 2 µL of recombinant DNase I (rDNase I) and 10× DNase buffer per reaction. The

DNase master mix was added to 16 µL of RNA, and samples were gently mixed by pipetting. DNase digestion was performed by incubating samples in a 37 °C water bath for 30 minutes.

Following incubation, DNase activity was quenched by adding 6 µL of DNase inactivation beads to each sample, followed by vortexing for approximately 30 seconds. Samples were allowed to stand at room temperature for 2 minutes and then centrifuged at 13,000 rpm for 5 minutes at 4 °C. The supernatant (19 µL) containing DNase-treated RNA was carefully transferred to a new RNase-free 1.5 mL microcentrifuge tube, ensuring that no inactivation beads were carried over.

RNA concentration and purity were assessed using NanoDrop spectrophotometry. RNA integrity was evaluated by measuring the A260/A280 ratio, and samples with values between 1.8 and 2.0 were considered of high purity and suitable for downstream applications.

Table 5. DNase I treatment setup for genomic DNA removal from RNA samples.

Reagent (DNA-free DNA removal kit, AM1906)	**Volume per RXN (20ul RXN)**
rDNase I	2uL
10X DNase Buffer	2uL
RNA	16uL
Inactivation Beads	6uL (Added Post Reaction)

Reverse Transcription of RNA to cDNA

RNA concentrations were determined using NanoDrop spectrophotometry, and the sample with the lowest RNA concentration was used to calculate the maximum RNA mass that could be used within a 16 µL input volume. This RNA mass was then used for all samples to ensure that reverse transcription was performed using equal amounts of RNA for each reaction.

All reagents were thawed on ice, and the volume required to load the total RNA per reaction was calculated for each sample. Reaction components were prepared according to the composition listed in Table 9 using the All-In-One 5X RT MasterMix with gDNA Removal (Cat No. G592; Applied Biological Materials Inc.) and a mixture of oligo (dT) and random primers for cDNA synthesis. Components were combined in 0.2 mL PCR tubes. Nuclease-free water was added as

needed to achieve a final reaction volume of 20 µL. Reaction mixtures were briefly vortexed and centrifuged to ensure homogeneity.

Reverse transcription was performed using the following thermal cycling conditions: 25 °C for 10 minutes, 42 °C for 50 minutes, 85 °C for 5 minutes, followed by a 4 °C hold. Upon completion of the reaction, cDNA samples were transferred to 1.5 mL microcentrifuge tubes and diluted 1:10 by adding 180 µL of RNase-free water to 20 µL of cDNA.

Diluted cDNA samples were aliquoted into 100 µL volumes for long-term storage and 20-40 µL working stocks for short-term use and stored at appropriate temperatures for downstream applications.

Table 6. cDNA synthesis reaction setup using 5× All-in-One RT Mastermix (Abcam)

Reagent (Abcam)	**Volume per RXN (20ul RXN)**
5X All-in-One Master mix	4uL
RNA(1-2ug)	Up to 16uL
Water	Varies up to 16uL
Final Volume	20uL

Quantitative PCR (qPCR) Reaction Setup

A qPCR master mix was prepared according to the composition listed in Table 10, excluding cDNA. qPCR reaction tubes were labeled with their corresponding sample identifiers, and 16 µL of master mix, containing SYBR Green Master Mix, STAU1 forward and reverse primers, and nuclease-free water was dispensed into each tube. Subsequently, 4 µL of cDNA was added to the appropriate tubes to achieve a final reaction volume of 20 µL.

Reaction mixtures were briefly vortexed and centrifuged to ensure homogeneity and to collect contents at the bottom of the tubes. Tubes were then placed into a QuantStudio™ 3 Real-Time PCR System (Applied Biosystems, Thermo Fisher Scientific) for amplification and fluorescence detection.

Table 7. qPCR reaction setup for STAU1 and GAPDH gene expression analysis.

Reagent	Volume per sample (20 µL RXN)
SSoAdvanced Universal SYBR Green MasterMix	10
STAU1 Forward Primer (5'-TGC AAG CTA CAG ACA GCC C-3')	0.8
STAU1 Reverse Primer (5'-GGC TGT GAG GAG CAG TTG AT-3')	0.8
GAPDH Forward Primer (5'- TAC TGA CCA CAG TCC ATG CC -3')	0.8
GAPDH Reverse Primer (5' - TCA TAC TTG GCA GGT TTC TCC A -3)	0.8
cDNA	4
Nuclease-free Water	4.4

3.12 Protein Extraction and Western Blot Analysis

Tissue Pulverization for Protein

Approximately 2-3 kg of dry ice was obtained from the University of Ottawa Supply. All materials and tools were thoroughly cleaned with RNaseZap to prevent RNA degradation. The tissue pulverizer was disassembled and prechilled on dry ice for at least 15 minutes prior to use. Scraping tools and spatulas were prechilled in liquid nitrogen using a benchtop Dewar. The tissue pulverizer was assembled, ensuring that no frozen condensation was present on the crushing surfaces. Individual muscle samples were processed one at a time. A single muscle was placed in the center of the pulverizer, followed by the insertion of the piston. The sample was immediately crushed using two moderate strikes with a hammer to ensure complete pulverization. The piston was gently removed, and the crushed tissue was inspected to confirm that it was not adhered to the crushing surfaces. The compressed tissue powder was scraped into the center puck and further broken into small fragments (~1-2 mm). Pulverized tissue fragments were transferred into their respective prechilled, labeled microcentrifuge tubes designated for protein, RNA, or stock storage. Following transfer, samples were immediately returned to dry ice. All surfaces and tools were wiped thoroughly with 100% isopropanol to remove residual tissue powder. These steps were repeated for each sample, with careful cleaning between samples to prevent cross-contamination. Aliquoted

tissue samples designated for protein and RNA isolation were stored for downstream processing, and all individual sample stocks were returned to -80 °C for long-term storage.

Protein Isolation and Quantification by CB-X (Gbiosciences)

First, 10mL of 1.25X UREA-Thiourea mix was prepared using urea, thiourea, and water. If not used the same day, the solution was stored at -20 °C. Next,10mL of MEU buffer was prepared using 100mM DTT, 125mM Tris-HCL 6,8pH, 1.25X urea-thiourea, PIC and phosphor-stop, and water for protein isolation.

Protein Solubilization Using MEU Buffer

Aliquoted protein samples were retrieved from -80 °C storage and placed on ice. 300 µL of freshly prepared MEU buffer was added to each sample. Samples were vortexed for 30 minutes at room temperature using a pulsed vortexing protocol (30 s vortex, 10 s pause at 2000 rpm) to ensure efficient protein solubilization. Following vortexing, samples were centrifuged at 16,000 × g for 15 minutes at 4 °C. The supernatant containing solubilized protein was carefully transferred into a new 1.5 mL microcentrifuge tube, avoiding disturbance of the small cream-to-white pellet present at the bottom of each tube. Protein samples were either maintained on ice for immediate downstream processing or stored at -80 °C for long-term storage.

CB-X Protein Clean-Up/Quantification

Protein samples were retrieved from -80 °C storage and immediately placed on ice. 20 µL of each sample stock was transferred into a new 1.5 mL microcentrifuge tube, after which 1 mL of CB-X precipitation buffer was added. Tubes were capped immediately and briefly vortexed to disrupt the solution, promoting protein precipitation. Formation of a white protein precipitate was visually confirmed. Samples were centrifuged at 16,000 × g for 5 minutes at 4 °C. The supernatant was carefully removed, and tubes were left uncapped for 1-2 minutes to allow residual solvent to evaporate. As the solution contained acetone, all steps were performed under a chemical fume hood to minimize vapor exposure. Once fully dried, protein pellets were resuspended in 100 µL of CB-X Solubilizer Buffers 1 and 2 mixed at a 1:1 ratio. Samples were vortexed for 10 minutes at room temperature using a pulsed setting (30 s vortex, 10 s pause at 2000 rpm) to ensure complete solubilization of the protein pellet, which may vary depending on protein concentration. A 1:2 serial dilution of a 2.0 mg/mL CB-X protein standard was prepared to generate a standard curve ranging from 2.0 mg/mL to 0.0625 mg/mL (Figure 21). Experimental samples were diluted 1:5 by

mixing 10 µL of sample stock with 40 µL of distilled water. For quantification, 10 µL of each sample and standard was transferred in triplicate to a 96-well plate, followed by the addition of 200 µL of CB-X assay dye to each well. The plate was incubated for 5 minutes at room temperature with gentle agitation. Absorbance was measured at 595 nm using a microplate reader to determine protein concentration based on the standard curve. The CB-x precipitation was performed to accurately estimate protein concentration of High salt solution used for MEU protein extraction.

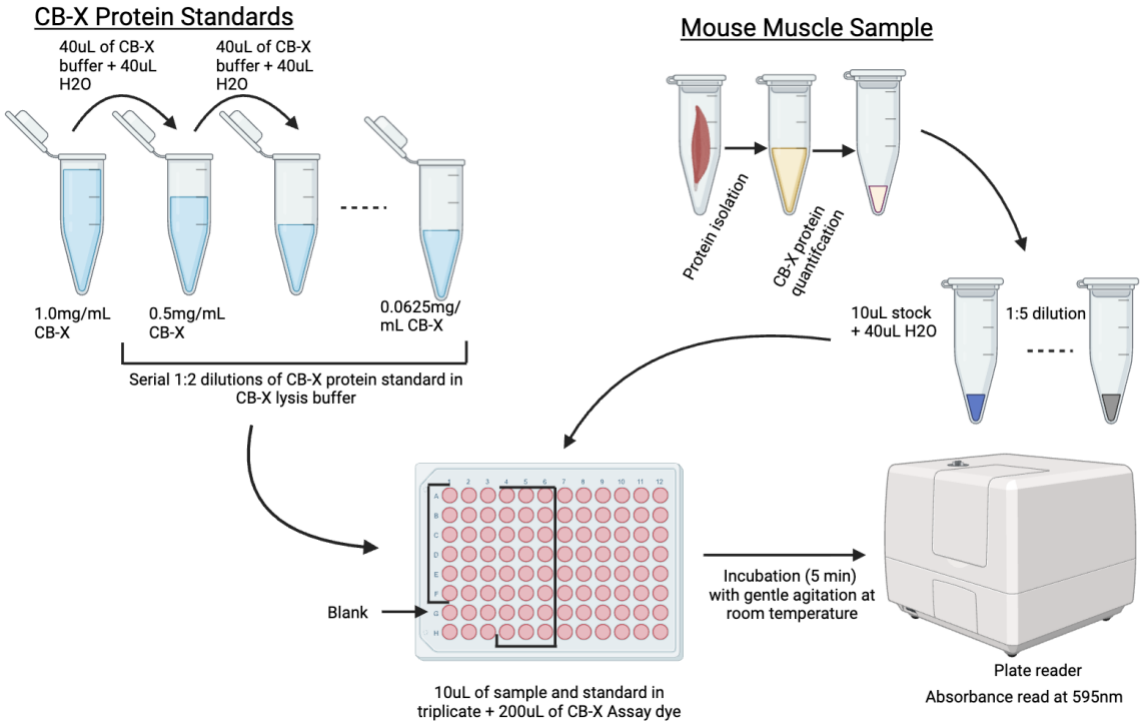

Figure 18. CB-X-based protein quantification workflow for in vivo skeletal muscle samples.

Skeletal muscle samples were subjected to protein isolation and precipitation, followed by centrifugation (16,000 × g, 5 min, 4 °C) to obtain protein pellets. In parallel, a CB-X protein standard curve was generated using a 1:2 serial dilution of a 2.0 mg/mL protein standard prepared in CB-X lysis buffer, ranging from 2.0 to 0.0625 mg/mL, with a blank included. The absorbance was measured at 595 nm using a microplate reader to determine protein concentration. Image created in BioRender.

Western Blot Run and Transfer

Following protein quantification, samples were normalized to equal protein concentrations and analyzed to determine STAU1 protein expression in vivo. Western blotting of muscle samples was performed using the same procedures described in Section 3.1.5, including gel electrophoresis, protein transfer, membrane blocking, antibody incubation, and signal detection.

4. Results

4.1. Investigating the Effect of FDA-Approved Drugs on STAU1 Expression in Starved C2C12 Myotubes

4.1.1. Effects of Drug 12 and Drug 15 on STAU1 Protein Expression in C2C12 Cells

A high-throughput screen of FDA-approved drugs revealed numerous candidates that might lower STAU1 expression while maintaining cell viability, as described in Sections 1.8 and 1.9. Five of these compounds consistently showed downregulation of STAU1 protein levels (Figure 12A). The top three candidates, Drugs 11, 12, and 15 reduced starvation-induced muscle atrophy, based on subsequent evaluation in C2C12 myotube atrophy in vitro model. The current work focuses on the molecular effects of Drugs 12 and 15 as Drug 11 is currently being studied by Marc Charron in our laboratory.

Aim 1 focused on determining whether selected FDA-approved drug candidates modulate STAU1 protein expression. Western blot analysis was performed to determine whether Drug 12 and Drug 15 modulate STAU1 protein expression in differentiated C2C12 myotubes. As shown in Figure 22A, two distinct STAU1 bands were detected at approximately 63 kDa and 55 kDa, consistent with the previously reported STAU1 isoforms (Ravel-Chapuis et al., 2014; Quesada, and DesGroseillers, 2022). β-actin (42 kDa) was used as a loading control.

Quantification of the 63 kDa (Figure 22B) and 55 kDa (Figure 22C) isoform showed a decreasing trend of STAU1 levels when treated with Drug 12; however, this reduction did not reach statistical significance relative to the control. When both isoforms were combined for total STAU1 quantification (Figure 22D), Drug 12 treatment produced a slight reduction in total STAU1 expression, but this change was not statistically significant. In addition, Drug 15 revealed a significant reduction in STAU1 protein levels compared to control ($p < 0.05$) at 63 kDa and 55kDa. Drug 15-treated cells showed a significant decrease in STAU1 abundance compared to control ($p < 0.05$) when the quantification of both isoforms was combined (figure 22D). Together, these results indicate that Drug 12 exhibits a milder, non-significant effect,

affecting both the 63 kDa and 55 kDa isoforms, while Drug 15 significantly reduces STAU1 protein expression in differentiated C2C12 myotubes.

These results were derived from six independent biological replicates (n = 6), with three experiments conducted by Marc Charron and three conducted by the author, demonstrating reproducibility of the observed effects across independent experiments sets.

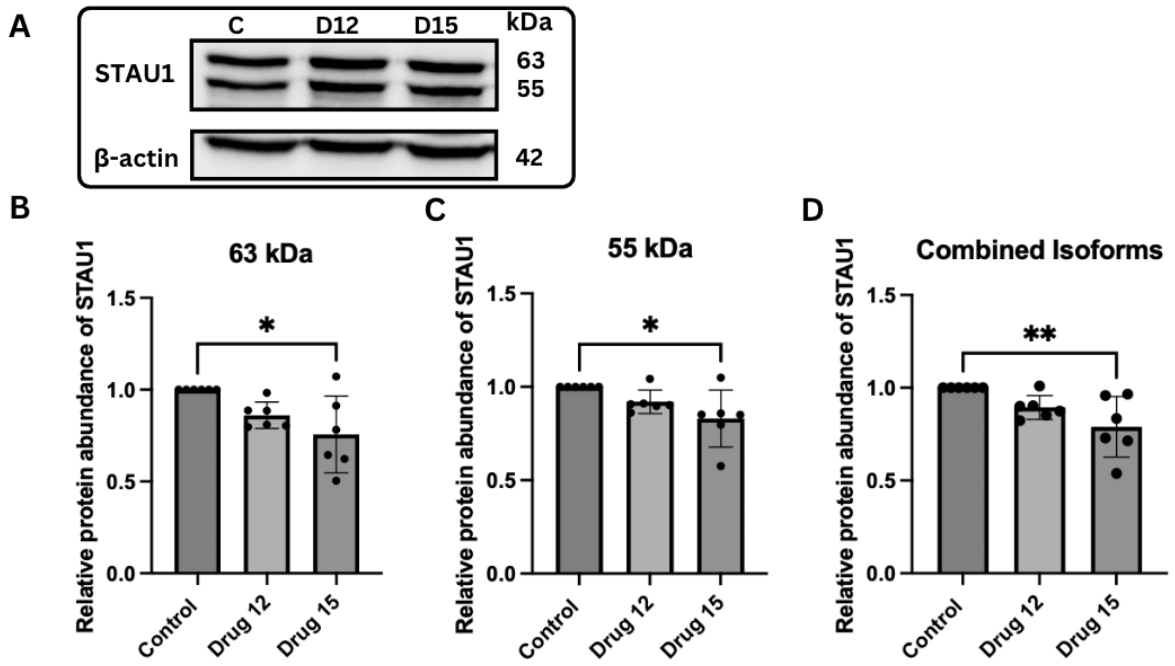

Figure 19. Effects of Drug 12 and Drug 15 reduce STAU1 protein expression in differentiated C2C12

(A) Representative Western blot showing STAU1 protein levels following 1-hour treatment with Drug 12 or Drug 15 compared to untreated control. Two STAU1 isoforms are detected at approximately 63 kDa and 55 kDa. β-actin (42 kDa) was used as a loading control.
(B) Quantification of the 63 kDa STAU1 isoform relative to β-actin.
(C) Quantification of the 55 kDa STAU1 isoform relative to β-actin.
(D) Combined quantification of both STAU1 isoforms.

Data are presented as mean ± SEM from independent experiments (n = 6). Statistical significance was determined using one-way ANOVA, where $p < 0.05$ (*) and $p < 0.01$ (**).

4.1.2. Drug 12 and Drug 15 Attenuate Starvation-Induced Upregulation of STAU1 mRNA

To determine whether pharmacological treatments influence STAU1 expression at the mRNA level, STAU1 transcript levels were measured by quantitative PCR in C2C12 myotubes following starvation. Gene expression analysis was conducted by Marc Charron (PhD student) in our lab. Relative STAU1 mRNA levels were normalized against the expression of a housekeeping gene, GAPDH, and compared to those of non-starved control condition.

C2C12 myoblasts were differentiated into myotubes for four days before treatment. Differentiated myotubes were then treated with Drugs 12 and 15 at final concentration of 1 μM or DMEM as a control for 1 hour. Following this treatment, cells were incubated for 6 hours in either differentiation medium or starvation medium to induce atrophic conditions. At 5 hours into the starvation period, a separate set of myotubes maintained in differentiation medium (non-starved group) received the same 1-hour drug treatment. All samples were collected at the 6-hour timepoint for subsequent analysis (Figure 14)

Treatment with Drug 12 or Drug 15 under non-starved conditions did not lead to a significant alteration in STAU1 expression compared to untreated controls, implying that these compounds mainly function to inhibit stress-induced upregulation of STAU1 rather than affecting its basal expression (Figure 23). As expected, starvation significantly increased STAU1 mRNA expression, with approximately a 2.9-fold elevation compared to non-starved control group ($p < 0.01$). Treatment with Drug 12 significantly reduced STAU1 mRNA levels during starvation compared to non-treated starved cells ($p < 0.05$), bringing expression levels back to those like non-starved controls (Figure 23). Likewise, Drug 15 diminished the increase in STAU1 expression induced by starvation, with a significant reduction noted relative to non-treated starved cells ($p < 0.01$).

Note that the 55 kDa ($STAU1^{55}$) and 63 kDa ($STAU1^{63}$) isoforms of STAU1 are both detected by the STAU1 primers used in this investigation because they are not isoform specific. This technique was chosen because it is challenging to create primers that can distinguish between the two isoforms without affecting amplification efficiency as they are produced by alternative splicing of the same STAU1 gene and have a high degree of sequence homology (Duchaine et

al., 2002; Wickham et al., 1999). As a result, rather than reflecting isoform-specific regulation, the qPCR findings represent total STAU1 expression.

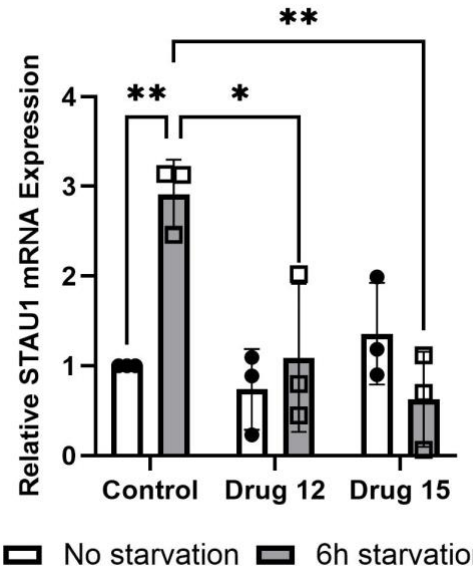

Figure 20. Drug 12 and Drug 15 reduce starvation-induced STAU1 mRNA expression.

Relative STAU1 mRNA levels were measured by qPCR in C2C12 myotubes under control and starvation conditions following 1 hour of drug treatment. Data are expressed relative to non-treated controls and analyzed by two-way ANOVA with appropriate post hoc comparisons. *$p < 0.05$, **$p < 0.01$. Individual biological replicates are shown as dots.

4.1.3 Drug 12 and Drug 15 Attenuate Starvation-Induced Myotube Atrophy

To determine whether pharmacological reduction of STAU1 contributes to protection against skeletal muscle atrophy, myotube diameter was assessed in differentiated C2C12 myotubes using immunofluorescence staining with anti-myosin heavy chain (MF20 antibody) following starvation. Myotubes were prepared and treated as described in Section 4.1.2 (Figure 14). Cells received either vehicle control, Drug 12, or Drug 15 for 1 hour under non-starved conditions or following 6 hours of starvation.

Representative immunofluorescence shows myotubes in the 6-hour starvation control group and drug treatment post-starvation (Figure 24A). In line with an atrophic response, starvation for 6 hours resulted in an approximate 30% reduction in myotube diameter in control cell group (Figure 24B) compared to the non-starved control group ($p < 0.01$), confirming a strong

induction of myotube atrophy. Conversely, treatment with Drug 12 notably reduced the starvation-induced decrease in myotube diameter ($p < 0.05$). Likewise, Drug 15 treatment preserved myotube diameter after starvation, with a significant protective effect observed in comparison to 6-hour starvation control myotubes ($p < 0.05$) (Figure 24B).

However, neither Drug 12 nor Drug 15 altered myotube diameter under no starvation conditions, suggesting that these compounds do not cause hypertrophic or atrophic effects under basal conditions. The myotube diameter results indicate that Drug 12 and Drug 15 provide significant protection against myotube atrophy induced by starvation. The effects of treatment on key atrogenes, including MuRF1 and Atrogin-1, were also assessed; however, their expression

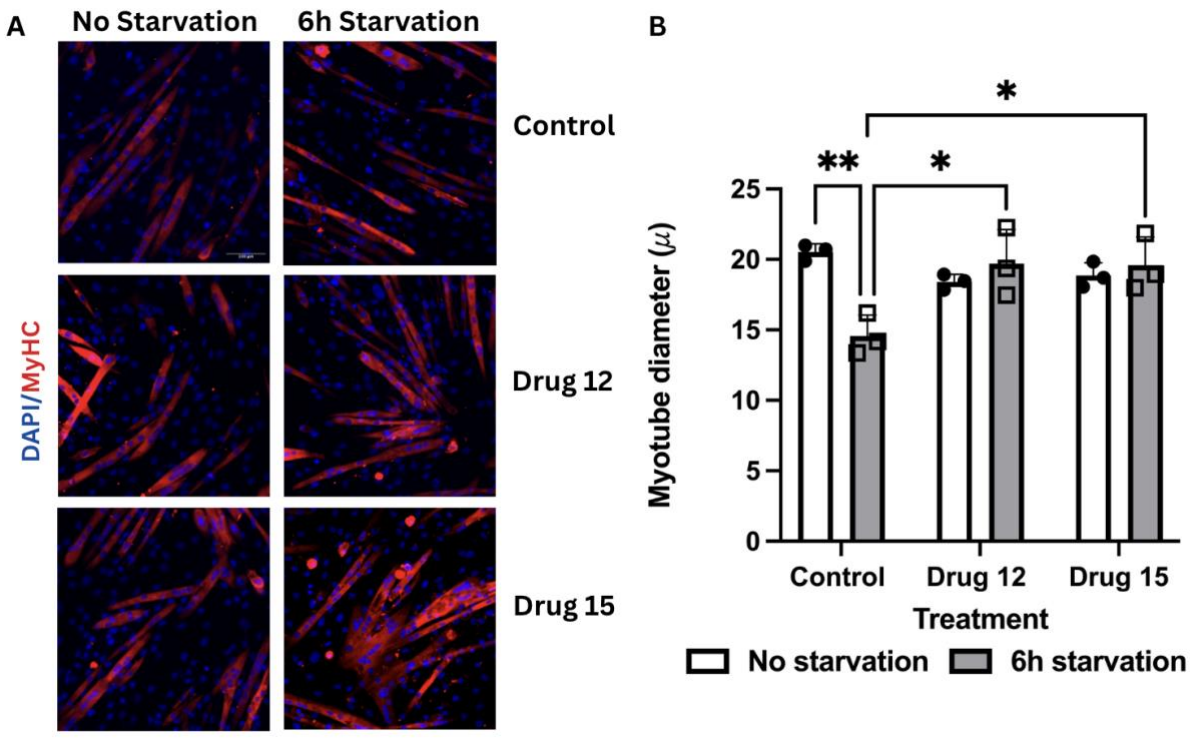

Figure 21. Drug 12 and Drug 15 attenuate starvation-induced myotube atrophy in differentiated C2C12 myotubes.

(A) Representative immunofluorescence images of differentiated C2C12 myotubes under non-starved conditions and after 6 h of starvation media. Myotubes were treated for 1 h with vehicle (Control), Drug 12, or Drug 15 before incubation in differentiation medium or starvation medium. Myosin heavy chain is shown in red and nuclei (DAPI) in blue. Scale bar = 100 µm.
(B) Quantification of myotube diameter (µm).

Data are presented as mean ± SEM from independent experiments. Statistical analysis was performed using two-way ANOVA. *$p < 0.05$, **$p < 0.01$.

showed variability across treatment conditions, and no consistent pattern was observed (data not shown).

In summary, when considered alongside the observed reduction trend of Drug 12 and a significant decrease of Drug 15 in STAU1 protein levels and the significant decrease of both drugs at the mRNA levels under starvation, these findings support a functional relationship between STAU1 downregulation and the preservation of myotube integrity following drug treatment during the early stages of atrophic stress. Collectively, these in vitro results demonstrate that pharmacological reduction of STAU1 using FDA-approved drugs helps maintain myotube diameter under atrophic conditions, providing a strong rationale to next assess whether these protective effects translate to an in vivo model of skeletal muscle atrophy induced by sciatic nerve denervation.

4.2.1 Assessing the Therapeutic Potential of FDA-Approved Drugs Targeting STAU1 in a Mouse Model of Denervation-Induced Muscle Atrophy

4.2.1.1 Baseline STAU1 expression across tissues and skeletal muscle types

The baseline distribution of STAU1 protein levels across skeletal muscle tissues prior to examining its regulation during denervation-induced atrophy was determined. Western blot analysis was performed on protein lysates obtained from the tibialis anterior (TA), extensor digitorum longus (EDL), soleus (SOL), and gastrocnemius (GAS) from both male and female mice. Two distinct STAU1 isoforms were consistently detected at approximately 63 kDa and 55 kDa across all samples, with ponceau staining used to assess total STAU1 protein (Figure 25A).

The 63-kDa STAU1 isoform was quantified and shown to be relatively low in both male and female TA, whereas greater mean levels were found in a few other muscle groups, most notably the male and female SOL and GAS muscles. However, there was no noticeable sex-dependent pattern and substantial animal variability within a few of groupings, primarily the SOL muscles (Figure 25B).

There was greater variation in the 55-kDa STAU1 isoform amongst muscle groups. In females, the EDL and SOL showed higher mean abundance than the TA, with the SOL showing the greatest mean amount. In comparison to the TA, the 55-kDa isoform also seems to be more prevalent in the EDL, SOL, and GAS in men. Again, there was a great deal of variation, especially in the female SOL group (Figure 25C).

The 55- and 63-kDa isoforms were also assessed together to see if the total STAU1 abundance followed these isoform-specific patterns (Figure 25D). The combined STAU1 abundance showed greater in the EDL and SOL, with the female SOL showing the highest mean abundance, and was lowest in the TA muscles of both sexes. However, sex or muscle-specific differences are limited by the biological replicates to make solid conclusion. Together, our preliminary findings imply that baseline STAU1 protein abundance may differ among skeletal muscle types and encourage more research with larger cohorts to determine if sex or muscle fiber composition affects STAU1 expression.

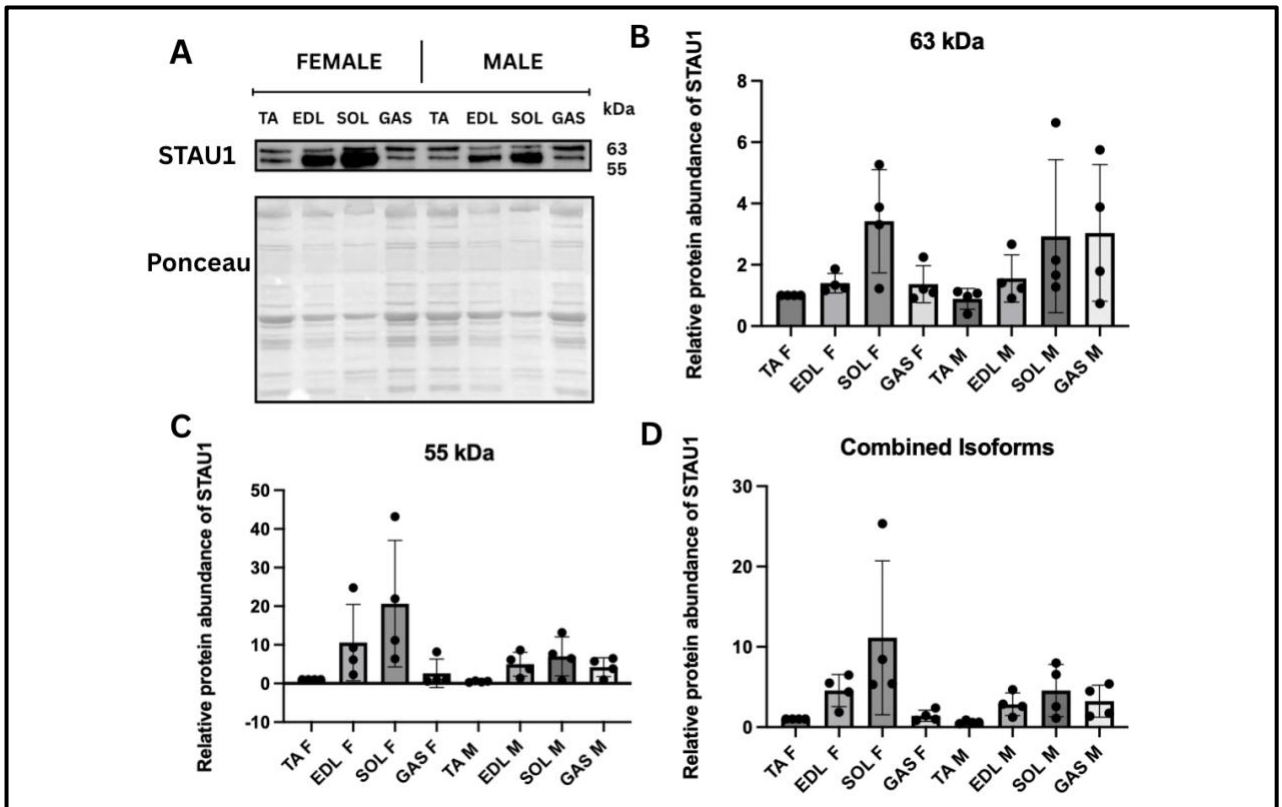

Figure 22. Baseline distribution of STAU1 protein across different skeletal muscle tissues in male and female mice.

(A) Representative Western blot showing STAU1 isoforms (~63 kDa and ~55 kDa) detected in the tibialis anterior (TA), extensor digitorum longus (EDL), soleus (SOL), and gastrocnemius (GAS) from male (M) and female (F) mice. Ponceau S staining is shown as a total protein loading control.
(B) Quantification of STAU1 protein level at 63 kDa normalized to total protein (Ponceau).
(C) Quantification of STAU1 protein level at 55 kDa normalized to total protein (Ponceau)
(D) Quantification of combined STAU1 isoforms

4.2.1.2 Effects of Sciatic Denervation and Drug 12 on STAU1 Protein Abundance In Vivo

Twelve-week-old FVB/N mice underwent unilateral sciatic nerve denervation on day 0, in which a small segment of the sciatic nerve was excised from the left leg (Figure 18). The right leg of the individual mouse was used as a control group (innervated). Following recovery from anesthesia, mice received daily intraperitoneal injections of Drug 12 (1.0 mg/kg) beginning 2-3 hours post-surgery (Figure 19).

To determine whether STAU1 protein expression is altered early during denervation-induced skeletal muscle atrophy and whether Drug 12 modulates this response, Western blot analysis was

performed on tibialis anterior muscles collected at day 5 post-denervation (Figure 26). Day 5 was selected as previous work from our laboratory has demonstrated that STAU1 levels increase in denervated muscle within the first week, with a marked rise occurring at days 3, 5, and 7 following nerve injury, consistent with published reports showing STAU1 upregulation in response to denervation-induced atrophic stress (Belanger et al., 2003; Parks et al., 2017).

As shown in Figure 26A, two distinct STAU1 bands corresponding to the 63 kDa and 55 kDa isoforms were detected. Ponceau stain for the total protein staining was used for normalization rather than a single housekeeping protein because commonly used loading controls (e.g., GAPDH, β-actin, α-tubulin) are themselves altered during denervation-induced skeletal muscle atrophy. Denervation triggers broad remodeling of cytoskeletal and metabolic proteins, and several reports have shown that the expression of traditional housekeeping proteins is not stable under atrophic or stress conditions, making them unreliable for accurate normalization (Aldridge et al., 2008). In contrast, total protein normalization using Ponceau stain provides a more consistent and unbiased method to correct for loading variability across lanes, particularly in models where global protein expression patterns are changing (Eaton et al., 2013).

Quantification of the 63 kDa isoform (Figure 26B) revealed a significant increase in STAU1 protein levels in saline-treated denervated (Sal DEN) muscles compared to saline-treated innervated controls (Sal INN) ($p < 0.01$). This represents an approximate ~1.7-fold increase in the 63 kDa STAU1 isoform at day 5 following denervation. Next, treatment with Drug 12 in denervated mice (D12 DEN) did not significantly reduce this elevation, as levels remained comparably high to saline denervated group ($p < 0.01$). In contrast, analysis of the 55 kDa isoform (Figure 26C) showed greater variability and not statistically significant indicating a decreasing trend between Drug 12 denervated group (D12 DEN) and saline denervated group (Sal DEN). When both isoforms were combined (Figure 26D), overall STAU1 protein abundance was significantly elevated in saline denervated muscles compared to saline innervated ($p < 0.05$). Drug 12 treatment showed a trend toward reduction but did not reach statistical significance at this early time point.

Together, these findings demonstrate that STAU1 protein expression is significantly elevated as early as day 5 following denervation, however, Drug 12 does not yet attenuate this early increase at this stage of atrophy progression.

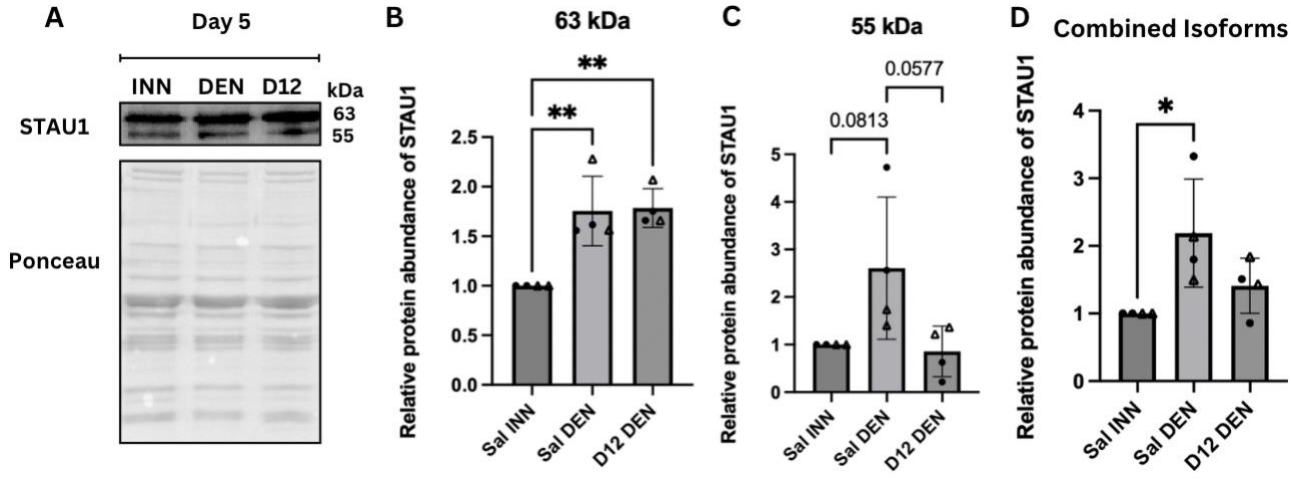

Figure 23. Early modulation of STAU1 protein expression following sciatic denervation and Drug 12 treatment at Day 5.

(A) Representative Western blot showing STAU1 isoforms (63 kDa and 55 kDa) in tibialis anterior muscles from saline-innervated controls (Sal INN), saline-denervated mice (Sal DEN), and Drug 12 treated denervated mice (D12 DEN) at Day 5 post-denervation. Total protein loading was verified using Ponceau S staining.
(B) Quantification of the 63 kDa STAU1 isoform
(C) Quantification of the 55 kDa STAU1 isoform
(D) Combined quantification of both STAU1 isoforms.

Individual data points represent biological replicates from male (triangles) and female (circles) mice. Data are presented as mean ± SEM, n = 4 biological replicates per group (both sexes included). Statistical analysis was performed using one-way ANOVA. *p < 0.05, ***p < 0.01; ns, not significant.*

4.2.1.3 Effects of Sciatic Denervation and Drug 12 on STAU1 mRNA Expression In Vivo

To assess if Drug 12 affects STAU1 expression at the transcript level after neurogenic atrophy, STAU1 mRNA levels were measured in skeletal muscle five days following sciatic nerve denervation. Gene expression levels were normalized against a housekeeping gene, GAPDH, and presented relative to controls from the innervated saline group. Even though atrophic stimuli can influence housekeeping genes, GAPDH expression in our investigation was steady under all experimental circumstances, as demonstrated by minimal variation in Ct values across groups. GAPDH was therefore chosen an appropriate internal control for transcript-level normalization based previous experiments performed for drug 11.

As noted in the protein level, sciatic denervation led to a ~3.4-fold increase in STAU1 mRNA expression when compared to the saline innervated muscles (Sal INN), indicating that STAU1 is upregulated during the early stages of atrophy caused by denervation. However, noticeable variability among individual animals was found in the denervated group, and this increase did not achieve statistical significance *(p = 0.1491)*. Treatment with Drug 12 reduced STAU1 mRNA levels in denervated muscle to ~1.8-fold, corresponding to an approximate 45% reduction relative to saline-denervated muscle. Although this trend suggests partial normalization of STAU1 expression with Drug 12 treatment, the difference between saline denervated (Sal DEN) and Drug 12 denervated (D12 DEN) was not statistically significant (*p = 0.4180*). Likewise, comparison between saline-innervated (Sal INN) and D12 DEN showed no significant difference.

Overall, these results indicate that STAU1 mRNA levels tend to increase early during denervation-induced atrophy, and Drug 12 treatment shows a trend toward moderating this response, although statistical significance was not reached at this early time point. These findings are consistent with the combined STAU1 isoform protein data (Figure 26D) and suggest that short-term Drug 12 treatment may be insufficient to substantially modulate STAU1 expression in vivo during the early stages of denervation-induced muscle atrophy.

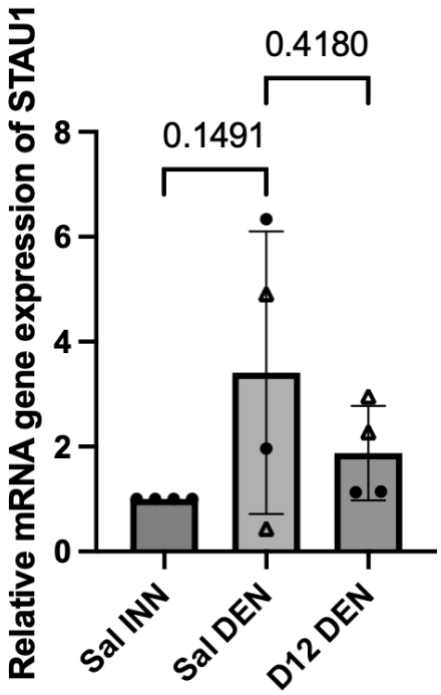

Figure 24. STAU1 mRNA expression in tibialis anterior muscle at day 5 following sciatic denervation.

Quantitative PCR analysis of STAU1 mRNA levels in the tibialis anterior muscle including saline innervated control (Sal INN), saline-treated denervated (Sal DEN), and Drug 12–treated denervated (D12 DEN) tibialis anterior muscles. STAU1 transcript levels were normalized to GAPDH and expressed relative to saline innervated control. Individual data points represent biological replicates from male (triangles) and female (circles) mice. Data are presented as mean ± SD, n = 4 biological replicates per group (both sexes included). Statistical analysis was performed using one-way ANOVA followed by Tukey's post hoc test.

4.2.1.4 Effects of Sciatic Denervation and Drug 12 on Myofiber Cross-Sectional Area

Sciatic denervation was performed on day 0 in 12-week-old FVB/N mice. Animals received daily intraperitoneal injections of Drug 12 (1.0 mg/kg), starting 2-3 hours post-surgery and continuing for 14 consecutive days (Figure 18 and 19). A two-week treatment period was selected to allow sufficient progression of denervation-induced muscle atrophy in saline-treated animals, characterized by pronounced reductions in muscle mass and myofiber size, thereby providing a clearer window to assess the protective effects of Drug 12 on muscle preservation.

At 14 days following sciatic denervation, clear morphological evidence of muscle atrophy was observed in saline-treated animals, as shown by hematoxylin and eosin-stained cross-sections of tibialis anterior muscle (Figure 28A). Denervated saline muscles exhibited visibly smaller and more angular myofibers compared to their innervated counterparts. Muscles from Drug 12-treated animals displayed similar fiber morphology as the saline denervated (Sal DEN) following denervation.

Quantitative analysis of mean cross-sectional area (CSA) confirmed these observations (Figure 28B). In saline-treated animals, denervation caused a significant reduction in mean CSA compared to innervated control group ($p<0.001$), corresponding to an approximate 42% decrease in fiber size. Drug 12-treated innervated mouse muscle samples showed CSA values comparable to saline innervated controls, indicating that the drug itself did not alter baseline muscle morphology. In the case of denervated muscles, the treatment with Drug 12 did not significantly maintain myofiber CSA compared to the denervated muscles treated with saline. The mean CSA was still significantly lower when compared to the innervated controls, and no notable statistical significance was present between the saline denervated and drug 12 denervated groups.

These differences were further reflected in the calculated atrophy percentage (Figure 28C). At day 14, saline denervated group resulted in approximately 45% atrophy relative to innervated muscle ($p<0.001$) (Figure 28C). Consistent with the mean CSA observation, the calculated atrophy percentage in Drug 12 denervated mice muscle was not significantly different from saline denervated muscle. No significant differences were observed between saline and Drug 12 innervated groups, confirming that Drug 12 alone does not affect myofiber size under normal conditions.

In summary, Drug 12 did not significantly decrease STAU1 protein and mRNA levels during the early stages following denervation. It did not mitigate muscle loss at day 14 and therefore does not confer protection against denervation-induced skeletal muscle atrophy.

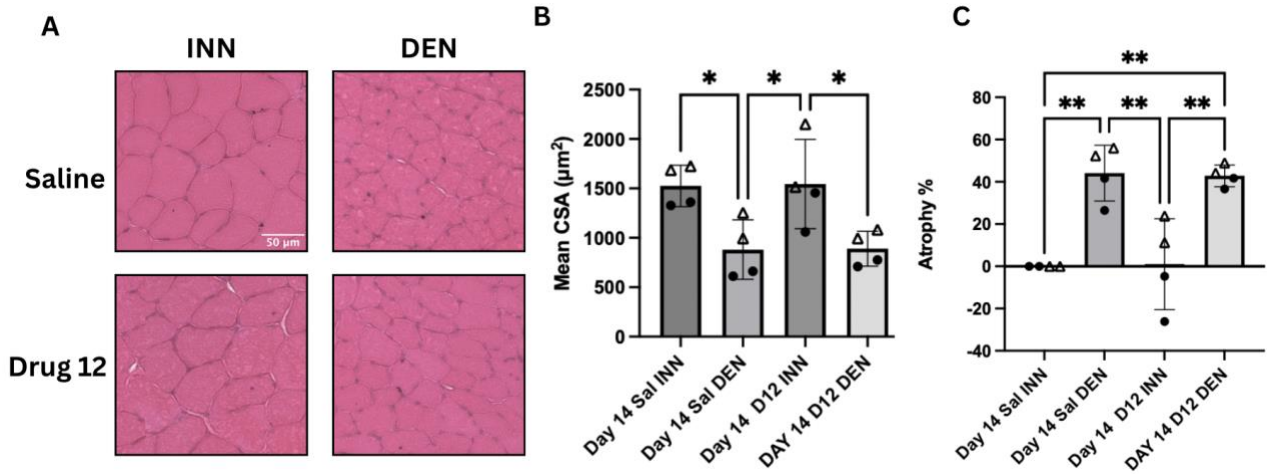

Figure 25. Effect of Drug 12 on myofiber size and atrophy 14 days after sciatic denervation.

(A) Representative H&E-stained transverse sections of tibialis anterior muscle from saline and Drug 12-treated mice under innervated (INN) and denervated (DEN) conditions at day 14 post-surgery. Scale bar = 50 µm.
(B) Quantification of mean myofiber cross-sectional area (CSA).
(C) Percent atrophy relative to Saline innervated.

Individual data points represent biological replicates from male (triangles) and female (circles) mice. Data are presented as mean ± SD, n = 4 biological replicates per group (both sexes included). Statistical analysis was performed using one-way ANOVA with post-hoc multiple comparisons.

4.2.2 Assessing the Therapeutic Potential of FDA-Approved Drugs Targeting STAU1 in a Mouse Model of Denervation-Induced Muscle Atrophy

4.2.2.1 Effects of Sciatic Denervation and Drug 15 on STAU1 Protein Abundance In Vivo

We further assessed whether Drug 15 could enhance modulation of STAU1 expression and provide better protection after sciatic nerve injury. Given the in vitro results indicating that Drug 15 significantly lowered STAU1 levels and reduced myotube atrophy, this compound was chosen for further in vivo study to evaluate whether these effects carry over to a model of skeletal muscle atrophy induced by denervation.

To determine whether Drug 15 modulates STAU1 protein expression during the early phase following sciatic denervation, western blot analysis was performed and collected at day 5 post-denervation (Figure 19). Representative blots and Ponceau normalization are shown in Figure 29A. Quantification of the 63 kDa isoform (Figure 29B) showed Drug 15 treated denervated (D15 DEN) muscle displayed a reduction in STAU1 levels relative to vehicle denervated (Veh DEN) but this difference was not significant ($p = 0.4114$). A similar pattern was observed for the 55 kDa isoform (Figure 29C). Drug 15 treatment did not significantly alter STAU1 expression compared to vehicle denervated (Veh DEN), ($p = 0.3158$), nor compared to vehicle inverted (Veh INN). When both isoforms were combined (Figure 29D), Drug 15 treatment did not significantly reduce STAU1 levels compared to vehicle denervated group (Veh DEN), ($p = 0.3550$).

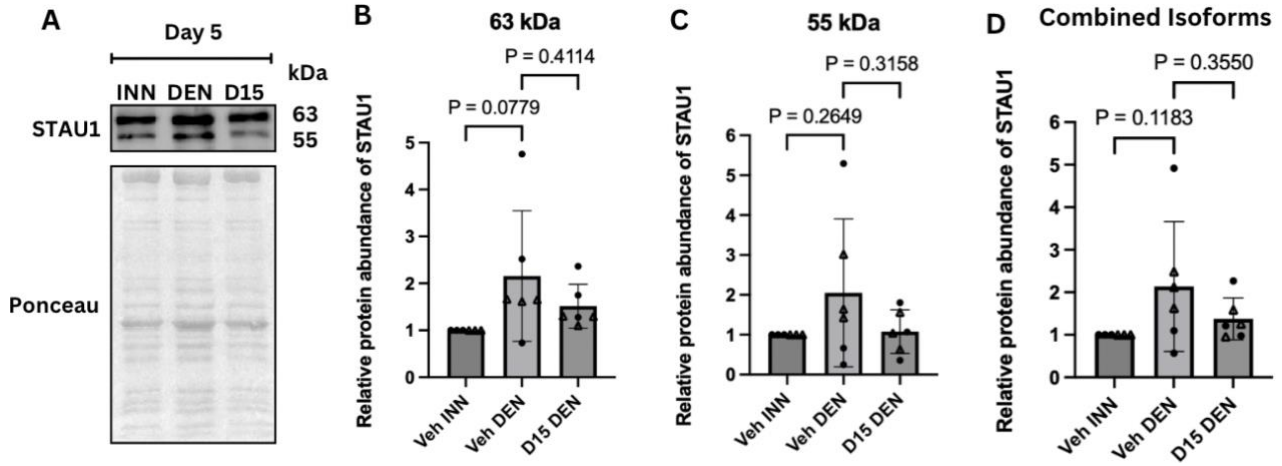

Figure 26. Effect of Drug 15 on STAU1 protein expression at day 5 following sciatic denervation.

(A) Representative Western blot showing STAU1 isoforms (~63 kDa and ~55 kDa) in tibialis anterior muscle from vehicle-innervated (Veh INN), vehicle-denervated (Veh DEN), and Drug 15-treated denervated (D15 DEN) mice at day 5 post-denervation. Ponceau staining was used to verify equal protein loading.
(B) Quantification of the 63 kDa STAU1 isoform normalized to total protein.
(C) Quantification of the 55 kDa STAU1 isoform normalized to total protein.
(D) Quantification of combined STAU1 isoforms.

Individual symbols denote biological replicates from both sexes (triangles: male; circles: female), illustrating variability between male and female samples. Data are presented as mean ± SD, n = 6 biological replicates per group (both sexes included). Statistical analysis was performed using one-way ANOVA with post-hoc multiple comparisons.

4.2.2.2 Effects of Sciatic Denervation and Drug 15 on STAU1 mRNA Expression In Vivo

To determine if Drug 15 influences the expression of STAU1 at the transcript level during neurogenic muscle atrophy, we measured STAU1 mRNA expression in skeletal muscle five days after sciatic nerve denervation with daily administration of the drug. The levels of gene expression were normalized to a housekeeping gene, GAPDH and presented in relation to innervated control muscles treated with a vehicle.

Following sciatic nerve denervation, STAU1 mRNA expression was ~1.4-fold higher in the innervated muscles ($p = 0.4519$) (Figure 30); however, this difference was not statistically significant due to variability within the experimental groups. Administration of Drug 15 after denervation did not significantly change STAU1 mRNA levels compared to those in denervated muscles treated with a vehicle ($p = 0.7111$) (Figure 30). Although we observed a slight decrease in average STAU1 transcript levels in samples treated with Drug 15, the expression remained higher when compared to innervated controls, and there was no statistically significant difference between the denervated groups.

In summary, these results suggest that Drug 15 does not significantly affect STAU1 mRNA expression in vivo five days following denervation. Consistent with the protein-level findings, Drug 15 demonstrated limited effects on STAU1 mRNA expression under the tested conditions, with no significant difference observed between the denervated vehicle group and Drug 15 treated muscles. Because denervation itself did not produce statistically significant increase of STAU1 mRNA in this cohort, it was not possible to determine whether Drug 15 reduced STAU1 mRNA levels under the experimental conditioned tested.

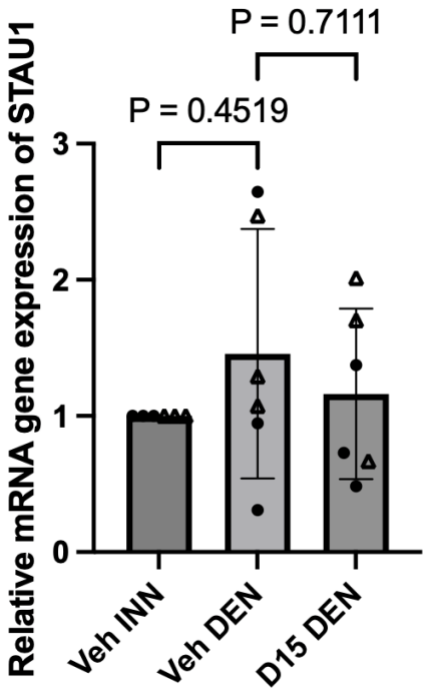

Figure 27. STAU1 mRNA expression following sciatic denervation and Drug 15 treatment.

Relative STAU1 mRNA levels were measured by qPCR in the tibialis anterior muscle indicating innervated vehicle-treated (V INN), denervated vehicle-treated (V DEN), and denervated Drug 15-treated (D15 DEN) muscles at day 5 post-denervation. Individual symbols denote biological replicates from both sexes (triangles: male; circles: female), illustrating variability between male and female samples. Data are presented as mean ± SEM, n = 6 biological replicates per group (both sexes included). Statistical analysis was performed using one-way ANOVA with post-hoc multiple comparisons.

4.2.2.3 Effect of Drug 15 on muscle fiber size and atrophy percent at day 14 post-denervation

To evaluate whether prolonged administration of Drug 15 alters the effects of denervation, tibialis anterior muscles were collected 14 days after sciatic denervation (Figure 18 and 19) and analyzed by H&E histology and cross-sectional area (CSA) measurements (Figure 31A). As expected, vehicle denervated group (Veh DEN) displayed marked fiber shrinkage compared to vehicle innervated group (Veh INN). Drug 15-treated denervated muscle (D15 DEN) showed a comparable degree of fiber reduction, with no visible preservation of fiber morphology relative to Vehicle denervated.

Quantification of mean CSA is shown in Figure 31B. Denervation in vehicle-treated mice resulted in a significant reduction in mean CSA compared to vehicle innervated ($p < 0.0001$),

representing an approximate 40-45% decrease in fiber size. Similarly, Drug 15-treated denervated muscle exhibited a reduction in CSA compared to drug 15 innervated muscle. There was no significant difference in CSA between vehicle denervated (Veh DEN) and drug 15 denervated group (D15 DEN), indicating that Drug 15 did not preserve myofiber size at this stage of denervation-induced atrophy.

Atrophy expressed as a percentage of loss relative to innervated controls is presented in Figure 31C. Vehicle denervation resulted in approximately 38% atrophy compared to vehicle innervated ($p < 0.0001$). Drug 15-treated denervated muscle exhibited a similar magnitude of atrophy (~34%), which remained significantly different from drug 15 innervated. No significant difference in atrophy percentage was observed between vehicle denervated and drug 15 denervated groups.

Together, these data demonstrate that, like Drug 12, prolonged in vivo treatment with Drug 15 did not prevent the loss of myofiber CSA nor reduce overall atrophy severity at day 14 following denervation (Figure 31).

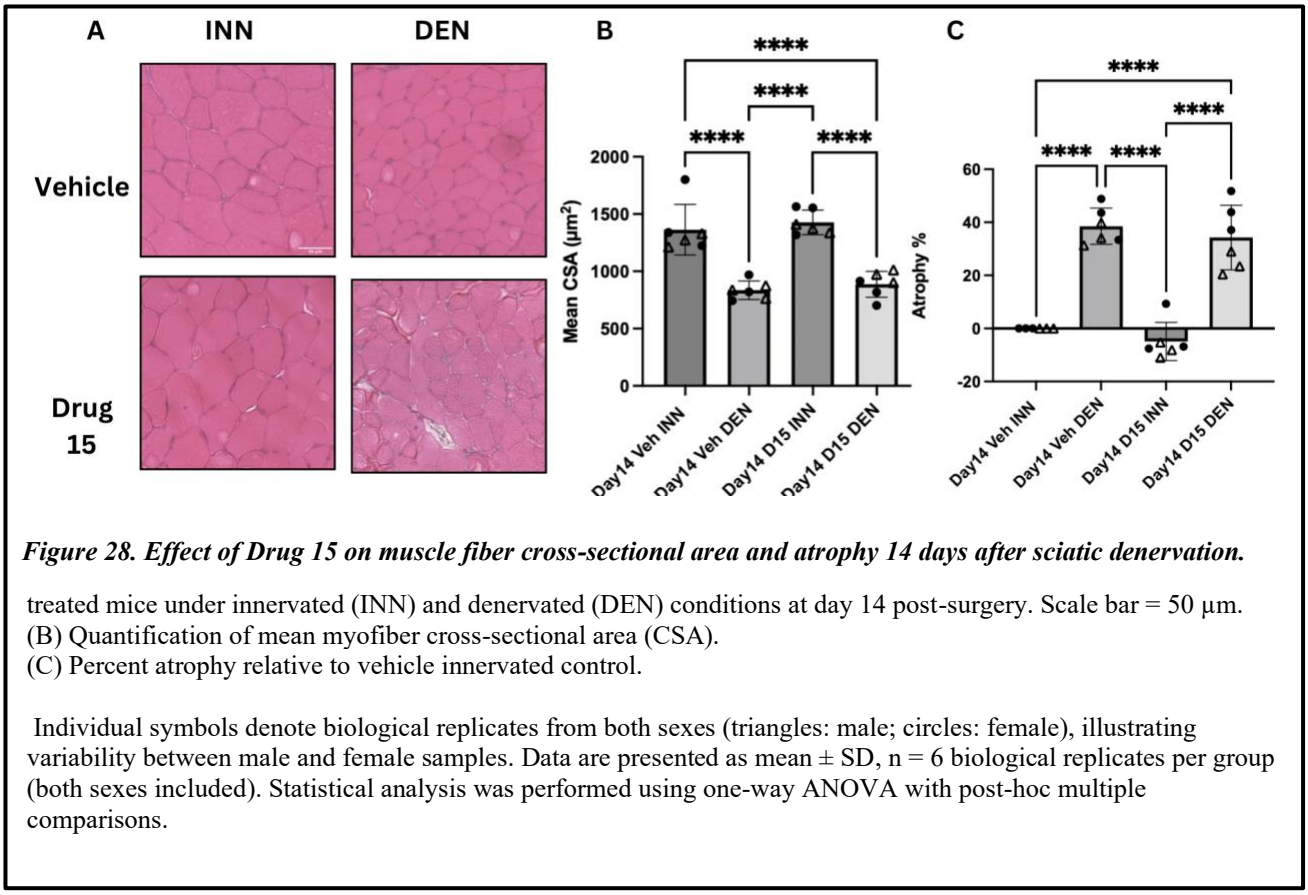

Figure 28. Effect of Drug 15 on muscle fiber cross-sectional area and atrophy 14 days after sciatic denervation.

treated mice under innervated (INN) and denervated (DEN) conditions at day 14 post-surgery. Scale bar = 50 µm.
(B) Quantification of mean myofiber cross-sectional area (CSA).
(C) Percent atrophy relative to vehicle innervated control.

Individual symbols denote biological replicates from both sexes (triangles: male; circles: female), illustrating variability between male and female samples. Data are presented as mean ± SD, n = 6 biological replicates per group (both sexes included). Statistical analysis was performed using one-way ANOVA with post-hoc multiple comparisons.

5. Discussion

This research aimed to determine whether skeletal muscle atrophy could be reduced by pharmacologically modulating STAU1 expression using FDA-approved drugs. It was hypothesized that lowering STAU1 expression might mitigate early molecular and morphological alterations associated with muscle atrophy, based on previous findings from our lab. To address this, two specific objectives were pursued: first, using differentiated C2C12 myotubes in an in vitro starvation model, the effects of drugs 12 and 15 on STAU1 expression and myotube atrophy were assessed, and second, the therapeutic potential of these compounds was evaluated in vivo using a denervation-induced mouse model of skeletal muscle atrophy.

In vitro results showed that specific compounds, notably Drugs 12 and 15, were able to decrease STAU1 expression and partially prevent starvation-induced myotube atrophy, as shown by preserved myotube diameter, which is consistent with the hypothesis. These findings demonstrate STAU1's potential as a pharmaceutical target in controlled environments and support its physiological significance in early atrophic signaling. The lack of a similar protective effects in the in vivo denervation paradigm, however, did not transfer to more intricate physiological system compared to the therapeutic efficacy seen in vitro. The difference possibly reflects the complex dynamics of muscle atrophy in vivo, where the efficacy of STAU1-targeting therapies may be limited by other variables, such as systemic signaling, drug bioavailability, tissue-specific uptake, and the degree of denervation-induced degeneration.

5.1 Pharmacological Modulation of STAU1 In C2C12 Myotubes

Aim 1 investigated whether FDA-approved compounds identified through high-throughput screening could modulate STAU1 expression and confer protection against early atrophic stress in differentiated C2C12 myotubes. Overall, the findings support a functional role for STAU1 in early catabolic signaling and reinforce its potential as a pharmacological target in skeletal muscle. Previous work from our laboratory demonstrated that increased STAU1 promotes muscle atrophy and suppresses PI3K/Akt/mTOR signaling, partly through upregulation of PTEN and enhanced FoxO activity (Parks et al., 2017). Building on this, the current data show that

pharmacological reduction of STAU1 is associated with preservation of myotube diameter under starvation conditions, supporting its role as an upstream regulator of early atrophic responses.

Importantly, Drug 15 markedly reduced both STAU1 isoforms at the protein level, whereas Drug 12 produced a milder effect while both protected myotubes against atrophy. This differential efficacy between drugs 12 and 15 suggests that partial suppression of STAU1 may be insufficient to elicit robust downstream morphological changes. Given STAU1's role in mRNA regulation (Kim et al., 2005; Park and Maquat, 2013), even subtle changes in its abundance may selectively influence stress-responsive transcripts. The observed attenuation of starvation-induced STAU1 upregulation further suggests that these compounds may interfere with early transcriptional or post-transcriptional stress adaptation. Atrophic stress initiates FoxO-dependent transcriptional changes alongside activation of proteolytic systems such as the ubiquitin-proteasome pathway and autophagy (Sandri, 2010; Bonaldo and Sandri, 2013). Accordingly, pharmacological inhibition of STAU1 may attenuate activation of this catabolic pathway during nutrient deprivation. Notably, neither compound altered myotube diameter under basal conditions, indicating that STAU1 modulation primarily affects stress-induced signaling rather than normal differentiation or homeostatic yield. This effect supports a model in which STAU1 contributes specifically to early adaptive responses to catabolic stress.

Collectively, these findings position STAU1 as a pharmacologically accessible regulator linking post-transcriptional RNA metabolism to early atrophic signaling. While serum starvation represents a simplified model, it reliably induces early molecular changes comparable to those observed in denervation-induced atrophy (Lecker et al., 2006; Sandri, 2010). Thus, the protective effects observed in vitro provided a strong rationale for evaluating whether similar modulation of STAU1 can translate into structural preservation in vivo.

5.2 Early Molecular Modulation of STAU1 Does Not Translate to Structural Rescue In Vivo

Although there is evidence of early STAU1 participation after denervation based on our preliminary data (Figure 8), altering its expression did not result in a significant structural preservation in vivo. In line with this, the current data show that STAU1 expression is increased

early following sciatic nerve denervation, which is consistent with its function in transcriptional regulation and catabolic response (Parks et l., 2017). Nevertheless, neither Drug 12 nor Drug 15 significantly suppressed this denervation-induced increase in STAU1 expression. Accordingly, neither treatment improved myofiber cross-sectional area after 14 days of denervation, suggesting a lack of substantial protection against muscle atrophy. These results imply that the lack of structural rescue in vivo was probably caused by inadequate target engagement. Partial or temporary modification of STAU1 might not have been sufficient to significantly change downstream catabolic pathways given the quick and complex course of denervation-induced atrophy. Muscle degeneration is further exacerbated by neuromuscular dysfunction and inflammatory remodeling, which may not be adequately mitigated by STAU1 modulation alone, in addition to prolonged activation of proteolytic systems and compromised anabolic signaling. Therefore, the interpretation that adequate reduction of STAU1 may be required prior to achieving structural protection in vivo is supported by the current data. Overall, these findings highlight the context-dependent function of STAU1 during early atrophic signaling and imply that to achieve quantifiable structural effect, treatment approaches that target RNA-regulatory pathways may need to use combinatorial techniques or prolonged target suppression.

5.3 Pharmacokinetic and Dosing Challenges In Vivo Target Engagement

A key factor contributing to the difference between in vitro and in vivo outcomes is the difference in experimental context and drug exposure. In cell culture, compounds maintain consistent concentrations and directly reach target cells, allowing for ongoing modulation of signaling pathways. Conversely, in vivo effectiveness relies on pharmacokinetic limitations, including short systemic half-life and limited tissue retention, and likely reduced sustained target engagement in skeletal muscle (Lin and Lu, 1997; Toutain and Bousquet-Mélou, 2004). As a result, once-daily dosing may not have maintained sufficient drug levels during the early, rapidly evolving phase of denervation-induced signaling. Next, denervation leads to considerable changes in skeletal muscle blood flow, inflammation, metabolic processes, and protein dynamics, which could additionally affect drug absorption and retention (Bonaldo and Sandri, 2013; Bodine and Baehr, 2014). Early denervation is characterized by rapid transcriptional changes and activation of proteolytic pathways (Bodine et al., 2001; Parks et al., 2017), suggesting that pharmacological intervention may require ongoing target suppression within a

limited time frame. For example, if Drug 12 is quickly flushed into the bloodstream, as indicated by reports of rapid dilution and systemic elimination after injection in humans, its pharmacodynamic availability in muscle may have been insufficient to combat these initial catabolic processes. Thus, the absence of notable protection on day 14 does not automatically rule out STAU1 as a biologically important regulator of atrophy induced by denervation but may instead indicate inadequate pharmacokinetic exposure. Although STAU1 expression were observed at the protein and mRNA levels, the pharmacokinetic limitations mentioned may have restricted ongoing suppression in muscle tissue. Taken together, these findings suggest that insufficient target engagement during early denervation likely limited the translation of molecular changes into sustained structural protection.

An additional interpretation of these findings highlights the importance of therapeutic timing when targeting RNA-regulatory pathways during muscle atrophy. Following denervation, rapid alterations in transcription and translation occur within the first few days of injury (Bodine et al., 2001; Lecker et al., 2006; Sandri, 2010). Although STAU1 modulation occurs during this early phase, morphological outcomes were assessed at later stages when downstream catabolic pathways are already established. These findings further indicate that STAU1 modulation alone may be insufficient to counteract established catabolic processes and may be most effective when combined with strategies that directly target anabolic signaling or proteolytic pathways (Bodine and Baehr, 2014). Given that STAU1 regulates mRNA stability, localization, and translation, its modulation may influence upstream signaling sensitivity without fully preventing downstream protein degradation. Therefore, STAU1 may function as a mechanistic leverage point that enhances the effectiveness of broader therapeutic strategies rather than acting as a standalone target.

An additional limitation relates to the dosing and formulation constraints. Despite initial plans for higher doses for Drug 15 (98mg/kg) based on our animal care protocol, practical issues with solubility limited the maximum injectable dose to around 30 mg/kg, significantly lower than the desired exposure range. The compound showed enhanced solubility solely at higher temperatures, conditions that are unsuitable for standard in vivo delivery. Limited solubility is a frequent obstacle in translational pharmacology, resulting in decreased bioavailability and

variable tissue exposure, which restricts target interaction even when cellular effects are encouraging (Savjani et al., 2012). Drug 12, on the other hand, did not exhibit similar solubility restrictions. Nonetheless, its pharmacokinetic profile could have had an impact in the absence of reported effectiveness in vivo. In addition, Drug 15 is given clinically through the oral route instead of parenteral injection, indicating that its pharmacokinetic profile in this study probably varied from its optimized clinical delivery setting. Oral administration allows for prolonged systemic exposure via absorption kinetics and multiple doses, while bolus intraperitoneal injection may lead to temporary peak concentrations that quickly decrease (Rowland & Tozer, 2011). Collectively, these formulation and dosing constraints indicate that the lack of structural protection in vivo may signify insufficient drug dosage instead of an absence of biological activity, emphasizing the necessity of pharmacokinetic enhancement, different delivery methods, and dose-escalation research in upcoming studies. These findings highlight how formulation constraints can limit translational efficacy, especially when compounds found via screening platforms are repurposed without optimization for delivering to skeletal muscle.

5.4 Model Differences: Starvation Versus Neurogenic Atrophy

Both serum starvation and sciatic nerve injury lead to skeletal muscle atrophy. However, these models differ in their biological complexity. Although both models activate overlapping pathways, denervation introduces additional systemic and multicellular factors that are not captured in vitro, contributing to differences in therapeutic response. Moreover, in vivo drug efficacy is influenced by factors such as half-life, absorption, metabolism, and clearance, which may limit effective target engagement within skeletal muscle. (Lecker et al., 2006; Bonaldo and Sandri, 2013; Bodine and Baehr, 2014). Thus, pharmacological interventions that successfully modify molecular responses in vitro may not be sufficient to address the systemic and multicellular factors contributing to neurogenic muscle loss in vivo. In addition, denervation triggers rapid alterations in neuromuscular signaling, inflammatory responses, and satellite cell activity, all of which influence the timeline and progression of muscle atrophy (Sartori, Romanello, and Sandri, 2021). These additional layers influence drug distribution, target engagement, and tissue response, thereby limiting therapies targeting cell-autonomous pathways. Therefore, modulation of RNA-binding proteins such as STAU1 may influence early signaling

dynamics but may not be sufficient to prevent structural decline when systemic drivers of atrophy predominate.

5.5 STAU1: Biological Relevance Beyond its Pharmacological Outcome

Earlier molecular modulation did not translate into any measurable structural protection in vivo. This difference, however, doesn't reduce STAU1's biological significance, but rather implies that its function may be more significant in the first stages of atrophic signaling than in maintaining or reversing existing muscle degeneration. The ability to reduce STAU1 in vitro without altering myotube morphology suggests that STAU1 impacts stress adaptation rather than constitutive muscle maintenance. The evidence showing that STAU1 is upregulated after denervation suggests that it plays a role in the first cellular reaction to atrophic stress, possibly via regulating translation, mRNA stability, and stress-responsive pathways (Kim et al., 2005; Almasi and Jasmin, 2021). As a post-transcriptional regulator, STAU1 may contribute to the early remodeling process by facilitating the muscle transcriptome's rapid adaptation in response to catabolic stressors. However, STAU1 regulation might not be enough to change the course of muscle loss if downstream pathways like proteolysis and compromised anabolic signaling are completely activated.

A key observation from this study is that the only consistent feature across both in vitro and in vivo models was the induction of STAU1 in response to atrophic stimuli. As previous research has mainly concentrated on transcriptional atrogenes or subsequent proteolytic pathways, the current results emphasize that post-transcriptional RNA regulation at an early phase, and possibly a limiting factor in determining the course of atrophy. STAU1 is dynamically regulated in both metabolic and neurogenic stress (Thomas et al., 2009; Paul et al., 2018). Pharmacological reduction of STAU1 primarily affected early molecular responses in vitro, without translating into structural improvements in vivo. These findings expand current models of muscle wasting, which focus on proteostasis imbalance, by highlighting RNA regulation as an additional layer contributing to the modulation of catabolic signaling (Kim et al., 2007; Park & Maquat, 2013; Bonaldo & Sandri, 2013). The noted separation between molecular changes and preservation of morphology in vitro offers experimental support for the idea that targeting RNA-regulatory pathways might require continuous or combinatorial therapeutic strategies. Overall, these

findings suggest that effective intervention may require targeting regulatory networks before structural deterioration occurs. Together, these results shift the conceptual focus from inhibiting downstream catabolism to comprehending how early RNA regulatory mechanisms establish the therapeutic window.

5.6 STAU1 in the Broader Context of RNA-Binding Proteins and Post-Transcriptional Regulation in Muscle Atrophy

Expanding upon the well-established function of RNA-binding proteins in skeletal muscle biology (Section 1.5), the current results allow for a more focused consideration of STAU1 in the post-transcriptional regulatory network during atrophy. STAU1 likely works as a component of a coordinated network of RBPs that together influence the muscle transcriptome under atrophic stress rather than functioning independently. Recent findings have significantly broadened the range of RBP activity, emphasizing their function as dynamic regulators of cellular adaptability through extensive regulation of protein synthesis and RNA fate (Hentze et al., 2025; Koletsou and Huppertz, et al., 2025).

In this regard, several RBPs have been linked to muscle atrophy via different but related pathways. For example, the dysregulation of CUGBP1/CELF1 has been shown to control alternative splicing and translation, promoting atrophic and disease-associated phenotypes (Lutz et al., 2023). Like this, HuR (ELAVL1) also affects the stability and translation of transcripts related to stress responses and myogenesis (Figueroa et al., 2003). Importantly, new research indicates that RBPs may display temporary and context-dependent expression patterns during muscle remodeling, as evidenced by elements like Zfp697, which is dynamically produced during muscle injury and recovery (Correia et al., 2023).

In addition to specific RBPs, a variety of post-transcriptional processes, such as RNA decay pathways and non-coding RNAs, are involved in the control of muscle mass. MicroRNAs and long non-coding RNAs (lncRNAs) have been identified as important regulators of muscle atrophy, including denervation, age, and cachexia (McCarthy, 2011; Zhang et al., 2025). By focusing on important genes involved in muscle development and proteostasis, microRNAs such as 1, miR-133, and miR-206 control myogenic differentiation and atrophy-related pathways

(McCarthy, 2011). During muscle development and regeneration, RNA modifications, such as N6-methyladenosine (m6A), have also been identified as significant regulators of mRNA stability and translation (Sun et al., 2023). These mechanisms function together to create an integrated regulatory network that regulates gene expression on several levels.

In this wider context, STAU1 may be seen as a multifunctional RBP that incorporates translation, decay, and mRNA transport, among other levels of post-transcriptional regulation. It serves as an early regulator of RNA dynamics in response to muscle stress due to its participation in stress-responsive pathways and its overexpression under atrophic environments. The present study highlights the complexity of post-transcriptional regulatory networks by showing that modification of STAU1 alone is insufficient to change structural results in vivo. These findings provide support to the notion that effective treatment methods that target RNA metabolism in skeletal muscle atrophy may need combinatorial approaches that take into consideration the interaction between numerous RBPs and regulatory pathways.

6. Potential Pitfalls and Limitations of the Study

In addition to the biological intricacies present in the denervation model, the genetic background could be an additional determinant of treatment response. The use of the FVB/N mouse strain in this study has physiological differences from the more frequently used C57BL/6J background seen in numerous denervation studies. Although FVB/N mice provide benefits for transgenic studies and demonstrate significant muscle development, they possess unique metabolic, neuromuscular, and regenerative traits that may influence the trajectory and variability of atrophy progression and the response to pharmacological treatments (Montagutelli, 2000). Compared with C57BL/6J mice, FVB/N mice exhibit differences in muscle fiber composition, inflammatory responses, and satellite cell function, which may have an impact on the degree and variety of denervation-related muscle atrophy (Zhang et al., 2024). Furthermore, depending on the muscle group and experimental settings, denervation for 14 days in mice usually causes significant muscular atrophy, with losses in muscle mass and fiber cross-sectional area observed in the range of ~30-50% in the TA muscle of FVB/N mice. Despite possible variations in underlying molecular responses, the available evidence indicates that the overall magnitude of

atrophy currently is generally comparable across commonly used mouse strains, despite the lack of direct comparisons between FVB/N and C57BL/6J in denervation models. Denervation causes a quick and severe loss of muscle mass in mice, with decreases of up to around 50% seen in just 14 days (Tang et al., 2014; You et al., 2021; You and Chen, 2021). In contrast, human muscle atrophy usually only results in a ~5-10% decrease of muscle mass over a similar two-week period, regardless of the cause, that is, through denervation, immobility, or disuse (Nedergaard et al., 2012; Deane et al., 2024). Although many of the biological and signaling processes driving muscle atrophy are replicated in rodent models, there are significant species differences in the temporal dynamics and degree of structural degradation. The therapeutic window may be condensed, and the capacity to identify protective effects of pharmacological therapies during experimental periods may be limited since the mouse denervation model reflects an accelerated and severe type of muscle wasting. This discrepancy implies that extended or persistent treatment approaches may be essential to therapies that target early molecular processes, such as STAU1 regulation, to produce quantifiable structural results in vivo.

Moreover, differences between animals and sex-specific variations in muscle adaptation might reduce statistical power to detect moderate pharmacological effects in denervation models (Della Peruta et al., 2023). Sex-dependent differences in inflammatory and neuromuscular responses have been reported after denervation, partly due to hormonal changes in muscle metabolism and immune signaling (Spangenburg et al., 2012; Della Peruta et al., 2023). Sex-specific variations have also been noted in human models of muscular atrophy, such as immobilization and bed rest which seem to depend on the situation. For instance, human short-term disuse studies show quantifiable reductions in muscle size (~3-5% after 7 days), along with changes in metabolic and inflammatory signaling pathways (Di Girolamo et al., 2021; Deane et al., 2024). According to new research, males and females may have different neuromuscular and inflammatory reactions to disuse. Depending on the model, some studies show more inflammatory disruptions in males after bed rest, while others suggest that females are more vulnerable to disuse-induced muscle loss (Rosa-Caldwell and Greane, 2019; Peruta et al., 2023). All these results demonstrate that sex is a significant biological factor in preclinical and human models of muscle atrophy, perhaps affecting the degree of muscle loss as well as the reaction to therapeutic interventions. Most denervation studies preferentially use male mice to reduce hormonal variability, which may

facilitate the identification of moderate treatment effects. In this study, female mice exhibited increased variability and more significant negative reactions during extended drug treatment, including swelling, self-harming actions like toe chewing, and occasional loss of tissue. These observations suggest that sex-dependent differences in inflammatory signaling, pain sensitivity, and regenerative capacity may have influenced treatment tolerance and variability in STAU1 responses. As female mice showed pronounced adverse responses during prolonged treatment, this suggests that their initial physiological condition may affect their tolerance to nerve damage and drug therapy (Spangenburg et al., 2012; Mogil, 2012). Hormonal modulation of immune and neuromuscular pathways has been shown to alter denervation outcomes and pharmacological responsiveness, indicating that therapeutic strategies targeting RNA regulatory mechanisms may require sex-specific optimization to achieve consistent efficacy. These behaviors align with findings that peripheral nerve damage can lead to sex-specific variations in pain sensitivity, stress reactions, and wound repair, potentially influencing muscle integrity and experimental results (Mogil, 2012; Sorge & Totsch, 2017). These sex-specific and interdisciplinary differences make it more challenging to extrapolate results from mouse denervation models to human muscle atrophy.

Another key factor is that in vivo assessments were limited to the tibialis anterior (TA) muscle, a fast-twitch glycolytic muscle highly responsive to denervation-induced atrophy but may not capture the full range of skeletal muscle adaptations. Research shows that fast-twitch (type II) fibers are often more susceptible to denervation-induced atrophy than slow-twitch (type I) fibers, with larger losses in cross-sectional area and more evident activation of catabolic pathways. (Wang and Pessin, 2013; Yao et al., 2024). Their greater proneness to metabolic and atrophic stress after denervation is believed to result from their decreased oxidative function, reduced mitochondrial content, and increased reliance on neural input for protein turnover maintenance (Wang and Pessin, 2013). However, slow-twitch fibers have higher oxidative metabolism and inherent resistance to proteolysis, which may help them maintain some of their structural integrity in similar environments (Wang and Pessin, 2013). Denervation predominantly disrupts fast-fiber gene patterns and enhances atrophic signaling pathways in glycolytic myofibers, according to recent transcriptomic and pharmacological investigations (Dos Santos et al., 2025). It's important to note that fiber-type-specific responses might vary depending on the muscle and

context, as some research has shown that slow muscles' susceptibility varies based on the model and length of denervation. Various muscle groups exhibit metabolic characteristics, regeneration abilities, and vulnerability to neurogenic atrophy, with oxidative muscles such as the soleus frequently showing distinct temporal and molecular responses compared to glycolytic muscles (Schiaffino & Reggiani, 2011; Bonaldo & Sandri, 2013). Since this thesis demonstrated that STAU1 expression differs among muscle types (Figure 25), concentrating solely on TA might have restricted the identification of muscle-specific therapeutic effects, especially if pharmacological adjustments primarily affect oxidative fibers or muscles exhibiting greater basal post-transcriptional activity. Assessing additional muscles would provide a more comprehensive evaluation of drug effectiveness and determine if STAU1-targeting methods have fiber-type-specific effects in vivo. Overall, these constraints underscore that the lack of structural rescue does not diminish the biological significance of STAU1. Instead, it highlights the critical role of experimental context, exposure dynamics, and the choice of models in translating early molecular regulation into therapeutic results.

7. Future Directions

A primary goal for future research is to ascertain how the regulation of STAU1 might be translated into significant structural protection of skeletal muscle in vivo. The results of this research show that although STAU1 can be regulated at the molecular level and is consistently activated during early atrophic stress, this does not lead in the maintenance of muscle structure under the investigated conditions. This demonstrates an essential gap between long-term tissue outcome and early post-transcriptional regulation. To fill this gap, it will be necessary to have a better knowledge of when STAU1 functions during muscle atrophy and if its function is limited to early signaling events or extends into later remodeling stages. STAU1 may work within a limited temporal window that is not sufficiently targeted by existing intervention efforts since denervation quickly activates post-transcriptional pathways before the development of classical atrogenes (Park & Maquat, 2013; Quesada & DesGroseillers, 2022). Designing strategies that integrate STAU1 regulation with the development of atrophic signaling will require defining this temporal link.

Building this temporal framework, altering dose and delivery tactics will be essential to guarantee adequate and sustained regulation of STAU1 in vivo. Given the solubility limitations and possible rapid elimination, the lack of structural protection seen in this investigation may indicate insufficient target engagement because of limited drug exposure. Therefore, if STAU1 activity is maintained after the initial phase of atrophic signaling, future research should investigate fractionated dosage techniques or repeated dosing regimens to maintain effective medication levels over time. Alternative delivery methods, such as sustained-release formulations or osmotic pump-mediated continuous administration, to maintain consistent suppression over time, should be investigated to improve target engagement. These methods would assist in determining if long-term, sustained STAU1 modulation is necessary to affect downstream remodeling processes and ultimately supply skeletal muscle with structural protection. In situations when the effective dose may not have been reached, for Drug 15, for example, future research should concentrate on improving dosing procedures to guarantee adequate and sustained target engagement. Repeated dose schedules (2-3 injections per day), or increased or fractionated dosing (where practical), could help maintain consistent drug levels over time. Furthermore, pharmacokinetic constraints may be avoided and tissue-specific targeting enhanced by alternate delivery methods such continuous delivery systems or sustained-release formulations.

Future research should investigate next-generation STAU1 modulators with enhanced potency, selectivity, and muscle-specific bioavailability and improved formulations. This could entail extending pharmacological screening beyond the original FDA-approved compound library from our Laboratory to include larger and more varied compounds, such as additional libraries for repurposing, collections of RNA-focused small molecules, and compounds found using high-throughput. The potential to target RNA-binding proteins (RBPs) and RNA-protein interactions with small molecules, such as substances that directly disrupt RNA-protein binding, change RBP stability, or modify RNA structure and accessibility, has been brought to light by recent developments in drug discovery (Shi et al., 2025; Konde et al., 2025). Specifically, the identification of bioactive compounds that specifically target RNA structures or RBP interactions has been made possible by the development of RNA-focused chemical libraries and enhanced screening technologies (Taghavi et al., 2025).

In parallel, new therapeutic approaches include antisense oligonucleotides and RNA-targeting small molecules that alter RNA processing and translation, as well as multifunctional molecules and targeted degradation techniques (such as PROTAC-like systems) intended to specifically remove disease-relevant RBPs (Konde et al., 2025; Ansari et al., 2025). Furthermore, it has been demonstrated that naturally occurring substances and nutraceuticals indirectly affect stress-responsive signaling pathways and RNA-binding protein activity; however, their specificity for certain RBPs, such as STAU1, is still unclear and demands further investigation. This is demonstrated by new research showing that cellular metabolites, signaling molecules, and environmental elements, such as bioactive compounds, which can alter RNA stability, translation, and metabolic pathways, dynamically regulate RBPs (Koletsou and Huppertz, 2025; Sun et al., 2025). When taken as a whole, these strategies demonstrate the evolving platform for focusing on post-transcriptional regulation and imply that future attempts to modify STAU1 could benefit from combining innovations in RNA-targeted drug discovery with better pharmacological design.

Simultaneously, genetic approaches like inducible or muscle-specific STAU1 knockdown models may help differentiate pharmacokinetic constraints from actual biological effects, thereby elucidating whether the lack of structural rescue seen in vivo is due to intrinsic pathway redundancy or inadequate drug exposure. The confirmation of STAU1 and associated RNA-binding proteins as potential therapeutic targets for skeletal muscle atrophy might be strengthened by combining these strategies.

Improving the selection and different experimental models will be essential to define STAU1's context-dependent functions. Comparative studies across atrophy models (denervation, disuse, metabolic stress), and muscle wasting due to disease will clarify whether STAU1 functions as a universal regulator of initial stress responses or has specific effects dependent on the model used. Previous research indicates that while different atrophy stimuli activate common proteolytic pathways, the regulatory mechanisms upstream vary notably, especially regarding RNA processing and translational control (Lecker et al., 2006; Sandri, 2010; Bonaldo & Sandri, 2013). Including various muscle groups with fiber types will help further elucidate whether STAU1-

influenced RNA regulation has different roles in glycolytic compared to oxidative muscle adaptation (Schiaffino & Reggiani, 2011). Future studies should incorporate sex as a biological variable and evaluate how hormonal signaling interacts with STAU1-mediated RNA regulation. Additionally, age-matching based on physiological maturity rather than chronological age may improve consistency and sensitivity in detecting treatment effects. To further develop this approach, it will be necessary to integrate tissue-specific responses in physiologically models with the temporal dynamics of STAU1 regulation. Determining if STAU1 shows comparable early and transient regulation during muscle atrophy and whether its modulation can affect disease progression in a clinically meaningful duration will be necessary to translate these findings to humans. These discoveries could facilitate the integration of RNA-targeted techniques into treatment plans intended to maintain muscular integrity in the initial phases of muscle atrophy. Together, these directions position STAU1 not as a standalone structural target but as a regulator of early vulnerability to muscle degeneration.

8. Significance and Relevance

This study provides important mechanistic and translational insights into the role of RNA-binding proteins in skeletal muscle atrophy, identifying Staufen1 (STAU1) as a previously underexplored regulator of early atrophic signaling. Skeletal muscle atrophy constitutes a significant clinical and societal challenge, leading to functional deterioration, reduced quality of life, and heightened morbidity associated with various conditions such as aging (sarcopenia), immobilization, denervation, and chronic illness (Bonaldo and Sandri, 2013; Sayer and Cruz-Jentoft, 2022). There is currently no widely used pharmaceutical treatments that consistently maintain muscle mass and function, despite substantial research into the molecular pathways behind muscle loss. This underscores an essential gap in translational muscle biology. Although transcriptional regulation and signaling pathways involving IGF-1/Akt/mTOR and ubiquitin-proteasome-mediated proteolysis have been the focus of traditional approaches, there is growing evidence that post-transcriptional regulation is just as important in determining muscle remodeling and degeneration (Schiaffino et al., 2013; Hentze et al., 2018).

RNA-binding proteins (RBPs) have become important gene expression regulators, allowing for fast, dynamic modulation of mRNA stability, localization, and translation in response to cellular

stress. By identifying STAU1 as a physiologically significant modulator of early atrophic signaling, my thesis adds to this emerging paradigm. STAU1's function as a conserved early response factor to muscle stress is supported by its constant increase in both in vitro and in vivo settings, placing it within the sequential pyramid of post-transcriptional regulation. This work offers functional evidence that targeting RNA metabolism can affect the early phases of muscle atrophy by showing that pharmacological regulation of STAU1 modifies early molecular responses in vitro.

The absence of structural protection observed in the in vivo data, despite early molecular modulation, highlights a significant conceptual advancement that early post-transcriptional regulators like STAU1 may initiate atrophic signaling but are inadequate alone to mitigate muscle loss progression. This result underscores the challenges of a specific-target treatment approach and the intricacy and diversity of regulatory networks controlling skeletal muscle homeostasis. By doing so, the emphasis shifts from identifying specific molecular factors to understanding how integrated regulatory systems, including signaling pathways, non-coding RNAs, and RBPs, interact over time to determine the fate of muscles.

From a translational perspective, this thesis offers key insight into why novel molecular targets might not provide functional results in vivo, especially in extreme and rapid models of muscle atrophy like denervation. This work adds to a more advanced framework for treatment development by pointing out limitations pertaining to dosage, administration, tissue selectivity, and temporal dynamics. It reinforces the idea that long-term or combinatorial approaches that target several nodes in the atrophy network, in contrast to a single regulator, may be essential for successful protective treatments. By expanding its relevance to skeletal muscle biology, this work broadens the scope of the developing field of RNA-targeted therapies. Although RNA-binding proteins have been thoroughly investigated in the contexts of cancer and neurological disorders, their therapeutic potential in muscle disorders remains unclear. This work establishes the groundwork for further research into RNA-based therapies, such as small compounds, antisense techniques, and other targeting strategies, by emphasizing the potential and limitations of targeting STAU1. In summary, these results add to the growing understanding that post-transcriptional regulation is a crucial and perhaps treatable mechanism for controlling muscle

atrophy, with implications for enhancing therapeutic effects across a variety of muscle-wasting disorders.

9. Conclusion

This thesis supports STAU1's function as an early and conserved mediator of skeletal muscle stress by showing that it is consistently elevated in response to atrophic stimuli in both in vitro and in vivo conditions. In vitro, pharmacological modification of STAU1 was sufficient to modify early molecular responses, demonstrating that post-transcriptional regulation plays a role in the onset of muscle atrophy. These changes, however, did not result in measurable structural protection in vivo, underlining a major gap between early molecular modulation and long-term tissue-specific implications. These results highlight the diverse and temporally dynamic nature of skeletal muscle atrophy. Although STAU1 seems to be an early regulator of RNA metabolism during atrophic signaling, the coordinated stimulation of proteolytic pathways, compromised anabolic signaling, and neuromuscular dysfunction that cause progressive muscle loss cannot be prevented by modulating STAU1 independently. In addition, this work serves as an important basis for comprehending why promising molecular targets may fail to yield beneficial results in vivo. The lack of structural rescue was probably caused by issues with drug administration, dosage restrictions, pharmacokinetics, and model severity, highlighting the need for advanced experimental and therapeutic approaches. These findings demonstrate that long-term modulation, enhanced tissue targeting, and combinatorial strategies that target several regulatory nodes at once would probably be necessary for successful treatments for muscle atrophy. In conclusion, STAU1 is a context-dependent, physiologically significant regulator of skeletal muscle atrophy. Although its early induction emphasizes its significance in initial response to muscle stress, a more thorough strategy will be needed to achieve sustained structural protection in vivo. These discoveries lay the groundwork for further research aimed at developing efficient treatments for conditions that cause muscular atrophy.

References

1. Acharyya, S., Ladner, K. J., Nelsen, L. L., Damrauer, J., Reiser, P. J., Swoap, S., & Guttridge, D. C. (2004). Cancer cachexia is regulated by selective targeting of skeletal muscle gene products. The Journal of clinical investigation, 114(3), 370–378. https://doi.org/10.1172/JCI20174
2. Aldridge, G. M., Podrebarac, D. M., Greenough, W. T., & Weiler, I. J. (2008). The use of total protein stains as loading controls: an alternative to high-abundance single-protein controls in semi-quantitative immunoblotting. Journal of neuroscience methods, 172(2), 250–254. https://doi.org/10.1016/j.jneumeth.2008.05.003
3. Almasi, S., & Jasmin, B. J. (2021). The multifunctional RNA-binding protein Staufen1: an emerging regulator of oncogenesis through its various roles in key cellular events. Cellular and molecular life sciences: CMLS, 78(23), 7145–7160. https://doi.org/10.1007/s00018-021-03965-
4. Almasi, S., SarmastiEmami, S., Baird, S., Ning, Z., Figeys, D., Côté, J., Cowan, K. N., & Jasmin, B. J. (2023). Staufen1 controls mitochondrial metabolism via HIF2α in embryonal rhabdomyosarcoma and promotes tumorigenesis. Cellular and Molecular Life Sciences: CMLS, 80(11), 328. https://doi.org/10.1007/s00018-023-04969-4
5. Ansari, N., Liu, C., Hédin, F., Hénin, J., Ponder, J. W., Ren, P., Piquemal, J. P., Lagardère, L., & El Hage, K. (2025). Targeting RNA with small molecules using state-of-the-art methods provides highly predictive affinities of riboswitch inhibitors. Communications Biology, 8(1), 1405. https://doi.org/10.1038/s42003-025-08809-y
6. Ashburn, T. T., & Thor, K. B. (2004). Drug repositioning: identifying and developing new uses for existing drugs. Nature reviews. Drug discovery, 3(8), 673–683. https://doi.org/10.1038/nrd1468
7. Bélanger, G., Stocksley, M. A., Vandromme, M., Schaeffer, L., Furic, L., DesGroseillers, L., & Jasmin, B. J. (2003). Localization of the RNA-binding proteins Staufen1 and Staufen2 at the mammalian neuromuscular junction. Journal of neurochemistry, 86(3), 669–677. https://doi.org/10.1046/j.1471-4159.2003.01883.x
8. Bodine, S. C., & Baehr, L. M. (2014). Skeletal muscle atrophy and the E3 ubiquitin ligases MuRF1 and MAFbx/atrogin-1. American journal of physiology. Endocrinology and metabolism, 307(6), E469–E484. https://doi.org/10.1152/ajpendo.00204.2014
9. Bodine, S. C., Latres, E., Baumhueter, S., Lai, V. K., Nunez, L., Clarke, B. A., Poueymirou, W. T., Panaro, F. J., Na, E., Dharmarajan, K., Pan, Z. Q., Valenzuela, D. M., DeChiara, T. M., Stitt, T. N., Yancopoulos, G. D., & Glass, D. J. (2001). Identification of ubiquitin ligases required for skeletal muscle atrophy. Science (New York, N.Y.), 294(5547), 1704–1708. https://doi.org/10.1126/science.106587
10. Bonaldo, P., & Sandri, M. (2013). Cellular and molecular mechanisms of muscle atrophy. Disease models & mechanisms, 6(1), 25–39. https://doi.org/10.1242/dmm.010389
11. Bondy-Chorney, E., Crawford Parks, T. E., Ravel-Chapuis, A., Klinck, R., Rocheleau, L., Pelchat, M., Chabot, B., Jasmin, B. J., & Côté, J. (2016). Staufen1 Regulates Multiple Alternative Splicing Events either Positively or Negatively in DM1 Indicating Its Role as a Disease Modifier. PLoS genetics, 12(1), e1005827. https://doi.org/10.1371/journal.pgen.1005827
12. Bonetto, A., Penna, F., Minero, V. G., Reffo, P., Bonelli, G., Baccino, F. M., & Costelli, P. (2009). Deacetylase inhibitors modulate the myostatin/follistatin axis without improving

cachexia in tumor-bearing mice. Current cancer drug targets, 9(5), 608–616. https://doi.org/10.2174/156800909789057015
13. Bonnet-Magnaval, F., Philippe, C., Van Den Berghe, L., Prats, H., Touriol, C., & Lacazette, E. (2016). Hypoxia and ER stress promote Staufen1 expression through an alternative translation mechanism. Biochemical and biophysical research communications, 479(2), 365–371. https://doi.org/10.1016/j.bbrc.2016.09.082
14. Brendel, C., Rehbein, M., Kreienkamp, H. J., Buck, F., Richter, D., & Kindler, S. (2004). Characterization of Staufen 1 ribonucleoprotein complexes. The Biochemical journal, 384(Pt 2), 239–246. https://doi.org/10.1042/BJ20040812
15. Broome, S. C., Whitfield, J., Karagounis, L. G., & Hawley, J. A. (2024). Mitochondria as Nutritional Targets to Maintain Muscle Health and Physical Function During Ageing. Sports medicine (Auckland, N.Z.), 54(9), 2291–2309. https://doi.org/10.1007/s40279-024-02072-7
16. Cacciatore, S., Calvani, R., Esposito, I., Massaro, C., Gava, G., Picca, A., Tosato, M., Marzetti, E., & Landi, F. (2024). Emerging Targets and Treatments for Sarcopenia: A Narrative Review. Nutrients, 16(19), 3271. https://doi.org/10.3390/nu16193271
17. Chakrabarti, A. M., Iosub, I. A., Lee, F. C. Y., Ule, J., & Luscombe, N. M. (2023). A computationally-enhanced hiCLIP atlas reveals Staufen1-RNA binding features and links 3' UTR structure to RNA metabolism. Nucleic acids research, 51(8), 3573–3589. https://doi.org/10.1093/nar/gkad221
18. Chen, P., Jia, F., Wang, M., & Yang, S. (2025). Analysis of the mechanism of skeletal muscle atrophy from the pathway of decreased protein synthesis. Frontiers in Physiology, 16, 1533394. https://doi.org/10.3389/fphys.2025.1533394
19. Chen, P., Jia, F., Wang, M., & Yang, S. (2025). Analysis of the mechanism of skeletal muscle atrophy from the pathway of decreased protein synthesis. Frontiers in physiology, 16, 1533394. https://doi.org/10.3389/fphys.2025.1533394
20. Chong, C. R., & Sullivan, D. J., Jr (2007). New uses for old drugs. Nature, 448(7154), 645–646. https://doi.org/10.1038/448645a
21. Chu, Y., Yuan, X., Tao, Y., Yang, B., & Luo, J. (2024). Autophagy in Muscle Regeneration: Mechanisms, Targets, and Therapeutic Perspective. International journal of molecular sciences, 25(22), 11901. https://doi.org/10.3390/ijms252211901
22. Colombrita, C., Zennaro, E., Fallini, C., Weber, M., Sommacal, A., Buratti, E., Silani, V., & Ratti, A. (2009). TDP-43 is recruited to stress granules in conditions of oxidative insult. Journal of neurochemistry, 111(4), 1051–1061. https://doi.org/10.1111/j.1471-4159.2009.06383.x
23. Connor, S. G., Fairchild, T. J., Learmonth, Y. C., Beer, K., Cooper, I., Boardman, G., Teo, S. Y. M., Shatahmasseb, B., Zhang, R., Hiscock, K., Coudert, J. D., Yeap, B. B., & Needham, M. (2023). Testosterone treatment combined with exercise to improve muscle strength, physical function and quality of life in men affected by inclusion body myositis: A randomised, double-blind, placebo-controlled, crossover trial. PloS one, 18(4), e0283394. https://doi.org/10.1371/journal.pone.0283394
24. Correia, J. C., Jannig, P. R., Gosztyla, M. L., Cervenka, I., Ducommun, S., Præstholm, S. M., Dumont, K., Liu, Z., Liang, Q., Edsgärd, D., Emanuelsson, O., Gregorevic, P., Westerblad, H., Venckunas, T., Brazaitis, M., Kamandulis, S., Lanner, J. T., Yeo, G. W., & Ruas, J. L. (2023). Zfp697 is an RNA-binding protein that regulates skeletal muscle inflammation and regeneration. BioRxiv, 2023.06.12.544338. https://doi.org/10.1101/2023.06.12.544338

25. Corsello, S. M., Bittker, J. A., Liu, Z., Gould, J., McCarren, P., Hirschman, J. E., Johnston, S. E., Vrcic, A., Wong, B., Khan, M., Asiedu, J., Narayan, R., Mader, C. C., Subramanian, A., & Golub, T. R. (2017). The Drug Repurposing Hub: a next-generation drug library and information resource. Nature medicine, 23(4), 405–408. https://doi.org/10.1038/nm.4306
26. Cox, D. C., Guan, X., Xia, Z., & Cooper, T. A. (2020). Increased nuclear but not cytoplasmic activities of CELF1 protein leads to muscle wasting. Human Molecular Genetics, 29(10), 1729. https://doi.org/10.1093/hmg/ddaa095
27. Crawford Parks, T. E., Ravel-Chapuis, A., Bondy-Chorney, E., Renaud, J. M., Côté, J., & Jasmin, B. J. (2017). Muscle-specific expression of the RNA-binding protein Staufen1 induces progressive skeletal muscle atrophy via regulation of phosphatase tensin homolog. Human molecular genetics, 26(10), 1821–1838. https://doi.org/10.1093/hmg/ddx085
28. Crawford, J., Prado, C. M., Johnston, M. A., Gralla, R. J., Taylor, R. P., Hancock, M. L., & Dalton, J. T. (2016). Study Design and Rationale for the Phase 3 Clinical Development Program of Enobosarm, a Selective Androgen Receptor Modulator, for the Prevention and Treatment of Muscle Wasting in Cancer Patients (POWER Trials). Current oncology reports, 18(6), 37. https://doi.org/10.1007/s11912-016-0522-0
29. Dalton, J. T., Barnette, K. G., Bohl, C. E., Hancock, M. L., Rodriguez, D., Dodson, S. T., Morton, R. A., & Steiner, M. S. (2011). The selective androgen receptor modulator GTx-024 (enobosarm) improves lean body mass and physical function in healthy elderly men and postmenopausal women: results of a double-blind, placebo-controlled phase II trial. Journal of cachexia, sarcopenia and muscle, 2(3), 153–161. https://doi.org/10.1007/s13539-011-0034-6
30. Dave HD, Shook M, Varacallo MA. Anatomy, Skeletal Muscle. [Updated 2023 Aug 28]. In: StatPearls [Internet]. Treasure Island (FL): StatPearls Publishing; 2026 Jan-. Available from: https://www.ncbi.nlm.nih.gov/books/NBK537236/
31. Deane, C. S., Piasecki, M., & Atherton, P. J. (2024). Skeletal muscle immobilisation-induced atrophy: Mechanistic insights from human studies. Clinical Science (London, England: 1979), 138(12), 741. https://doi.org/10.1042/CS20231198
32. DeFronzo, R. A., & Tripathy, D. (2009). Skeletal muscle insulin resistance is the primary defect in type 2 diabetes. Diabetes care, 32 Suppl 2(Suppl 2), S157–S163. https://doi.org/10.2337/dc09-S302
33. Della Peruta, C., Lozanoska-Ochser, B., Renzini, A., Moresi, V., Sanchez Riera, C., Bouché, M., & Coletti, D. (2023). Sex Differences in Inflammation and Muscle Wasting in Aging and Disease. International journal of molecular sciences, 24(5), 4651. https://doi.org/10.3390/ijms24054651
34. Di Girolamo, F. G., Fiotti, N., Milanović, Z., Situlin, R., Mearelli, F., Vinci, P., Šimunič, B., Pišot, R., Narici, M., & Biolo, G. (2021). The Aging Muscle in Experimental Bed Rest: A Systematic Review and Meta-Analysis. Frontiers in Nutrition, 8, 633987. https://doi.org/10.3389/fnut.2021.633987
35. Dirks, M. L., Wall, B. T., van de Valk, B., Holloway, T. M., Holloway, G. P., Chabowski, A., Goossens, G. H., & van Loon, L. J. (2016). One Week of Bed Rest Leads to Substantial Muscle Atrophy and Induces Whole-Body Insulin Resistance in the Absence of Skeletal Muscle Lipid Accumulation. Diabetes, 65(10), 2862–2875. https://doi.org/10.2337/db15-1661

36. Domaniku, A., Bilgic, S. N., & Kir, S. (2023). Muscle wasting: emerging pathways and potential drug targets. Trends in pharmacological sciences, 44(10), 705–718. https://doi.org/10.1016/j.tips.2023.07.006
37. Donaldson, J. G., & Jackson, C. L. (2000). Regulators and effectors of the ARF GTPases. Current opinion in cell biology, 12(4), 475–482. https://doi.org/10.1016/s0955-0674(00)00119-8
38. Dormoy-Raclet, V., Ménard, I., Clair, E., Kurban, G., Mazroui, R., Di Marco, S., von Roretz, C., Pause, A., & Gallouzi, I. E. (2007). The RNA-binding protein HuR promotes cell migration and cell invasion by stabilizing the beta-actin mRNA in a U-rich-element-dependent manner. Molecular and cellular biology, 27(15), 5365–5380. https://doi.org/10.1128/MCB.00113-07
39. Dos Santos, M., Bezprozvannaya, S., McAnally, J. R., Cai, C., Liu, N., & Olson, E. N. (2025). A mechanistic basis of fast myofiber vulnerability to neuromuscular diseases. Cell Reports, 44(7), 115959. https://doi.org/10.1016/j.celrep.2025.115959
40. Doyle, M., & Kiebler, M. A. (2011). Mechanisms of dendritic mRNA transport and its role in synaptic tagging. The EMBO journal, 30(17), 3540–3552. https://doi.org/10.1038/emboj.2011.278
41. Duan, K., Gao, X., & Zhu, D. (2021). The clinical relevance and mechanism of skeletal muscle wasting. Clinical nutrition (Edinburgh, Scotland), 40(1), 27–37. https://doi.org/10.1016/j.clnu.2020.07.029
42. Duchaîne, T. F., Hemraj, I., Furic, L., Deitinghoff, A., Kiebler, M. A., & DesGroseillers, L. (2002). Staufen2 isoforms localize to the somatodendritic domain of neurons and interact with different organelles. Journal of cell science, 115(Pt 16), 3285–3295. https://doi.org/10.1242/jcs.115.16.3285
43. Dugré-Brisson, S., Elvira, G., Boulay, K., Chatel-Chaix, L., Mouland, A. J., & DesGroseillers, L. (2005). Interaction of Staufen1 with the 5' end of mRNA facilitates translation of these RNAs. Nucleic acids research, 33(15), 4797–4812. https://doi.org/10.1093/nar/gki794
44. Eaton, S. L., Roche, S. L., Hurtado, M. L., Oldknow, K. J., Farquharson, C., Gillingwater, T. H., & Wishart, T. M. (2013). Total Protein Analysis as a Reliable Loading Control for Quantitative Fluorescent Western Blotting. PLOS ONE, 8(8), e72457. https://doi.org/10.1371/journal.pone.0072457
45. Figueroa, A., Cuadrado, A., Fan, J., Atasoy, U., Muscat, G. E., Muñoz-Canoves, P., Gorospe, M., & Muñoz, A. (2003). Role of HuR in Skeletal Myogenesis through Coordinate Regulation of Muscle Differentiation Genes. Molecular and Cellular Biology, 23(14), 4991. https://doi.org/10.1128/MCB.23.14.4991-5004.2003
46. Frontera, W. R., & Ochala, J. (2015). Skeletal muscle: a brief review of structure and function. Calcified tissue international, 96(3), 183–195. https://doi.org/10.1007/s00223-014-9915-y
47. Furic, L., Maher-Laporte, M., & DesGroseillers, L. (2008). A genome-wide approach identifies distinct but overlapping subsets of cellular mRNAs associated with Staufen1-and Staufen2-containing ribonucleoprotein complexes. Rna, 14(2), 324-335.
48. Fyfe, J. J., Hamilton, D. L., & Daly, R. M. (2022). Minimal-Dose Resistance Training for Improving Muscle Mass, Strength, and Function: A Narrative Review of Current Evidence and Practical Considerations. Sports medicine (Auckland, N.Z.), 52(3), 463–479. https://doi.org/10.1007/s40279-021-01605-8
49. Gan, Q., Salvi, J. S., D Klein, J. D., Akimenko, I., Quarta, M., Biressi, S., & Rando, T. A. (2017). Staufen1 inhibits MyoD translation to actively maintain muscle stem cell quiescence.

Proceedings of the National Academy of Sciences of the United States of America, 114(43), E8996. https://doi.org/10.1073/pnas.1708725114
50. Gebauer, F., Schwarzl, T., Valcárcel, J., & Hentze, M. W. (2021). RNA-binding proteins in human genetic disease. Nature reviews. Genetics, 22(3), 185–198. https://doi.org/10.1038/s41576-020-00302-y
51. Gilbert, C. J., Rabolli, C. P., Golubeva, V. A., Sattler, K. M., Wang, M., Ketabforoush, A., Arnold, W. D., Lepper, C., & Accornero, F. (2024). YTHDF2 governs muscle size through a targeted modulation of proteostasis. Nature communications, 15(1), 2176. https://doi.org/10.1038/s41467-024-46546-8
52. Gomes, M. D., Lecker, S. H., Jagoe, R. T., Navon, A., & Goldberg, A. L. (2001). Atrogin-1, a muscle-specific F-box protein highly expressed during muscle atrophy. Proceedings of the National Academy of Sciences of the United States of America, 98(25), 14440–14445. https://doi.org/10.1073/pnas.251541198.
53. Gonzalez Quesada, Y., & DesGroseillers, L. (2022). A Degradation Motif in STAU1 Defines a Novel Family of Proteins Involved in Inflammation. International journal of molecular sciences, 23(19), 11588. https://doi.org/10.3390/ijms231911588
54. González-Rocha, A., Mendez-Sanchez, L., Ortíz-Rodríguez, M. A., & Denova-Gutiérrez, E. (2022). Effect Of Exercise on Muscle Mass, Fat Mass, Bone Mass, Muscular Strength and Physical Performance in Community Dwelling Older Adults: Systematic Review and Meta-Analysis. Aging and disease, 13(5), 1421–1435. https://doi.org/10.14336/AD.2022.021
55. Gopal Krishnan, P. D., Lee, W. X., Goh, K. Y., Choy, S. M., Turqueza, L. R. R., Lim, Z. H., & Tang, H. W. (2025). Transcriptional regulation of autophagy in skeletal muscle stem cells. Disease models & mechanisms, 18(2), DMM052007. https://doi.org/10.1242/dmm.05200
56. Govindasamy, K., Rao, C. R., Chandrasekaran, B., Parpa, K., & Granacher, U. (2025). Effects of Resistance Training on Sarcopenia Risk Among Healthy Older Adults: A Scoping Review of Physiological Mechanisms. Life (Basel, Switzerland), 15(5), 688. https://doi.org/10.3390/life15050688
57. Gueugneau, M., Coudy-Gandilhon, C., Roche, F., Barthélémy, J. C., Féasson, L., & Béchet, D. (2018). Cellular and functional mechanisms underlying muscle aging and associated diseases. In Nestle Purina Companion Animal Nutrition (CAN) Summt
58. Harrison, D. E., Strong, R., Sharp, Z. D., Nelson, J. F., Astle, C. M., Flurkey, K., Nadon, N. L., Wilkinson, J. E., Frenkel, K., Carter, C. S., Pahor, M., Javors, M. A., Fernandez, E., & Miller, R. A. (2009). Rapamycin fed late in life extends lifespan in genetically heterogeneous mice. Nature, 460(7253), 392–395. https://doi.org/10.1038/nature08221
59. Hentze, M. W., Castello, A., Schwarzl, T., & Preiss, T. (2018). A brave new world of RNA-binding proteins. Nature Reviews Molecular Cell Biology, 19(5), 327-341. https://doi.org/10.1038/nrm.2017.130
60. Hentze, M. W., Sommerkamp, P., Ravi, V., & Gebauer, F. (2025). Rethinking RNA-binding proteins: Riboregulation challenges prevailing views. Cell, 188(18), 4811-4827. https://doi.org/10.1016/j.cell.2025.06.021
61. Heraud-Farlow, J. E., Sharangdhar, T., Li, X., Pfeifer, P., Tauber, S., Orozco, D., Hörmann, A., Thomas, S., Bakosova, A., Farlow, A. R., Edbauer, D., Lipshitz, H. D., Morris, Q. D., Bilban, M., Doyle, M., & Kiebler, M. A. (2013). Staufen2 regulates neuronal target RNAs. Cell reports, 5(6), 1511–1518. https://doi.org/10.1016/j.celrep.2013.11.039
62. Hostrup, M., Moesgaard, L., Fischer, M., Wickham, K. A., Pleshardt, M., Andersen, A. B., Bejder, J., Thomassen, M., Nielsen, J. J., Dehnes, Y., Bangsbo, J., Nordsborg, N. B., &

Jessen, S. (2025). Clenbuterol induces lean mass and muscle protein accretion, but attenuates cardiorespiratory fitness and desensitizes muscle β_2-adrenergic signalling. The Journal of physiology, 603(19), 5529–5545. https://doi.org/10.1113/JP289023
63. Hu, J., Wang, Y., Ji, X., Zhang, Y., Li, K., & Huang, F. (2024). Non-Pharmacological Strategies for Managing Sarcopenia in Chronic Diseases. Clinical interventions in aging, 19, 827–841. https://doi.org/10.2147/CIA.S455736
64. Jiang, S., Meng, X., Gu, H., Sun, J., Chen, S., Chen, Z., Liu, D., & Liang, X. (2023). STAU1 promotes adipogenesis by regulating the alternative splicing of Pparγ2 mRNA. Biochimica et biophysica acta. Molecular and cell biology of lipids, 1868(5), 159293. https://doi.org/10.1016/j.bbalip.2023.159293
65. Joshi, A. S., Tomaz da Silva, M., Kumar, S., & Kumar, A. (2025). Signaling networks governing skeletal muscle growth, atrophy, and cachexia. Skeletal muscle, 15(1), 29. https://doi.org/10.1186/s13395-025-00397-z
66. Kaur, M., & Cole, M. D. (2013). MYC acts via the PTEN tumor suppressor to elicit autoregulation and genome-wide gene repression by activation of the Ezh2 methyltransferase. Cancer research, 73(2), 695-705.
67. Kiebler, M. A., Hemraj, I., Verkade, P., Köhrmann, M., Fortes, P., Marión, R. M., Ortín, J., & Dotti, C. G. (1999). The mammalian staufen protein localizes to the somatodendritic domain of cultured hippocampal neurons: implications for its involvement in mRNA transport. The Journal of neuroscience: the official journal of the Society for Neuroscience, 19(1), 288–297. https://doi.org/10.1523/JNEUROSCI.19-01-00288.1999
68. Kim, Y. K., Furic, L., Desgroseillers, L., & Maquat, L. E. (2005). Mammalian Staufen1 recruits Upf1 to specific mRNA 3'UTRs so as to elicit mRNA decay. Cell, 120(2), 195–208. https://doi.org/10.1016/j.cell.2004.11.050
69. Kitajima, Y., Yoshioka, K., & Suzuki, N. (2020). The ubiquitin-proteasome system in regulation of the skeletal muscle homeostasis and atrophy: from basic science to disorders. The journal of physiological sciences: JPS, 70(1), 40. https://doi.org/10.1186/s12576-020-00768-9
70. Koletsou, E., & Huppertz, I. (2025). RNA-binding proteins as versatile metabolic regulators. Npj Metabolic Health and Disease, 3(1), 1. https://doi.org/10.1038/s44324-024-00044-z
71. Koletsou, E., & Huppertz, I. (2025). RNA-binding proteins as versatile metabolic regulators. Npj Metabolic Health and Disease, 3, 1. https://doi.org/10.1038/s44324-024-00044-z
72. Konde, O. M., Balela, W. B., & Tshitenge, T. B. (2025). Targeting RNA-binding proteins with small molecules: Perspectives and challenges. Frontiers in Chemistry, 13, 1649692. https://doi.org/10.3389/fchem.2025.1649692
73. Konde, O. M., Balela, W. B., & Tshitenge, T. B. (2025). Targeting RNA-binding proteins with small molecules: Perspectives and challenges. Frontiers in Chemistry, 13, 1649692. https://doi.org/10.3389/fchem.2025.1649692
74. Konopka, A. R., Laurin, J. L., Schoenberg, H. M., Reid, J. J., Castor, W. M., Wolff, C. A., Musci, R. V., Safairad, O. D., Linden, M. A., Biela, L. M., Bailey, S. M., Hamilton, K. L., & Miller, B. F. (2019). Metformin inhibits mitochondrial adaptations to aerobic exercise training in older adults. Aging cell, 18(1), e12880. https://doi.org/10.1111/acel.12880
75. Kubat, G. B., Bouhamida, E., Ulger, O., Turkel, I., Pedriali, G., Ramaccini, D., Ekinci, O., Ozerklig, B., Atalay, O., Patergnani, S., Nur Sahin, B., Morciano, G., Tuncer, M., Tremoli, E., & Pinton, P. (2023). Mitochondrial dysfunction and skeletal muscle atrophy: Causes,

mechanisms, and treatment strategies. Mitochondrion, 72, 33–58. https://doi.org/10.1016/j.mito.2023.07.003
76. Larsson, L., Degens, H., Li, M., Salviati, L., Thompson, W., Kirkland, J. L., & Sandri, M. (2018). Sarcopenia: Aging-Related Loss of Muscle Mass and Function. Physiological Reviews, 99(1), 427. https://doi.org/10.1152/physrev.00061.2017
77. Lazzaretti, D., Bandholz-Cajamarca, L., Emmerich, C., Schaaf, K., Basquin, C., Irion, U., & Bono, F. (2018). The crystal structure of Staufen1 in complex with a physiological RNA sheds light on substrate selectivity. Life science alliance, 1(5), e201800187. https://doi.org/10.26508/lsa.201800187
78. Lecker, S. H., Goldberg, A. L., & Mitch, W. E. (2006). Protein degradation by the ubiquitin-proteasome pathway in normal and disease states. Journal of the American Society of Nephrology: JASN, 17(7), 1807–1819. https://doi.org/10.1681/ASN.2006010083
79. Leduc-Gaudet, J. P., Franco-Romero, A., Cefis, M., Moamer, A., Broering, F. E., Milan, G., Sartori, R., Chaffer, T. J., Dulac, M., Marcangeli, V., Mayaki, D., Huck, L., Shams, A., Morais, J. A., Duchesne, E., Lochmuller, H., Sandri, M., Hussain, S. N. A., & Gouspillou, G. (2023). MYTHO is a novel regulator of skeletal muscle autophagy and integrity. Nature communications, 14(1), 1199. https://doi.org/10.1038/s41467-023-36817-1
80. Lee, K., Ku, J., Ku, D., & Kim, Y. (2024). Inverted Alu repeats: Friends or foes in the human transcriptome. Experimental & Molecular Medicine, 56(6), 1250-1262. https://doi.org/10.1038/s12276-024-01177-3
81. Levine, B., & Kroemer, G. (2019). Biological Functions of Autophagy Genes: A Disease Perspective. Cell, 176(1-2), 11–42. https://doi.org/10.1016/j.cell.2018.09.048c
82. Li, L., Huang, C., Pang, J., Huang, Y., Chen, X., & Chen, G. (2023). Advances in research on cell models for skeletal muscle atrophy. Biomedicine & pharmacotherapy = Biomedecine & pharmacotherapie, 167, 115517. https://doi.org/10.1016/j.biopha.2023.115517
83. Li, W., Xing, Y., Jiang, L., Meng, J., Wang, Y., Tan, R., & Zhang, Y. (2025). Systems biology and experimental validation indicate DDIT4, FOXO1, and STAT3 as shared key genes linking osteoporosis and sarcopenia. Frontiers in genetics, 16, 1630705. https://doi.org/10.3389/fgene.2025.1630705
84. Lim, C., Nunes, E. A., Currier, B. S., McLeod, J. C., Thomas, A. C. Q., & Phillips, S. M. (2022). An Evidence-Based Narrative Review of Mechanisms of Resistance Exercise-Induced Human Skeletal Muscle Hypertrophy. Medicine and science in sports and exercise, 54(9), 1546–1559. https://doi.org/10.1249/MSS.0000000000002929
85. Lin, J. H., & Lu, A. Y. (1997). Role of pharmacokinetics and metabolism in drug discovery and development. Pharmacological reviews, 49(4), 403-449.
86. Liu, D., Fan, Y. B., Tao, X. H., Pan, W. L., Wu, Y. X., Wang, X. H., He, Y. Q., Xiao, W. F., & Li, Y. S. (2021). Mitochondrial Quality Control in Sarcopenia: Updated Overview of Mechanisms and Interventions. Aging and disease, 12(8), 2016–2030. https://doi.org/10.14336/AD.2021.0427
87. Liu, S., Liao, S., He, J., Zhou, Y., & He, Q. (2025). IGF2BP2: An m6A reader that affects cellular function and disease progression. Cellular & Molecular Biology Letters, 30, 43. https://doi.org/10.1186/s11658-025-00723-9
88. Liu, W., Meng, P., Li, Z., Shen, Y., Meng, X., Jin, S., & Hu, M. (2025). The multifaceted impact of physical exercise on FoxO signaling pathways. Frontiers in cell and developmental biology, 13, 1614732. https://doi.org/10.3389/fcell.2025.1614732

89. Lo Scrudato, M., Poulard, K., Sourd, C., Tomé, S., Klein, A. F., Corre, G., Huguet, A., Furling, D., Gourdon, G., & Buj-Bello, A. (2019). Genome Editing of Expanded CTG Repeats within the Human DMPK Gene Reduces Nuclear RNA Foci in the Muscle of DM1 Mice. Molecular therapy : the journal of the American Society of Gene Therapy, 27(8), 1372–1388. https://doi.org/10.1016/j.ymthe.2019.05.021
90. Lu, L., Liu, C., & Wei, W. (2026). Resistance training for the prevention and management of sarcopenia in older adults: Mechanisms, efficacy, and future applications. Experimental gerontology, 216, 113085. https://doi.org/10.1016/j.exger.2026.113085
91. Luo, M., Duchaîne, T. F., & DesGroseillers, L. (2002). Molecular mapping of the determinants involved in human Staufen-ribosome association. The Biochemical journal, 365(Pt 3), 817–824. https://doi.org/10.1042/bj20020263
92. Lutz, M., Levanti, M., Karns, R., Gourdon, G., Lindquist, D., Timchenko, N. A., & Timchenko, L. (2023). Therapeutic Targeting of the GSK3β-CUGBP1 Pathway in Myotonic Dystrophy. International Journal of Molecular Sciences, 24(13), 10650. https://doi.org/10.3390/ijms241310650
93. Mao, X., Lv, K., Qi, W., Cheng, W., Li, T., Sun, Y., Jin, H., Pan, H., & Wang, D. (2025). Research progress on sarcopenia in the musculoskeletal system. Bone research, 13(1), 78. https://doi.org/10.1038/s41413-025-00455-8
94. Marcellus, K. A., Crawford Parks, T. E., Almasi, S., & Jasmin, B. J. (2021). Distinct roles for the RNA-binding protein Staufen1 in prostate cancer. BMC cancer, 21(1), 120. https://doi.org/10.1186/s12885-021-07844-2
95. McCarthy, J. J., & Esser, K. A. (2007). MicroRNA-1 and microRNA-133a expression are decreased during skeletal muscle hypertrophy. Journal of Applied Physiology. https://doi.org/JAP-00932-2006McCuller, C., Jessu, R., & Callahan, A. L. (2023). Physiology, Skeletal Muscle. In StatPearls. StatPearls Publishing.
96. McKinnell, I. W., & Rudnicki, M. A. (2004). Molecular mechanisms of muscle atrophy. Cell, 119(7), 907–910. https://doi.org/10.1016/j.cell.2004.12.007Mogil J. S. (2012). Sex differences in pain and pain inhibition: multiple explanations of a controversial phenomenon. Nature reviews. Neuroscience, 13(12), 859–866. https://doi.org/10.1038/nrn3360
97. Montagutelli X. (2000). Effect of the genetic background on the phenotype of mouse mutations. Journal of the American Society of Nephrology: JASN, 11 Suppl 16, S101–S105.
98. Morey-Holton, E. R., & Globus, R. K. (2002). Hindlimb unloading rodent model: technical aspects. Journal of applied physiology (Bethesda, Md: 1985), 92(4), 1367–1377. https://doi.org/10.1152/japplphysiol.00969.2001
99. Mukund, K., & Subramaniam, S. (2019). Skeletal muscle: A review of molecular structure and function, in health and disease. Wiley Interdisciplinary Reviews. Systems Biology and Medicine, 12(1), e1462. https://doi.org/10.1002/wsbm.1462
100. Mynatt, R. L., Noland, R. C., Elks, C. M., Vandanmagsar, B., Bayless, D. S., Stone, A. C., Ghosh, S., Ravussin, E., & Warfel, J. D. (2019). The RNA binding protein HuR influences skeletal muscle metabolic flexibility in rodents and humans. Metabolism: clinical and experimental, 97, 40–49. https://doi.org/10.1016/j.metabol.2019.05.010
101. Nedergaard, A., Jespersen, J. G., Pingel, J., Christensen, B., Sroczynski, N., Langberg, H., Kjaer, M., & Schjerling, P. (2012). Effects of 2 weeks lower limb immobilization and two separate rehabilitation regimens on gastrocnemius muscle protein turnover signaling and normalization genes. BMC Research Notes, 5, 166. https://doi.org/10.1186/1756-0500-5-166

102. Nishikawa, H., Goto, M., Fukunishi, S., Asai, A., Nishiguchi, S., & Higuchi, K. (2021). Cancer Cachexia: Its Mechanism and Clinical Significance. International journal of molecular sciences, 22(16), 8491. https://doi.org/10.3390/ijms22168491
103. Nosengo, N. (2016). Can you teach old drugs new tricks? https://doi.org/10.1038/534314a
104. Nunes, E. A., Stokes, T., McKendry, J., Currier, B. S., & Phillips, S. M. (2022). Disuse-induced skeletal muscle atrophy in disease and nondisease states in humans: mechanisms, prevention, and recovery strategies. American journal of physiology. Cell physiology, 322(6), C1068–C1084. https://doi.org/10.1152/ajpcell.00425.2021
105. Nunn, E., Jaiswal, N., Gavin, M., Uehara, K., Stefkovich, M., Drareni, K., Calhoun, R., Lee, M., Holman, C. D., Baur, J. A., Seale, P., & Titchenell, P. M. (2024). Antibody blockade of activin type II receptors preserves skeletal muscle mass and enhances fat loss during GLP-1 receptor agonism. Molecular metabolism, 80, 101880. https://doi.org/10.1016/j.molmet.2024.101880
106. Pang, X., Zhang, P., Chen, X., & Liu, W. (2023). Ubiquitin-proteasome pathway in skeletal muscle atrophy. Frontiers in physiology, 14, 1289537. https://doi.org/10.3389/fphys.2023.1289537
107. Pang, X., Zhang, P., Chen, X., & Liu, W. (2023). Ubiquitin-proteasome pathway in skeletal muscle atrophy. Frontiers in physiology, 14, 1289537. https://doi.org/10.3389/fphys.2023.1289537
108. Park, E., & Maquat, L. E. (2013). Staufen-mediated mRNA decay. Wiley interdisciplinary reviews. RNA, 4(4), 423–435. https://doi.org/10.1002/wrna.1168
109. Paul, S., Dansithong, W., Figueroa, K. P., Scoles, D. R., & Pulst, S. M. (2018). Staufen1 links RNA stress granules and autophagy in a model of neurodegeneration. Nature Communications, 9(1), 3648. https://doi.org/10.1038/s41467-018-06041-3
110. Pedersen, B. K., & Febbraio, M. A. (2012). Muscles, exercise and obesity: skeletal muscle as a secretory organ. Nature reviews. Endocrinology, 8(8), 457–465. https://doi.org/10.1038/nrendo.2012.49
111. Permpoon, U., Moon, J., Kim, C. Y., & Nam, T. G. (2025). Glucocorticoid-Mediated Skeletal Muscle Atrophy: Molecular Mechanisms and Potential Therapeutic Targets. International journal of molecular sciences, 26(15), 7616. https://doi.org/10.3390/ijms26157616
112. Peruta, C. D., Lozanoska-Ochser, B., Renzini, A., Moresi, V., Riera, C. S., Bouché, M., & Coletti, D. (2023). Sex Differences in Inflammation and Muscle Wasting in Aging and Disease. International Journal of Molecular Sciences, 24(5), 4651. https://doi.org/10.3390/ijms24054651
113. Phillips, S. M., & Van Loon, L. J. (2011). Dietary protein for athletes: from requirements to optimum adaptation. Journal of sports sciences, 29 Suppl 1, S29–S38. https://doi.org/10.1080/02640414.2011.619204
114. Powers, S. K., Lynch, G. S., Murphy, K. T., Reid, M. B., & Zijdewind, I. (2016). Disease-Induced Skeletal Muscle Atrophy and Fatigue. Medicine and science in sports and exercise, 48(11), 2307–2319. https://doi.org/10.1249/MSS.0000000000000975
115. Prado, C. M., Purcell, S. A., & Laviano, A. (2020). Nutrition interventions to treat low muscle mass in cancer. Journal of cachexia, sarcopenia and muscle, 11(2), 366–380. https://doi.org/10.1002/jcsm.12525
116. Pushpakom, S., Iorio, F., Eyers, P. A., Escott, K. J., Hopper, S., Wells, A., Doig, A., Guilliams, T., Latimer, J., McNamee, C., Norris, A., Sanseau, P., Cavalla, D., & Pirmohamed,

M. (2019). Drug repurposing: progress, challenges and recommendations. Nature reviews. Drug discovery, 18(1), 41–58. https://doi.org/10.1038/nrd.2018.168
117. Qu, H., & Qu, Y. (2025). Can coenzyme Q10 supplementation reduce exercise-induced muscle damage and oxidative stress in athletes? A systematic review and meta-analysis. Complementary therapies in clinical practice, 60, 102001. https://doi.org/10.1016/j.ctcp.2025.102001
118. Ravel-Chapuis, A., Bélanger, G., Yadava, R. S., Mahadevan, M. S., DesGroseillers, L., Côté, J., & Jasmin, B. J. (2012). The RNA-binding protein Staufen1 is increased in DM1 skeletal muscle and promotes alternative pre-mRNA splicing. The Journal of cell biology, 196(6), 699–712. https://doi.org/10.1083/jcb.201108113
119. Ravel-Chapuis, A., Crawford, T. E., Blais-Crépeau, M. L., Bélanger, G., Richer, C. T., & Jasmin, B. J. (2014). The RNA-binding protein Staufen1 impairs myogenic differentiation via a c-myc-dependent mechanism. Molecular biology of the cell, 25(23), 3765–3778. https://doi.org/10.1091/mbc.E14-04-0895
120. Riaz, M., Raz, Y., van Putten, M., Paniagua-Soriano, G., Krom, Y. D., Florea, B. I., & Raz, V. (2016). PABPN1-Dependent mRNA Processing Induces Muscle Wasting. PLoS genetics, 12(5), e1006031. https://doi.org/10.1371/journal.pgen.1006031
121. Ricci, E. P., Kucukural, A., Cenik, C., Mercier, B. C., Singh, G., Heyer, E. E., Ashar-Patel, A., Peng, L., & Moore, M. J. (2014). Staufen1 senses overall transcript secondary structure to regulate translation. Nature structural & molecular biology, 21(1), 26–35. https://doi.org/10.1038/nsmb.2739
122. Richter, E. A., & Hargreaves, M. (2013). Exercise, GLUT4, and skeletal muscle glucose uptake. Physiological reviews, 93(3), 993–1017. https://doi.org/10.1152/physrev.00038.2012
123. Rolland, Y., Dray, C., Vellas, B., & Barreto, P. S. (2023). Current and investigational medications for the treatment of sarcopenia. Metabolism: clinical and experimental, 149, 155597. https://doi.org/10.1016/j.metabol.2023.155597
124. Rommel, C., Bodine, S. C., Clarke, B. A., Rossman, R., Nunez, L., Stitt, T. N., Yancopoulos, G. D., & Glass, D. J. (2001). Mediation of IGF-1-induced skeletal myotube hypertrophy by PI(3)K/Akt/mTOR and PI(3)K/Akt/GSK3 pathways. Nature cell biology, 3(11), 1009–1013. https://doi.org/10.1038/ncb1101-1009
125. Rooks, D., Swan, T., Goswami, B., Filosa, L. A., Bunte, O., Panchaud, N., Coleman, L. A., Miller, R. R., Garcia Garayoa, E., Praestgaard, J., Perry, R. G., Recknor, C., Fogarty, C. M., Arai, H., Chen, L. K., Hashimoto, J., Chung, Y. S., Vissing, J., Laurent, D., Petricoul, O., … Roubenoff, R. (2020). Bimagrumab vs Optimized Standard of Care for Treatment of Sarcopenia in Community-Dwelling Older Adults: A Randomized Clinical Trial. JAMA network open, 3(10), e2020836. https://doi.org/10.1001/jamanetworkopen.2020.20836
126. Rosa-Caldwell, M. E., & Greene, N. P. (2019). Muscle metabolism and atrophy; let's talk about sex. Biology of sex differences, 10(1), 43. https://doi.org/10.1186/s13293-019-0257-3
127. Ryall, J. G., Plant, D. R., Gregorevic, P., Sillence, M. N., & Lynch, G. S. (2003). β2-Agonist administration reverses muscle wasting and improves muscle function in aged rats. The Journal of Physiology, 555(Pt 1), 175. https://doi.org/10.1113/jphysiol.2003.056770
128. Sánchez, J. L. C., Gallardo-Gómez, D., Alfonso-Rosa, R. M., Cruz, B. D. P., Ramos-Munell, J., & Del Pozo-Cruz, J. (2025). Effectiveness of different types of exercise based-interventions in sarcopenia: A systematic review and meta-analysis. Geriatric nursing (New York, N.Y.), 63, 635–642. https://doi.org/10.1016/j.gerinurse.2025.04.019

129. Sandri, M. (2010). Autophagy in skeletal muscle. FEBS Letters, 584(7), 1411-1416. https://doi.org/10.1016/j.febslet.2010.01.056
130. Santos, B. F., Grenho, I., Martel, P. J., Ferreira, B. I., & Link, W. (2023). FOXO family isoforms. Cell Death & Disease, 14(10), 702. https://doi.org/10.1038/s41419-023-06177-1
131. Sartori, R., Romanello, V., & Sandri, M. (2021). Mechanisms of muscle atrophy and hypertrophy: implications in health and disease. Nature communications, 12(1), 330. https://doi.org/10.1038/s41467-020-20123-1
132. Savjani, K. T., Gajjar, A. K., & Savjani, J. K. (2012). Drug solubility: importance and enhancement techniques. ISRN pharmaceutics, 2012, 195727. https://doi.org/10.5402/2012/195727
133. Sayed, R. K. A., Hibbert, J. E., Jorgenson, K. W., & Hornberger, T. A. (2023). The Structural Adaptations That Mediate Disuse-Induced Atrophy of Skeletal Muscle. Cells, 12(24), 2811. https://doi.org/10.3390/cells12242811
134. Sayer, A. A., & Cruz-Jentoft, A. (2022). Sarcopenia definition, diagnosis and treatment: Consensus is growing. Age and Ageing, 51(10). https://doi.org/10.1093/ageing/afac220
135. Sayer, A. A., Cooper, R., Arai, H., Cawthon, P. M., Ntsama Essomba, M. J., Fielding, R. A., Grounds, M. D., Witham, M. D., & Cruz-Jentoft, A. J. (2024). Sarcopenia. Nature reviews. Disease primers, 10(1), 68. https://doi.org/10.1038/s41572-024-00550-w
136. Schakman, O., Kalista, S., Barbé, C., Loumaye, A., & Thissen, J. P. (2013). Glucocorticoid-induced skeletal muscle atrophy. The international journal of biochemistry & cell biology, 45(10), 2163–2172. https://doi.org/10.1016/j.biocel.2013.05.036
137. Schiaffino, S., & Reggiani, C. (2011). Fiber types in mammalian skeletal muscles. Physiological reviews, 91(4), 1447–1531. https://doi.org/10.1152/physrev.00031.2010
138. Schiaffino, S., Dyar, K. A., Ciciliot, S., Blaauw, B., & Sandri, M. (2013). Mechanisms regulating skeletal muscle growth and atrophy. The FEBS journal, 280(17), 4294–4314. https://doi.org/10.1111/febs.12253
139. Schmidt, S. F., Rohm, M., Herzig, S., & Berriel Diaz, M. (2018). Cancer Cachexia: More Than Skeletal Muscle Wasting. Trends in cancer, 4(12), 849–860. https://doi.org/10.1016/j.trecan.2018.10.001
140. Severinsen, M. C. K., & Pedersen, B. K. (2020). Muscle-Organ Crosstalk: The Emerging Roles of Myokines. Endocrine reviews, 41(4), 594–609. https://doi.org/10.1210/endrev/bnaa016
141. Sharma, N., Chahal, A., Balasubramanian, K., Sanjeevi, R. R., Rai, R. H., Bansal, N., Muthukrishnan, R., & Sharma, A. (2023). Effects of resistance training on muscular strength, endurance, body composition and functional performance among sarcopenic patients: a systematic review. Journal of diabetes and metabolic disorders, 22(2), 1053–1071.
142. Shi, D. L., & Grifone, R. (2021). RNA-Binding Proteins in the Post-transcriptional Control of Skeletal Muscle Development, Regeneration and Disease. Frontiers in cell and developmental biology, 9, 738978. https://doi.org/10.3389/fcell.2021.738978
143. Shi, Y., Feng, D., Zhou, J., Liu, L., Li, X., Yuan, Z., Wu, J., & Yao, H. (2026). Targeting RNA binding proteins with small-molecule inhibitors: Advances, challenges, and therapeutic opportunities. Acta Pharmaceutica Sinica B, 16(3), 1292-1335. https://doi.org/10.1016/j.apsb.2025.12.010
144. Sinclair, M., Grossmann, M., Hoermann, R., Angus, P. W., & Gow, P. J. (2016). Testosterone therapy increases muscle mass in men with cirrhosis and low testosterone: A randomised controlled trial. Journal of hepatology, 65(5), 906–913. https://doi.org/10.1016/j.jhep.2016.06.007

145. Singh, A., D'Amico, D., Andreux, P. A., Fouassier, A. M., Blanco-Bose, W., Evans, M., Aebischer, P., Auwerx, J., & Rinsch, C. (2022). Urolithin A improves muscle strength, exercise performance, and biomarkers of mitochondrial health in a randomized trial in middle-aged adults. Cell reports. Medicine, 3(5), 100633.
146. Smith, G. I., Atherton, P., Reeds, D. N., Mohammed, B. S., Rankin, D., Rennie, M. J., & Mittendorfer, B. (2011). Omega-3 polyunsaturated fatty acids augment the muscle protein anabolic response to hyperinsulinaemia-hyperaminoacidaemia in healthy young and middle-aged men and women. Clinical science (London, England: 1979), 121(6), 267–278. https://doi.org/10.1042/CS20100597
147. Smith, G. I., Atherton, P., Reeds, D. N., Mohammed, B. S., Rankin, D., Rennie, M. J., & Mittendorfer, B. (2011). Omega-3 polyunsaturated fatty acids augment the muscle protein anabolic response to hyperinsulinaemia-hyperaminoacidaemia in healthy young and middle-aged men and women. Clinical science (London, England: 1979), 121(6), 267–278. https://doi.org/10.1042/CS20100597
148. Song, C. Y., Zhou, T. Y., Shi, H. B., Li, X. Y., & Hong, K. (2025). FoxO1 in skeletal muscle atrophy: Multifaceted regulatory mechanisms and therapeutic opportunities. Acta histochemica, 127(4), 152293. https://doi.org/10.1016/j.acthis.2025.152293
149. Sorge, R. E., & Totsch, S. K. (2017). Sex Differences in Pain. Journal of neuroscience research, 95(6), 1271–1281. https://doi.org/10.1002/jnr.2384
150. Souza, A. L. G., Alves, A. L. R., Martinez, C. G., Sousa, J. C., & Kurtenbach, E. (2025). Biomarkers of Skeletal Muscle Atrophy Based on Atrogenes Evaluation: A Systematic Review and Meta-Analysis Study. International journal of molecular sciences, 26(8), 3516. https://doi.org/10.3390/ijms26083516
151. Spangenburg, E. E., Geiger, P. C., Leinwand, L. A., & Lowe, D. A. (2012). Regulation of Physiological and Metabolic Function of Muscle by Female Sex Steroids. Medicine and Science in Sports and Exercise, 44(9), 1653. https://doi.org/10.1249/MSS.0b013e31825871fa
152. Stevenson, E. J., Koncarevic, A., Giresi, P. G., Jackman, R. W., & Kandarian, S. C. (2005). Transcriptional profile of a myotube starvation model of atrophy. Journal of applied physiology (Bethesda, Md.: 1985), 98(4), 1396–1406. https://doi.org/10.1152/japplphysiol.01055.2004
153. Sugimoto, Y., Vigilante, A., Darbo, E., Zirra, A., Militti, C., Luscombe, N. M., & Ule, J. (2015). HiCLIP reveals the in vivo atlas of mRNA secondary structures recognized by Staufen 1. Nature, 519(7544), 491-494. https://doi.org/10.1038/nature14280
154. Sun, H., Li, K., Liu, C., & Yi, C. (2023). Regulation and functions of non-m6A mRNA modifications. Nature Reviews Molecular Cell Biology, 24(10), 714-731. https://doi.org/10.1038/s41580-023-00622-x
155. Sun, S., Li, X., Zhai, J., Lu, C., Yu, W., Wu, W., & Chen, J. (2025). Orchestrating Nutrient Homeostasis: RNA-Binding Proteins as Molecular Conductors in Metabolic Disease Pathogenesis. Nutrients, 17(14), 2367. https://doi.org/10.3390/nu17142367
156. Sun, S., Li, X., Zhai, J., Lu, C., Yu, W., Wu, W., & Chen, J. (2025). Orchestrating Nutrient Homeostasis: RNA-Binding Proteins as Molecular Conductors in Metabolic Disease Pathogenesis. Nutrients, 17(14), 2367. https://doi.org/10.3390/nu17142367
157. Taghavi, A., Springer, N. A., Zanon, P. R. A., Li, Y., Li, C., Childs-Disney, J. L., & Disney, M. D. (2025). The evolution and application of RNA-focused small molecule libraries. RSC chemical biology, 6(4), 510–527. https://doi.org/10.1039/d4cb00272e

158. Tang, H., Inoki, K., Lee, M., Wright, E., Khuong, A., Khuong, A., Sugiarto, S., Garner, M., Paik, J., DePinho, R. A., Goldman, D., Guan, K. L., & Shrager, J. B. (2014). mTORC1 promotes denervation-induced muscle atrophy through a mechanism involving the activation of FoxO and E3 ubiquitin ligases. Science signaling, 7(314), ra18.
159. Thomas, M. G., Martinez Tosar, L. J., Desbats, M. A., Leishman, C. C., & Boccaccio, G. L. (2009). Mammalian Staufen 1 is recruited to stress granules and impairs their assembly. Journal of cell science, 122(Pt 4), 563–573. https://doi.org/10.1242/jcs.038208
160. Timchenko, N. A., Iakova, P., Cai, Z. J., Smith, J. R., & Timchenko, L. T. (2001). Molecular basis for impaired muscle differentiation in myotonic dystrophy. Molecular and cellular biology, 21(20), 6927–6938. https://doi.org/10.1128/MCB.21.20.6927-6938.2001
161. Tortora, G. J., & Derrickson, B. H. (2018). Principles of anatomy and physiology. John wiley & sons.
162. TOUTAIN, P. L., & BOUSQUET-MÉLOU, A. (2004). Plasma terminal half-life. Journal of Veterinary Pharmacology and Therapeutics, 27(6), 427-439. https://doi.org/10.1111/j.1365-2885.2004.00600.x
163. Vainshtein, A., & Sandri, M. (2020). Signaling Pathways That Control Muscle Mass. International journal of molecular sciences, 21(13), 4759. https://doi.org/10.3390/ijms21134759
164. Van Pelt, D. W., Confides, A. L., Judge, A. R., Vanderklish, P. W., & Dupont-Versteegden, E. E. (2018). Cold shock protein RBM3 attenuates atrophy and induces hypertrophy in skeletal muscle. Journal of muscle research and cell motility, 39(1-2), 35–40. https://doi.org/10.1007/s10974-018-9496-x
165. Vessey, J. P., Macchi, P., Stein, J. M., Mikl, M., Hawker, K. N., Vogelsang, P., Wieczorek, K., Vendra, G., Riefler, J., Tübing, F., Aparicio, S. A., Abel, T., & Kiebler, M. A. (2008). A loss of function allele for murine Staufen1 leads to impairment of dendritic Staufen1-RNP delivery and dendritic spine morphogenesis. Proceedings of the National Academy of Sciences of the United States of America, 105(42), 16374–16379. https://doi.org/10.1073/pnas.0804583105
166. Viezuină, D. M., Burlacu, I. M., Greșiță, A., Matache, I. M., Târtea, E. A., Mușat, M. I., Amzoiu, M. O., Cătălin, B., Sfredel, V., & Mitran, S. I. (2025). Phase-Specific Evaluation of Sciatic Nerve Regeneration in Preclinical Studies: A Review of Functional Assessment, Emerging Therapies, and Translational Value. International journal of molecular sciences, 27(1), 419. https://doi.org/10.3390/ijms27010419
167. Wall, B. T., Morton, J. P., & van Loon, L. J. (2015). Strategies to maintain skeletal muscle mass in the injured athlete: nutritional considerations and exercise mimetics. European journal of sport science, 15(1), 53–62. https://doi.org/10.1080/17461391.2014.936326
168. Walton, R. G., Dungan, C. M., Long, D. E., Tuggle, S. C., Kosmac, K., Peck, B. D., Bush, H. M., Villasante Tezanos, A. G., McGwin, G., Windham, S. T., Ovalle, F., Bamman, M. M., Kern, P. A., & Peterson, C. A. (2019). Metformin blunts muscle hypertrophy in response to progressive resistance exercise training in older adults: A randomized, double-blind, placebo-controlled, multicenter trial: The MASTERS trial. Aging cell, 18(6), e13039. https://doi.org/10.1111/acel.13039
169. Wang, Y., & Pessin, J. E. (2013). Mechanisms for fiber-type specificity of skeletal muscle atrophy. Current Opinion in Clinical Nutrition and Metabolic Care, 16(3), 243. https://doi.org/10.1097/MCO.0b013e328360272d
170. Weihl, C. C., Temiz, P., Miller, S. E., Watts, G., Smith, C., Forman, M., Hanson, P. I., Kimonis, V., & Pestronk, A. (2008). TDP-43 accumulation in inclusion body myopathy muscle

suggests a common pathogenic mechanism with frontotemporal dementia. Journal of neurology, neurosurgery, and psychiatry, 79(10), 1186–1189. https://doi.org/10.1136/jnnp.2007.131334
171. Wickham, L., Duchaîne, T., Luo, M., Nabi, I. R., & DesGroseillers, L. (1999). Mammalian staufen is a double-stranded-RNA- and tubulin-binding protein which localizes to the rough endoplasmic reticulum. Molecular and cellular biology, 19(3), 2220–2230. https://doi.org/10.1128/MCB.19.3.2220
172. Wisdom, K. M., Delp, S. L., & Kuhl, E. (2014). Review. Use it or lose it: Multiscale skeletal muscle adaptation to mechanical stimuli. Biomechanics and Modeling in Mechanobiology, 14(2), 195. https://doi.org/10.1007/s10237-014-0607-3
173. Wong, J. P., Ng, Y. K., Kjærgaard, J., Blazev, R., Deshmukh, A. S., & Parker, B. L. (2025). Skeletal muscle proteomics: Considerations and opportunities. Npj Metabolic Health and Disease, 3(1), 30. https://doi.org/10.1038/s44324-025-00073-2
174. Yamaguchi, Y., Oohinata, R., Naiki, T., & Irie, K. (2008). Stau1 negatively regulates myogenic differentiation in C2C12 cells. Genes to cells : devoted to molecular & cellular mechanisms, 13(6), 583–592. https://doi.org/10.1111/j.1365-2443.2008.01189.x
175. Yang, X., Li, M., Ji, Y., Lin, Y., Xu, L., Gu, X., Sun, H., Wang, W., Shen, Y., Liu, H., & Zhu, J. (2022). Changes of Gene Expression Patterns of Muscle Pathophysiology-Related Transcription Factors During Denervated Muscle Atrophy. Frontiers in Physiology, 13, 923190. https://doi.org/10.3389/fphys.2022.923190
176. Yao, Z., Guo, L., Zhang, L., & Nie, Q. (2024). Transcriptome and Metabolome Profiling Provide New Insights into Disuse Muscle Atrophy in Chicken: The Potential Role of Fast-Twitch Muscle Fibers. International Journal of Molecular Sciences, 25(6), 3516. https://doi.org/10.3390/ijms25063516
177. Yokogawa, A., Kido, K., Miura, I., Oyama, E., Takakura, D., Tanaka, K., Wilkinson, D. J., Smith, K., Atherton, P. J., & Kawanaka, K. (2025). Low-Carbohydrate Diet Exacerbates Denervation-Induced Atrophy of Rat Skeletal Muscle Under the Condition of Identical Protein Intake. Journal of cachexia, sarcopenia and muscle, 16(2), e13738. https://doi.org/10.1002/jcsm.13738
178. Yoshida, T., & Delafontaine, P. (2020). Mechanisms of IGF-1-Mediated Regulation of Skeletal Muscle Hypertrophy and Atrophy. Cells, 9(9), 1970. https://doi.org/10.3390/cells9091970
179. You, J. S., & Chen, J. (2021). Aging Does Not Exacerbate Muscle Loss During Denervation and Lends Unique Muscle-Specific Atrophy Resistance With Akt Activation. Frontiers in Physiology, 12, 779547. https://doi.org/10.3389/fphys.2021.779547
180. You, J. S., Kim, K., Steinert, N. D., Chen, J., & Hornberger, T. A. (2021). mTORC1 mediates fiber type-specific regulation of protein synthesis and muscle size during denervation. Cell death discovery, 7(1), 74. https://doi.org/10.1038/s41420-021-00460-w
181. Zhang, G., Hu, F., Huang, T., Ma, X., Cheng, Y., Liu, X., Jiang, W., Dong, B., & Fu, C. (2024). The recent development, application, and future prospects of muscle atrophy animal models. MedComm – Future Medicine, 3(4), e70008. https://doi.org/10.1002/mef2.70008
182. Zhang, H., Lan, T., Yan, X., Gu, H., Li, Y., & He, E. (2025). Effects of creatine supplementation on muscle strength gains-a meta-analysis and systematic review. PeerJ, 13, e20380. https://doi.org/10.7717/peerj.20380
183. Zhang, L., Peng, Z., Ding, W., Wu, H., Guo, R., Li, D., Niu, L., & Wei, X. (2025). STAU1 exhibits oncogenic characteristics and modulates alternative splicing and gene

expression in lung adenocarcinoma cells. Scientific reports, 15(1), 17031. https://doi.org/10.1038/s41598-025-01883-6
184. Zhang, X., Liao, S., Huang, L., & Wang, J. (2025). Prospective Intervention Strategies Between Skeletal Muscle Health and Mitochondrial Changes During Aging. Advanced biology, 9(1), e2400235. https://doi.org/10.1002/adbi.202400235
185. Zhang, Y., Wang, T., Wang, Z., & Jin, J. (2025). Functions and Therapeutic Potentials of Long Noncoding RNA in Skeletal Muscle Atrophy and Dystrophy. Journal of Cachexia, Sarcopenia and Muscle, 16(2), e13747. https://doi.org/10.1002/jcsm.13747
186. Zhao, R., Huang, S., Li, J., Gu, A., Fu, M., Hua, W., Mao, Y., Lei, Q. Y., Lu, B., & Wen, W. (2024). Excessive STAU1 condensate drives mTOR translation and autophagy dysfunction in neurodegeneration. The Journal of cell biology, 223(8), e202311127. https://doi.org/10.1083/jcb.202311127